Fourth EPAC Technical Report for the ISTAC

May 2024

Contents

1. Introduction

This technical report is the fourth to be presented to the International Scientific and Technical Advisory Committee (ISTAC) for the EPAC project.

The report is intended to provide an overview of the progress made over the past 18 months in all technical and scientific areas of the project. As this is the fourth report, it does not repeat the detailed overviews for the laser system, experimental areas, detectors and data management system that were included in the first report[1], but rather builds on the details provided in the second[2] and third[3] reports, with each section providing a simplified overview such that progress and scope can be gauged.

The building was completed and handed over to the CLF in April 2022, and the ISTAC will have the opportunity to visit the building again after the meeting, to see the progress with installation and commissioning for themselves.

The team has continued to progress the design of the facility informed by input from user consultation, modelling and testing. This report contains details of modelling conducted in key areas, in order to ensure that the expected performance is achieved, and testing that will prove performance or enable the team to make any necessary changes to optimise the design. The report also describes the approach taken to mitigate some of the key technical risks, and highlights the progress made with the procurement of components for different parts of the facility.

Good progress has been made against the installation plan, despite supply chain issues and other calls on staff. The Installation Manager will present the installation schedule and plans for the coming year to the ISTAC.

Commissioning of the laser systems has commenced, in parallel with service installation, and details will be included in presentations delivered during the meeting.

The Project Manager will also provide an overview of the overall progress.

2. Laser system

2.1 Overview of the laser system

The EPAC laser aims to deliver a PW-class system operating at 10 Hz by the end of the commissioning phase of the project. The laser system will be located on the second floor of the EPAC building, with a beam transport system required to propagate the beam to the Experimental Areas (EA) on the ground floor. The specification for the output of the EPAC laser as delivered into the EAs is given in **Table 1**.

Table 1: Specification of the EPAC laser

Parameter	Design requirement
Pulse energy	30 J; Day 1 = 20 J [1]
Pulse duration	≤ 30 fs FWHM
Peak power	1 PW; Day 1 = 0.67 PW
Central wavelength	800 ± 10 nm
Pulse repetition rate	10 Hz, 1 Hz, Shot on demand
Output bandwidth	> 75 nm FWHM
Shot-to-shot pulse energy stability	< 2.5 % RMS
Power contrast	@ -100 ps > 10^{12}; @ -20 ps > 10^{9}; @ -2 ps > 10^{5}
Beam shape	Circular, super-Gaussian (N ≥ 8)
Beam size	220 mm FWHM
Beam spatial intensity modulation	< 10% peak to valley
Beam pointing stability	< 5 µrad RMS
Beam quality	2.2 x Diffraction Limited [2]
Polarisation	Horizontal
Energy modes (Day 1)	E1 = 0.5 J to 20 J; E2 = 5 mJ to 0.5 J E3 = 0.2 mJ to 5 mJ; E4 = 0.5 nJ to 200 µJ

The laser will comprise a set of subsystems, namely: EPAC Front End, EPAC Pump Source, Green conversion, Titanium-doped Sapphire (Ti:Sa) High Energy Amplifier (HEA), Pulse compressor and Beam propagation, whose linkages are shown in **Figure 1**. The layout of the laser subsystems on the second floor of the EPAC building is shown in **Figure 2**.

Progress on these subsystems is reported in the following sections.

[1] Day 1 corresponds to initial operations, where output will be reduced whilst de-risking high peak / average power operation.
[2] Quality of beam entering EA1 prior to final adaptive optic correction.

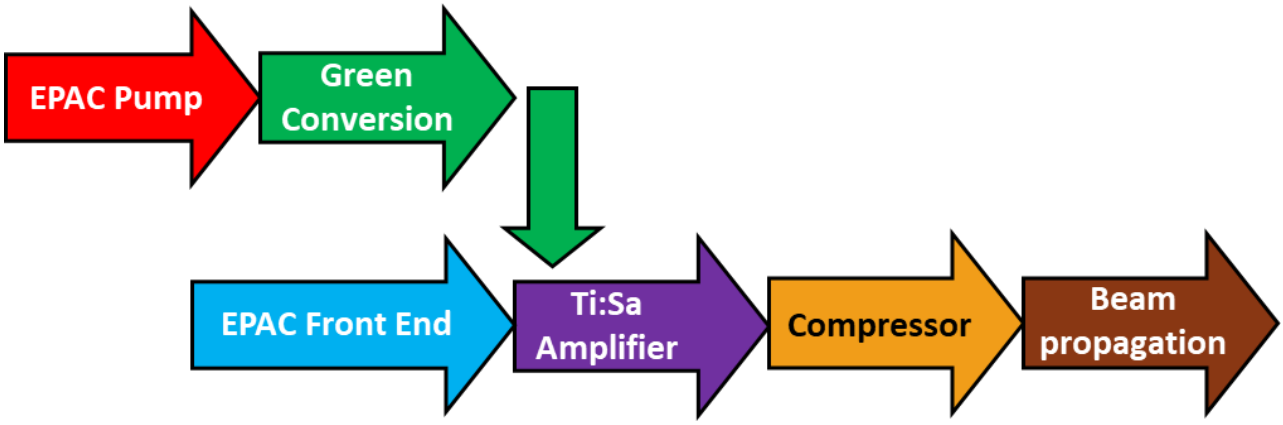

Figure 1: Concept of the EPAC laser

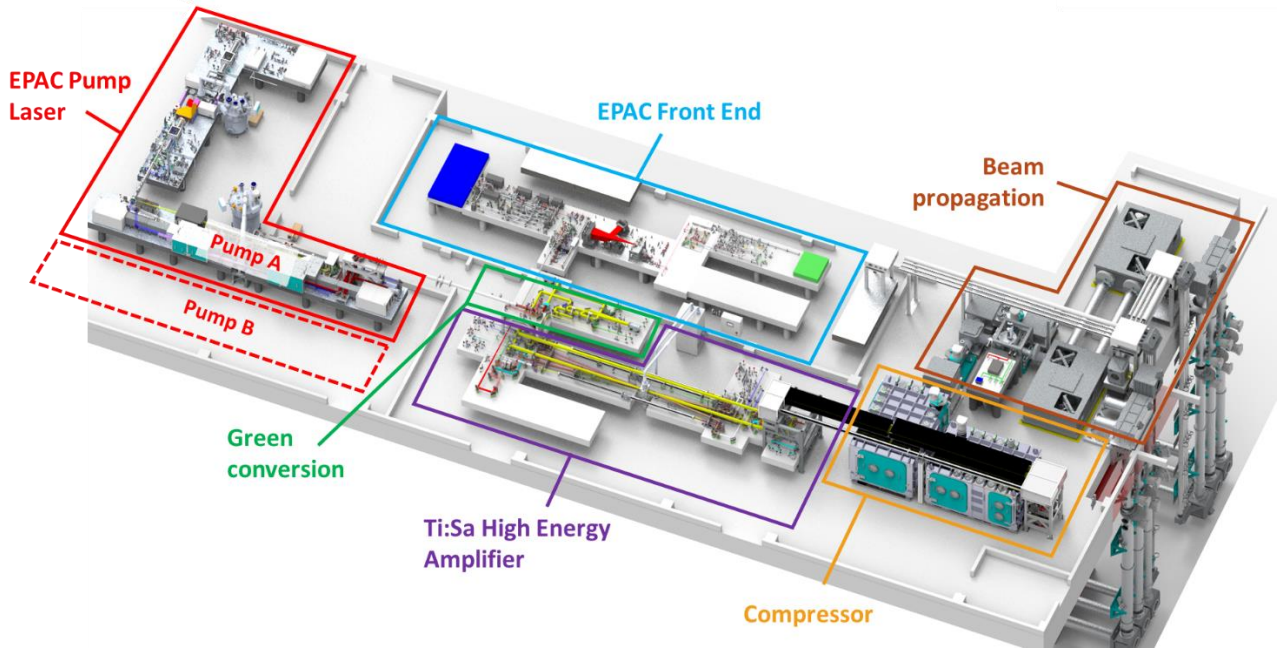

Figure 2: Layout of EPAC laser subsystems in EPAC building

2.2 Front End

The Front End of the EPAC laser is responsible for the first 10^8 net energy gain to deliver 1.5 J, 4 ns pulses of 110 nm FWHM bandwidth to seed the Ti:Sa multi-pass amplifier (**Section 2.4**). The amplification of the Front End is split into a picosecond-pumped OPCPA and a nanosecond-pumped OPCPA section, followed by an 'Energy Control' section that handles energy attenuation modes, fast stabilisation, repetition-rate control and optical isolation of the front end. The output specifications of the Front End are described in **Table 2**, and a schematic of the Front End amplification architecture and CAD drawing of the system are provided in **Figure 3** and **Figure 4**, respectively.

Table 2: Specifications of the EPAC Front End

Parameter	Design requirement
Pulse energy	1.5 J full spectrum > 500 mJ shaped spectrum
Pulse duration	4 ns FWHM
Amplification bandwidth	> 100 nm FWHM
Central wavelength	800 +/- 10 nm
Pulse repetition rate	10 Hz, 1 Hz, Shot on Demand
Subsystem output pulse energy: • **Master oscillator seed** • **ps-OPCPA** • **ns-OPCPA** • **After shaping**	 5 nJ 1.5 mJ 1.5 J > 500 mJ
Subsystem output pulse durations (FWHM): • **Master oscillator seed** • **ps-OPCPA** • **Tuneable stretcher** • **Stretcher**	 8 fs 15 ps 70 to 120 ps 4 ns
Shot-to-shot pulse energy stability	< 2 % RMS
Power contrast	10^{10}
Beam shape	Circular, super-Gaussian ($N \geq 8$)
Beam size	20 mm FWHM
Beam spatial intensity modulation	< 10 % peak to valley
Beam pointing stability	< 5 µrad RMS
Beam quality	1.5 x Diffraction Limited
Single shot capability	Yes
Polarisation	Vertical
Polarisation purity	100:1

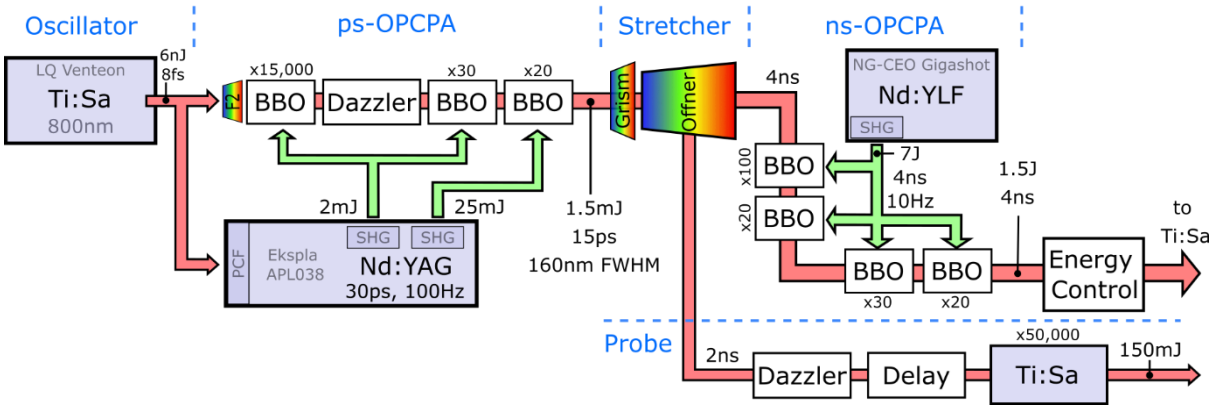

Figure 3: Schematic of the EPAC OPCPA front end amplification sections

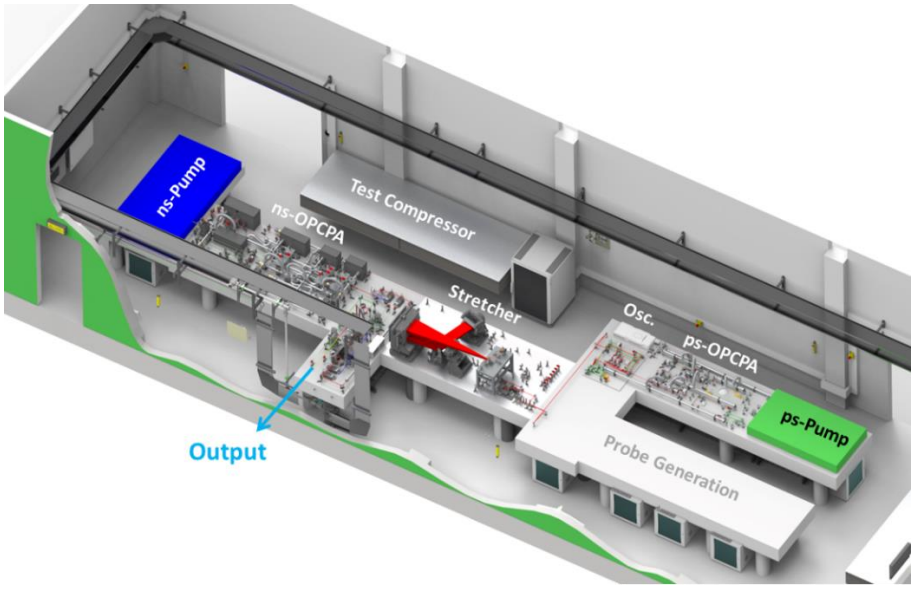

Figure 4: CAD drawing of the EPAC Front End

Since the last report[3], there has been significant progress with the Front End installation, with all major components required to deliver 4 ns to the Ti:Sa main amplifier now on the optical table. The overall design of the Front End is unchanged from that reported last time, with three 30 ps pumped OPCPA stages and four 4 ns pumped OPCPA stages. Commissioning of the laboratory and laser system began in November 2023 with the turning on of the Master Oscillator, and the aim is to deliver a usable pulsed alignment seed for Ti:Sa commissioning in June/July 2024.

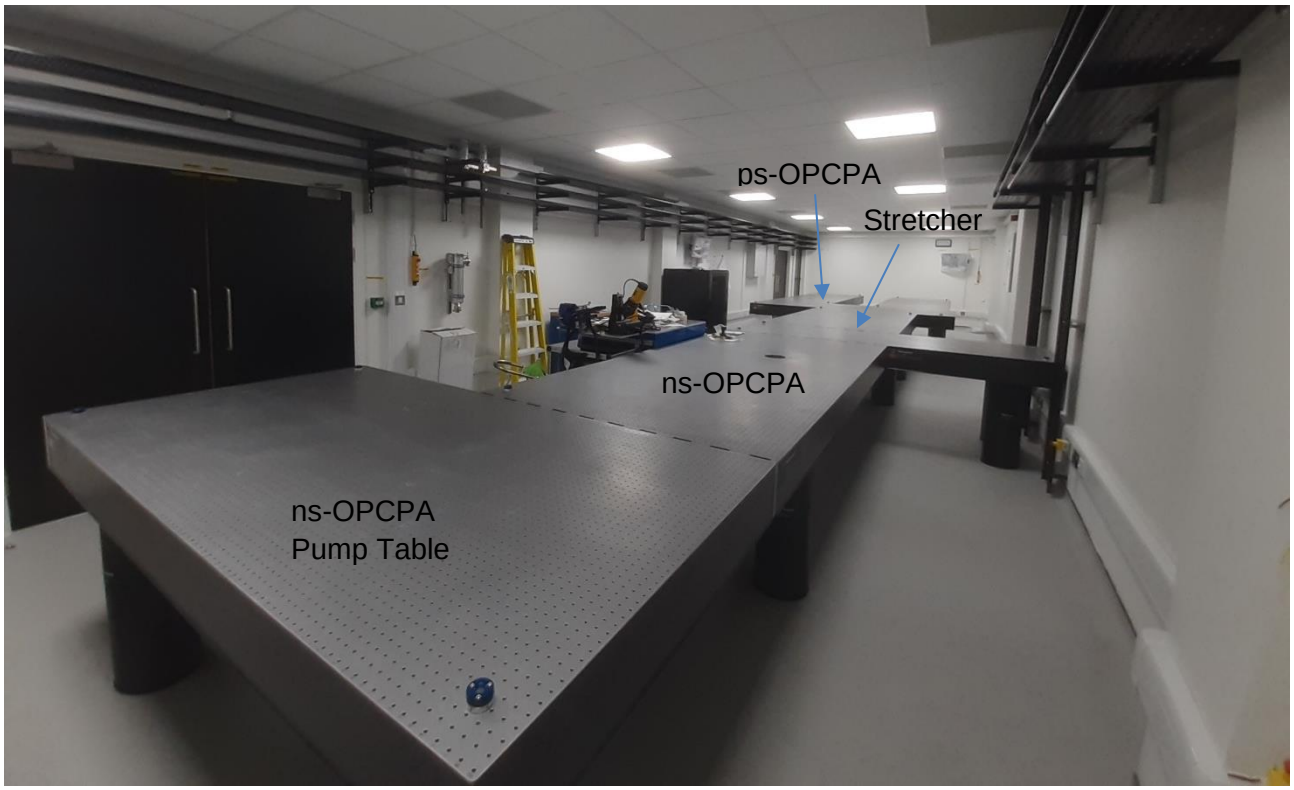

Figure 5: Photograph of the EPAC Front End Room in March 2023, when the main optical tables were installed

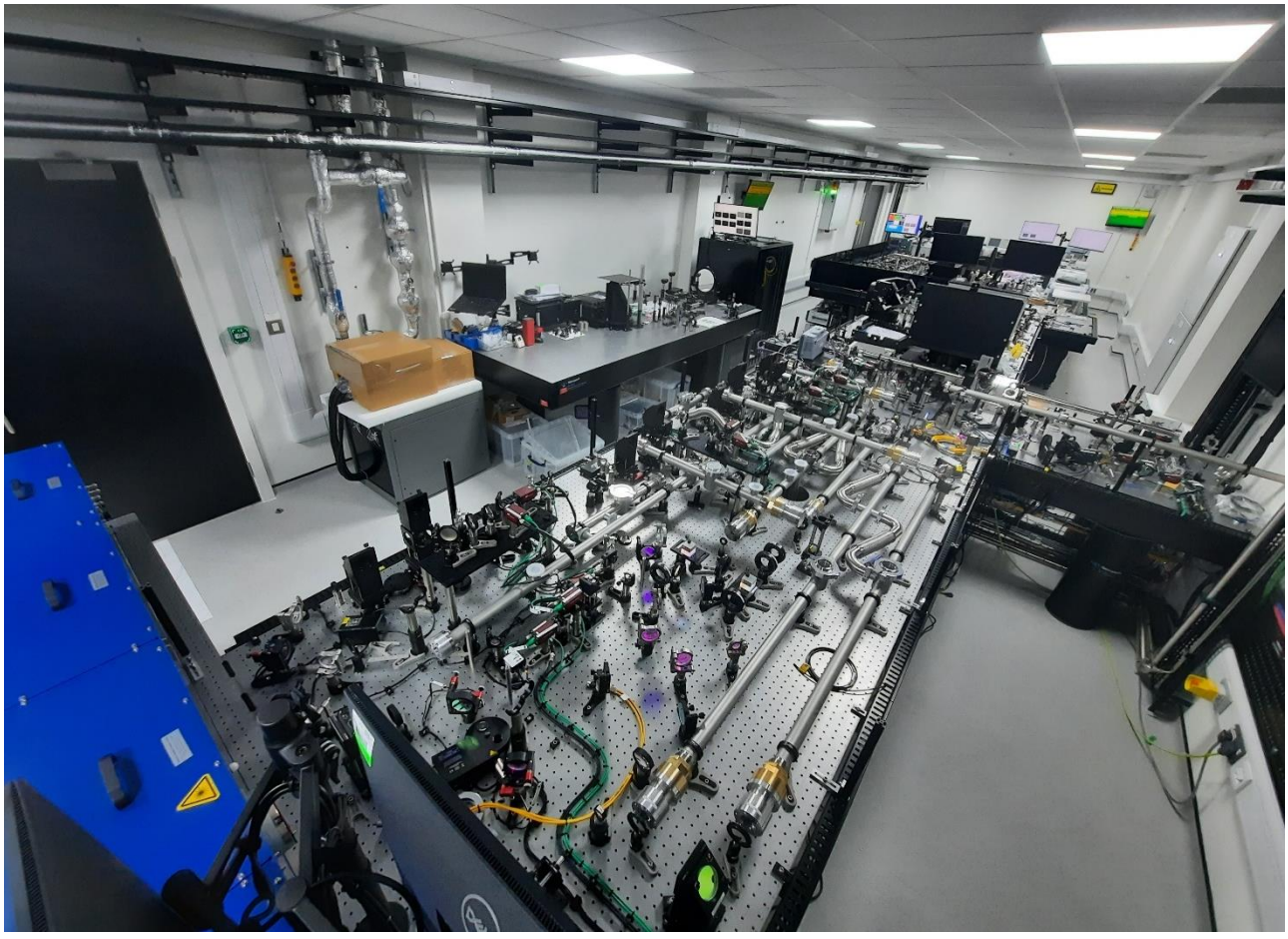

Figure 6: Photograph of the EPAC Front End Room in April 2024

The following sections describe progress since the last ISTAC report on development of the picosecond-pumped OPCPAs, stretcher, nanosecond-pumped OPCPAs, output energy control and isolation, and provision of a probe beamline.

2.2.1 Picosecond-pumped OPCPAs (ps-OPCPAs)

The ps-OPCPA section has been fully installed and is currently undergoing optimisation to provide reliable 1.5 mJ energy, >110nm output bandwidth, with energy and spectral stability, and uniform super-Gaussian beam profile, to seed the stretcher and ns-OPCPAs.

The first ps-OPCPA stage was designed to output 20 – 100 µJ and is currently producing ~10 µJ, x 5000 gain with >100 nm bandwidth. Current optimisation work is focused on avoiding excessive spatial walk-off effects, which uses 1 mm beams, an 11 mm crystal and the 2.4 deg non-collinear broadband phase-matching angle in BBO. These small beams are required to achieve benefits from amplifier saturation to pulse bandwidth, energy, energy stability and pulse contrast.

Optical gain in the second and third picosecond OPCPA stages has been achieved. The 1.5 mJ target, with 25 mJ available pump energy into the final stage, is still reasonable, where spatial walk-off effects become negligible for the ~10 mm beam diameters used.

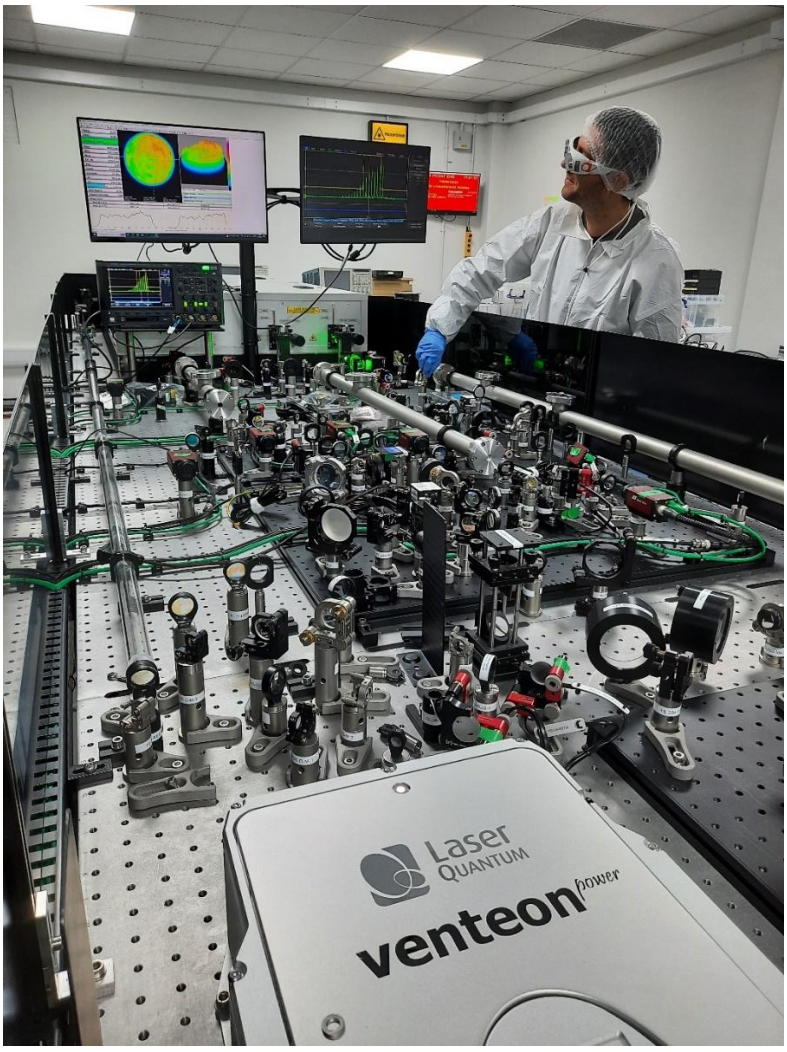

Figure 7: Veselin Aleksandrov aligning the 25mJ, 30ps pump laser into the final ps-OPCPA stage. In the foreground is the EPAC Master Oscillator.

2.2.1.1 ps pump laser

For any OPCPA system, the pump laser is a critical component that must perform reliably and stably. The 100 Hz diode-pumped picosecond pump laser, APL038, manufactured by Ekspla, was moved into the EPAC laboratory and has, so far, performed to expectations. The laser is currently set up to have optical synchronisation from the femtosecond Master Oscillator, with ~120 mW of its 550 mW output diverted to effectively seed the pump laser. The 800 nm of the Maser oscillator is spectrally shifted to 1064 nm by Raman scattering in a photonic crystal fibre, before amplification in an Nd:YAG regenerative amplifier, the output of which is then split into Gaussian and top-hat channels. The Gaussian channel is amplified with a single pass Nd:YAG booster amplifier and frequency doubled to 2 mJ; the top-hat channel routinely emits up to 25 mJ at 527 nm via a two-pass booster amplifier of larger rod diameter. A standard deviation of <0.3% in energy is regularly achieved, which will in turn lead to high stability OPCPA performance.

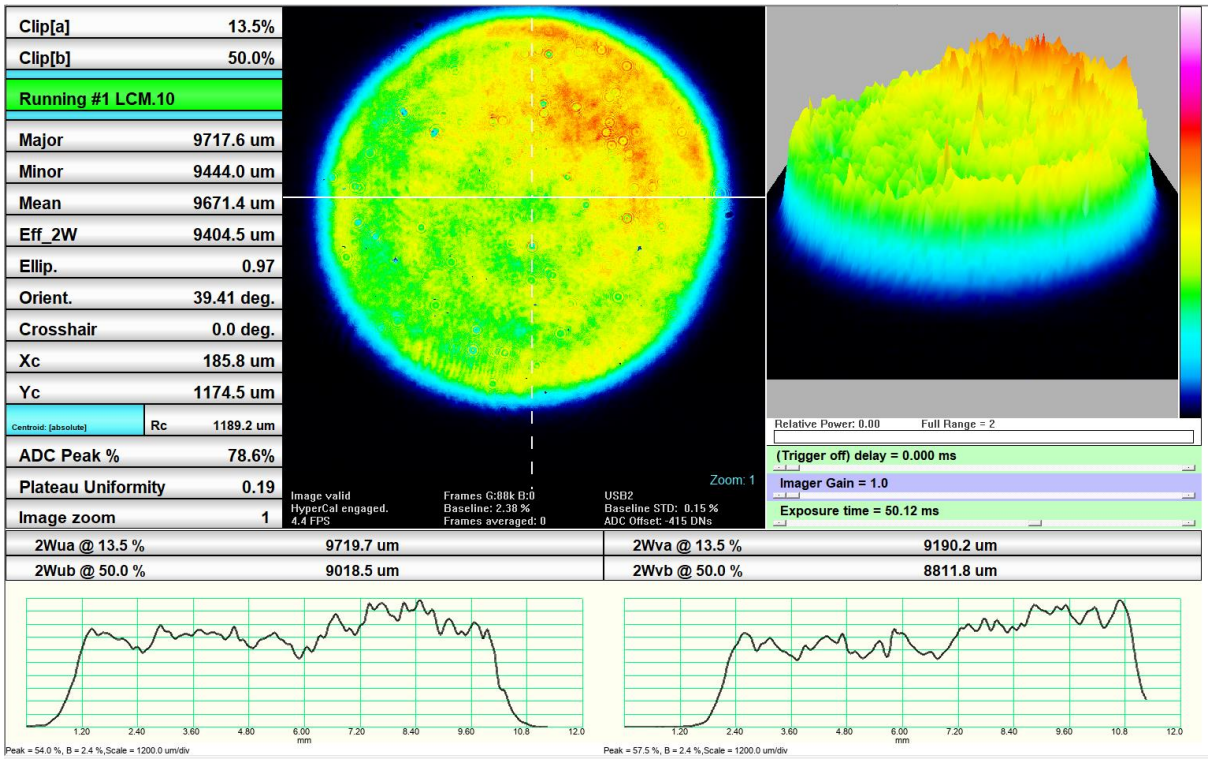

Figure 8: Beam profile of the 25mJ flat-top 527nm pumping pulses into the final OPCPA stage. Intensity uniformity can be improved with further service engineer led optimisation if required.

2.2.2 Stretcher scheme

The seed for the ns-OPCPAs will be output from the transmission grating Offner stretcher, with design for up to fifth-order spectral phase dispersion control of the entire short-pulse beamline. A delay in the manufacturing of optics was identified as a likely and significant risk to progression of the ns-OPCPA initial delivery. In response, we escalated the design and build of the "test compressor" for the Front End, to be used as a temporary stretcher. This uses CLF ex-Gemini stock 1480 l/mm gold reflective gratings operated at Littrow angle in a four-pass, two-grating out-of-plane Treacy configuration to produce ~4 ns pulses required to seed the ns-OPCPA beamline. This temporary stretcher is currently operational, producing 25% throughput after its eight grating reflections.

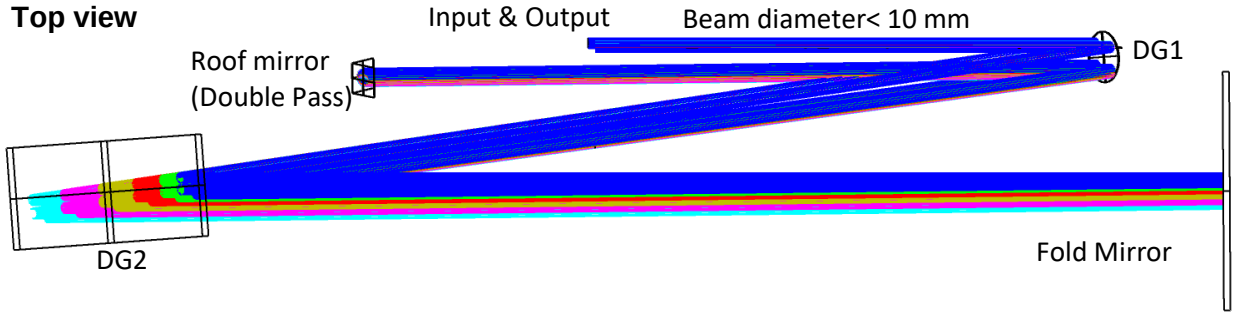

Figure 9: Optic schematic of the four-pass, two-grating Treacy configuration temporary stretcher/test compressor. A slight angle on the input or fold mirror orthogonal to the diffraction plane allows a geometric two-pass, where a roof mirror is positioned to translate the beam height and retrieve a four-pass output beam.

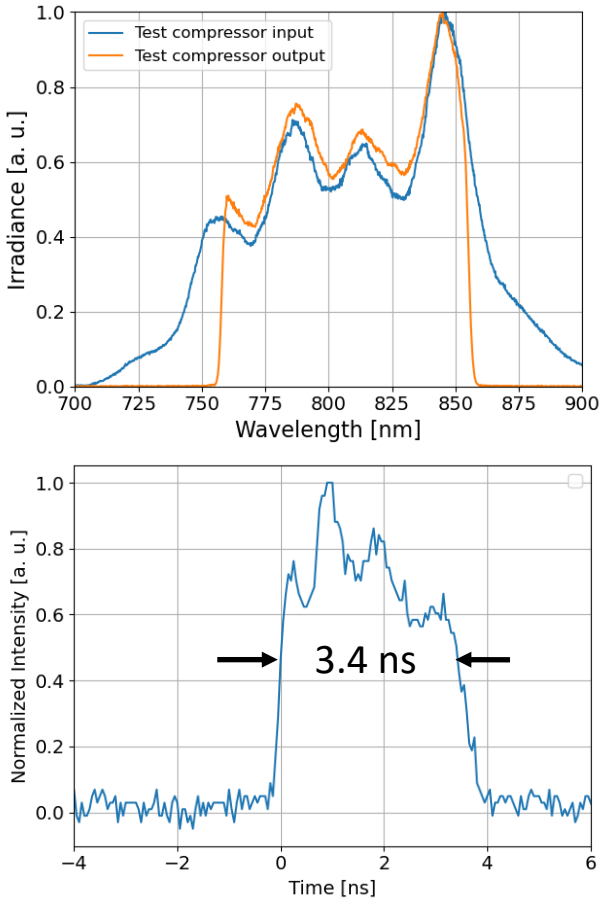

Figure 10: (Top) Spectral transmission of the test compressor/temporary stretcher. (Bottom) Output 3.4ns pulse duration of the stretcher, which is acceptable for initial ns-OPCPA operation until the main stretcher optics are delivered.

Some of the optics for the primary Offner stretcher have been received. Of particular importance is the surface irregularity of the convex spherical fold mirror at the Fourier plane of this achromatic imaging stretcher configuration, which is widely accepted to be the dominant contributor to laser pulse contrast noise pedestal. The real data from the manufactured optic is very similar to the modelling assumptions used in 2020 during the design stage, and lay behind the decision to invest in the highest optical quality polish available. We currently expect the noise contributions from this critical optic to be within contrast specification outlined in **Table 2**.

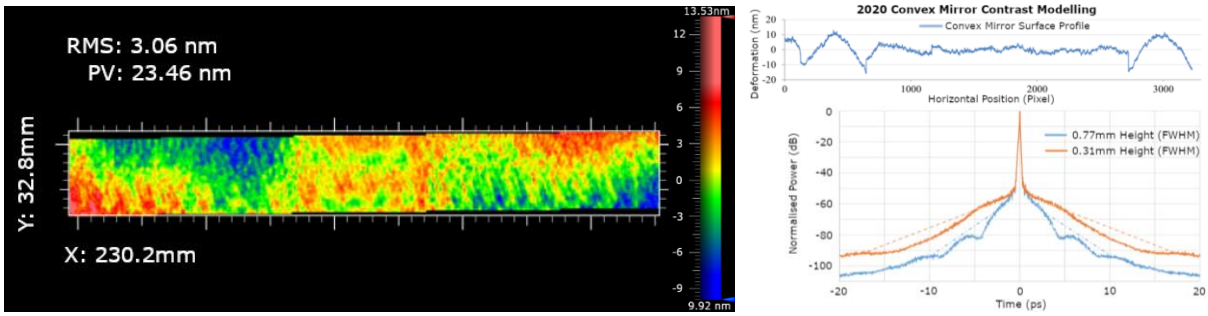

Figure 11: (Left) Surface irregularity from a perfect sphere of the EPAC Offner stretcher convex mirror. The laser will be incident on this optic as a ~1 mm height line focus (shaded blue). (Right) Modelling of pulse contrast contribution of the convex mirror with a similar surface profile.

2.2.3 Nanosecond-pumped OPCPAs (ns-OPCPAs)

The ns-OPCPA section of the Front End is currently being installed, with the first experimental results expected in June 2024. Since the last report, the design fluence of the amplifiers has been reduced to below book values of damage thresholds, to further ensure the longevity of the optical chain. The first three BBO OPCPA stages will operate at half the quoted laser induced damage threshold. Due to its higher damage threshold, we have chosen to use LBO in the final amplifier to achieve the design signal energy and beam size. The phase-matching of LBO has been checked and found to not be an issue.

The design operating parameters for the four, 4 ns pumped OPCPA stages are shown in **Table 3**. The design also incorporates a 50% energy loss between stages for system tolerancing. A variable gain in stage 1 accounts for the worst case energy output from the preceding optical chain, showing that the energy is recoverable. In the best case scenario, it is possible to shut off pumping the first or second amplifier stage.

Table 3: Design operating parameters and performance of the four ns-OPCPA stages

	Energies				Diameters			
Stage	**Seed (mJ)**	**Pump (mJ)**	**Signal (mJ)**	**Gain**	**Seed mm)**	**Pump (mm)**	**Crystal lLength (mm)**	**Signal bandwidth (nm FWHM)**
1, BBO	0.01-0.15	30	2.0	290 - 22	2.50	1.96	17 -11	107
2, BBO	0.9	28	15	27	2.35	1.89	15	108
3, BBO	3.8	182	105	39	5.66	4.81	15	108
4, LBO	52	4600	3000	72	19.25	17.11	27	109

Greater than 60% energy conversion efficiency per stage is expected due to the flat-top spatial and temporal profiles employed, and the operation of nonlinear amplification in the saturated regime.

2.2.3.1 ns-Pump Laser

The nanosecond OPCPA pump laser (ns-pump) characteristics will directly imprint onto the amplified 800 nm signal of the EPAC short-pulse beamline, and will have a large contribution of the final 30 – 50 J output profile of the EPAC Ti:Sa high energy amplifier. The placement of the contract was a significant technical decision: as previously reported, it was awarded to Photonic Solutions for a Northrop Grumman Core Edge Optronics (NGCEO) 7 J, 527 nm, 10 Hz Gigashot Nd:YLF DPSS system. The manufacture of this laser has recently been completed, and it is being installed in the EPAC Front End lab in April/May 2024.

A flat-top 4 ns temporal and spatial profile is being achieved. With care, the temporal profile is fully programmable in intensity with <100 ps resolution and a small variation, ~10%, in pulse duration. The 7 J energy stability is ~0.25% and the spatial profile has a standard deviation intensity uniformity of 9%. Due to the x 10 beam size and angular magnification into the first ns-OPCPA stage, the measured 9 µrad pointing stability will ensure phase-matching is stable for broadband OPCPA.

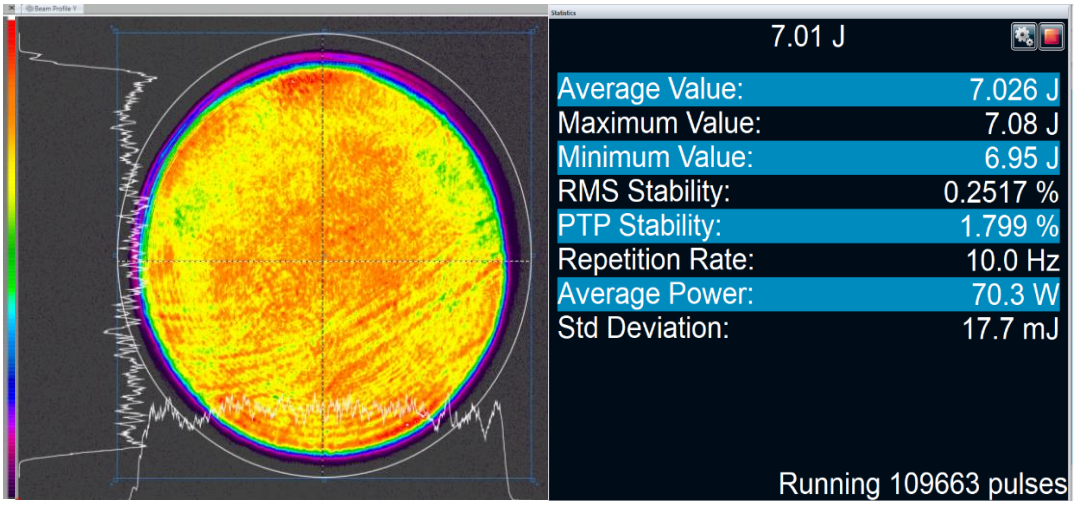

Figure 12: Spatial profile, 527 nm energy and energy stability of the ns-pump laser at its factory acceptance test

2.2.4 Probe beamline

Since the last report, a contract for a commercial 10 Hz Ti:Sa amplifier system has been awarded to Amplitude, for the production of an Nd:YAG 532 nm pumped regenerative amplifier and multi-pass system (ARCO X 150). This is a pre-existing design that is being made to order for UKRI, i.e. it is a low technical risk. This system will produce 150 mJ 2 ns pulses at 800 nm centre wavelength, optically seeded and synchronised to the EPAC stretcher first pass output. An independent AOPDF (Fastlite HR800 Dazzler) will control the spectral phase and amplitude for optimal compression to <30 fs.

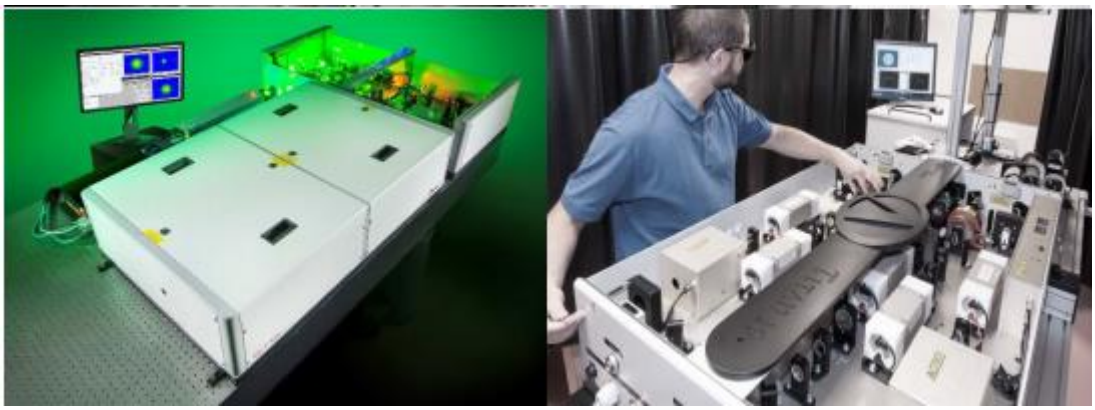

Figure 13: Representative photo of Amplitude ARCO X (150) Ti:Sa laser solution being made for EPAC

The probe pulses will be transported directly towards the EPAC experimental areas. A small in-air switchyard will be constructed adjacent to the primary 30 J in-vacuo beam switchyard, before transport down through the vertical riser and concrete labyrinth bunker into the experimental areas. While mirrors will be housed in air, near-field beam stability and profile will be maintained via image relay from the Front End via ~f/50 singlet lenses and vacuum tubes to enclose laser foci and long propagation paths, e.g. 12 m vertical riser path.

Each experimental area will have an in-air laser pulse compressor for probing, with pulse length control via compressor grating separation and Dazzler phase control. Due to financial constraints, the current design utilises ex-Gemini stock gratings and a slight angle through the optical system out of the diffraction plane, with long throw distance, to extract a 50 mm beam diameter output pulse. This will produce ~1 cm spatial chirp on the beam and, with an expected >60% total transport and compression efficiency, up to 100 mJ will be available to experimental users as a flexible probe laser source.

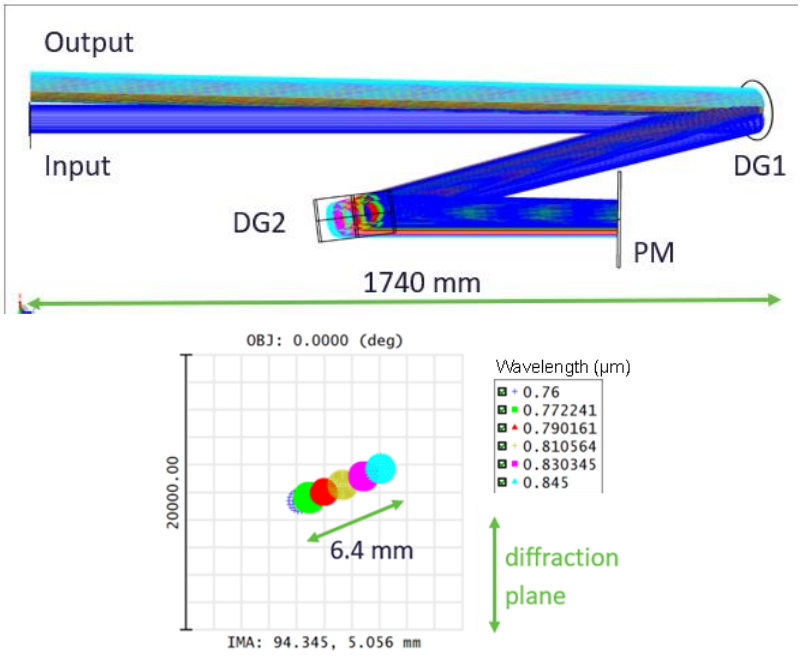

Figure 14: Optical design of the probe compressor using ex-Gemini stock gold gratings. A small angle orthogonal to the diffraction plane allows retrieval of the double-pass output of the two-grating compressor with a long injection throw. The 6.4 mm spatial chirp will contribute to 5% broadening of the pulse duration in the near-field.

As part of the probe transport design and delivery, provision for future probe/auxiliary beams is being allocated in the beam transport, to ensure that there are no physical constraints for future facility improvements. An in-vacuum 85 mm diameter beam auxiliary beamline is provisioned with 3-off in-air 50 mm beam diameter beamlines, as shown in **Figure 15**.

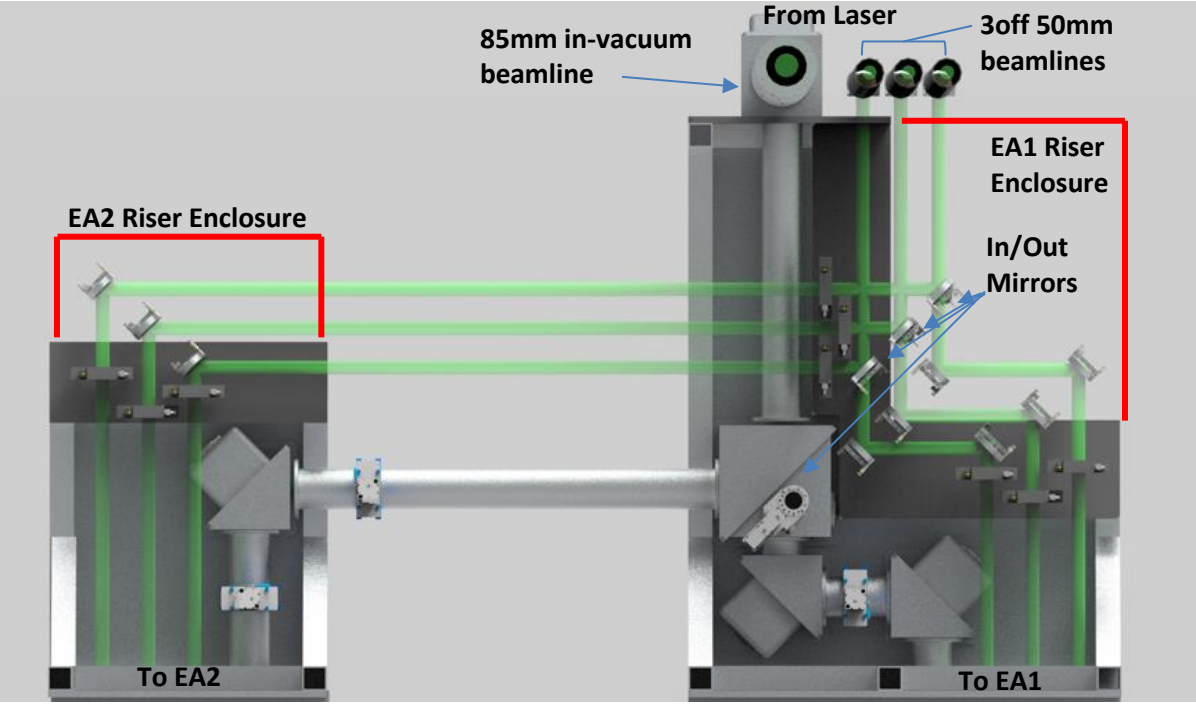

Figure 15: Agreed conceptual design of the EPAC probe/auxiliary beamline and switching configuration between EA1 and EA2. Switching mirrors will be driven in/out on linear stages, with default alignment to EA1 when switching mirrors are driven out of the beam path.

2.3 Pump source

The EPAC pump laser is based on the CLF's DiPOLE amplifier technology and is the third 100 J-scale system that the CLF has produced to date. It will be the fourth kW-scale system, as a parallel project developed a 100 Hz, 10 J system for colleagues in HiLASE.[4] The specification at the output of the EPAC Pump laser prior to propagation to the green conversion stage (**Section 2.4.1**) is given in **Table 4**.

Table 4: Specification of the EPAC Pump Laser

Parameter	Design requirement
Pulse energy	200 J with Pump A & B Day 1 = 120 J with Pump A only
Pulse duration	15 ns FWHM
Central wavelength	1029 to 1030 nm
Pulse repetition rate	10 Hz, 1 Hz
Shot-to-shot pulse energy stability	< 2.0% RMS
Power contrast	10^4
Beam shape	Square, super-Gaussian (N ≥ 8)
Beam size	75 ± 2 mm FWHM
Beam spatial intensity modulation	< 15 % peak to valley
Beam pointing stability	≤ 30 µrad
Beam quality	2 to 2.5 x Diffraction Limited
Polarisation	Horizontal
Polarisation purity	Better than 7:1

The last ISTAC report [3] mentioned that the design was based on the previous DiPOLE-100 systems, with changes made to accommodate the laboratory space available and specific improvements taken from new design work carried out in the 100 Hz project. The layout is shown in **Figure 16**, which also shows the rack room, where all the services for the system are located. In the time since the last ISTAC report, 95% of the installation phase has been completed. The final installation task to be completed is for the 100 J Pumps, which recently completed their factory acceptance test (FAT) and are being shipped to EPAC before the end of April 2024, ready for installation in May 2024. We have also started the alignment of the 10 J beam transport and 100 J sections.

The sections below provide a more detailed status update of the three main areas of the pump laser: front end, 10 J cryo-amplifier, and 120 J cryo-amplifier

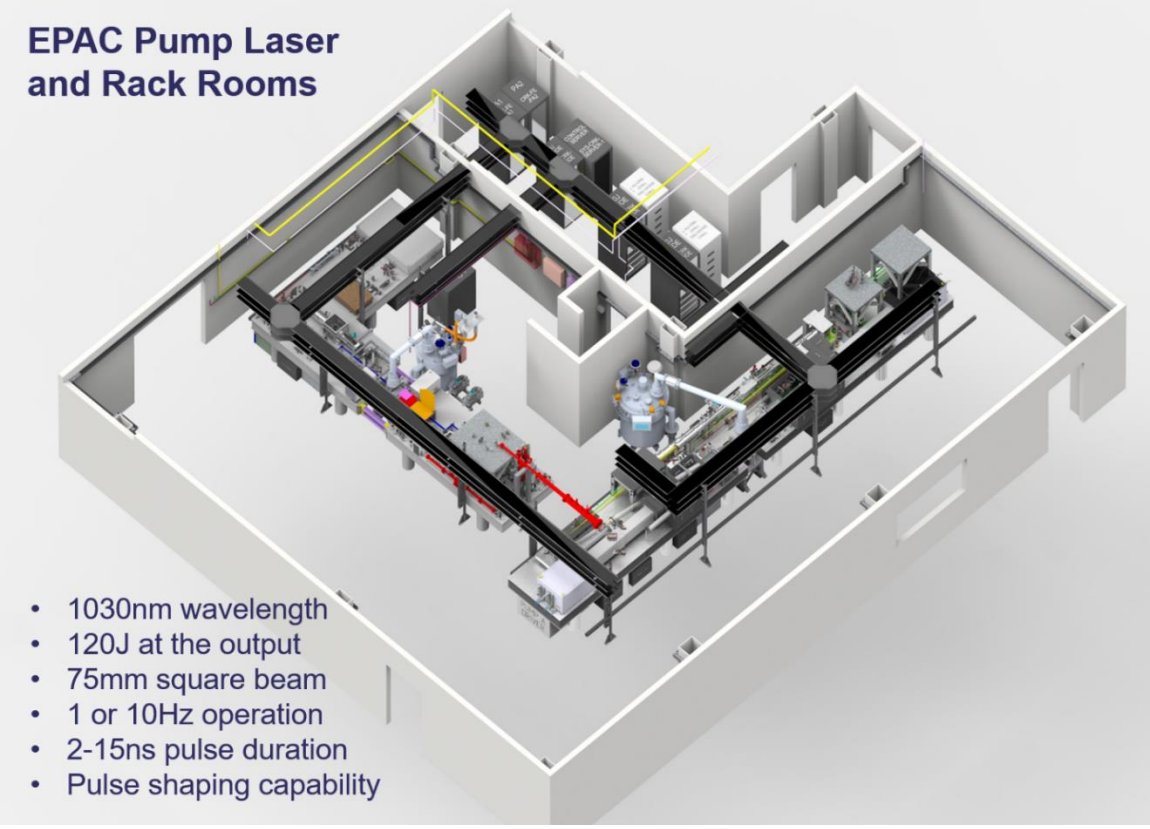

Figure 16: Isometric view of the pump laser and rack rooms, showing the full system in CAD including the services

2.3.1 Pump Source Front End

A summary of the pump Front End layout has been presented in the previous ISTAC reports in 2021[2] and 2022[3].

Since the last report, Preamplifier 2 (PA2) has been delivered, installed and tested in the EPAC Pump room. There remains an outstanding issue with PA2, in that the input lens requires changing to image the correct Gaussian pulse at the input. This lens change has been delayed, because the company that supplied PA2 has been concentrating on delivering the 100 J pump diodes. When the site acceptance test (SAT) for the pump diodes takes place, the suppliers will also address the issue with PA2. The full setup of the Front End is shown in **Figure 17**, while a 2-D plot of the Front End showing the evolution of the image sizes of the beam is given in **Figure 18**.

In October 2023, the installation phase was completed, and CLF safety paperwork was singed off, enabling a move into the commissioning phase of the programme. Since then, items such as cables for cameras, 10 J debris shields, opto-mechanics on the 10 J and 100 J optical tables, vacuum systems and cooling systems have been put in place. Optics have also been placed on the table and CW beams have been used to align the 10 J and 100 J sections.

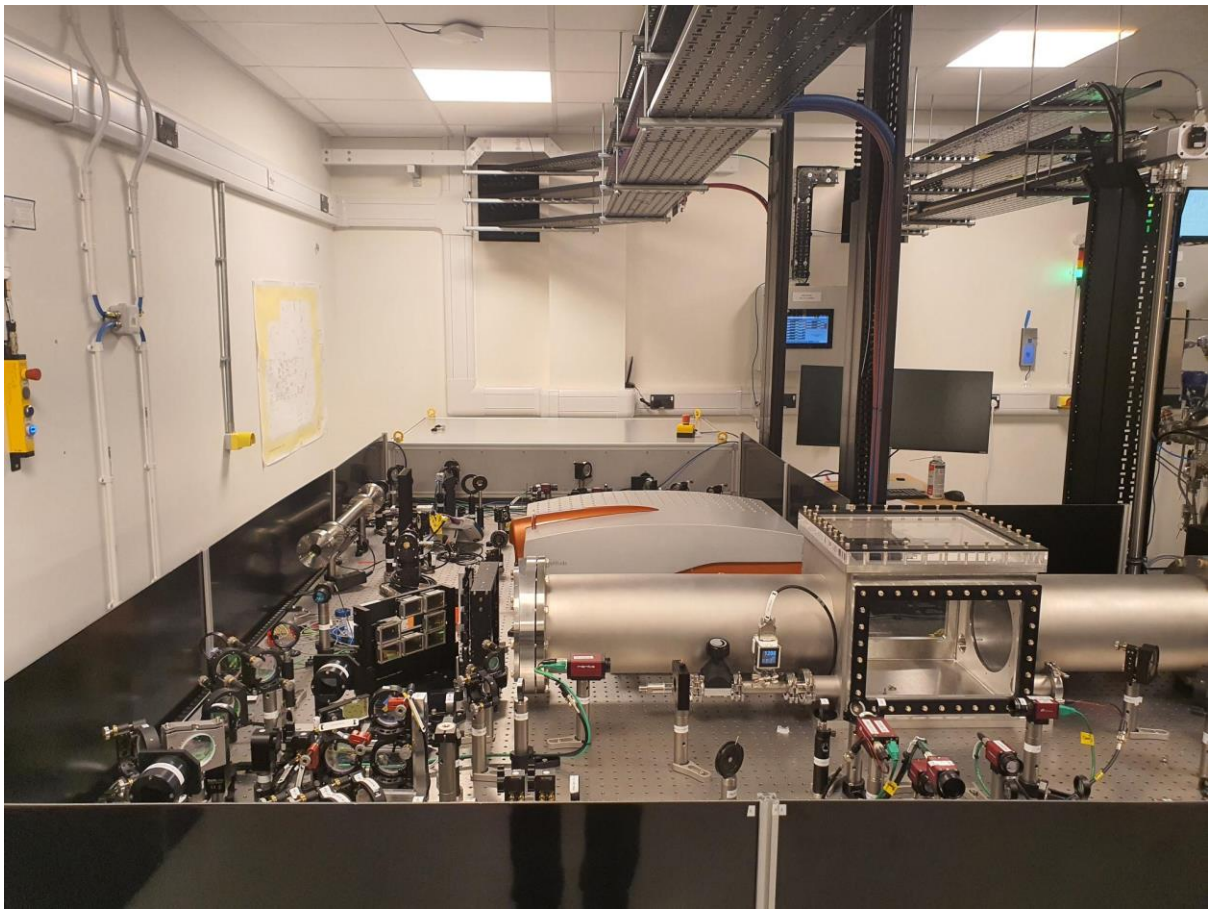

Figure 17: The pump laser Front End table in the EPAC lab, showing PA1 and PA2. The fibre seed source is located under the optical table, while the two Front End control racks are in the rack room.

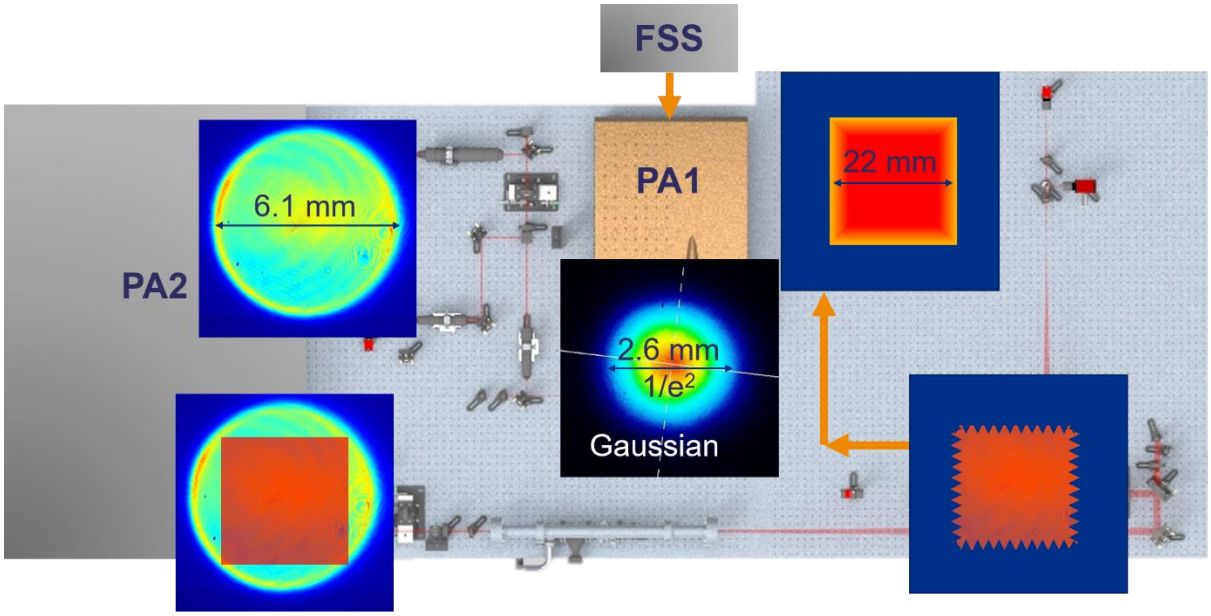

Figure 18: 2-D plot of the Front End, showing the evolution of the image sizes of the beam, where FFS is Fibre Seed Source, PA1 is Preamplifier 1 (Amplitude), and PA2 is Preamplifier 2 (Lastronics)

2.3.2 10 J cryo-amplifier

The SAT for the 10 J Cryo Amplifier was completed in February 2023 and it has been installed in the EPAC Pump room. **Figure 19** shows the 10 J cryo-amplifier in place, while **Figure 20** shows the current CAD design for the Front End, 10 J cryo-amplifier and beam transport stages.

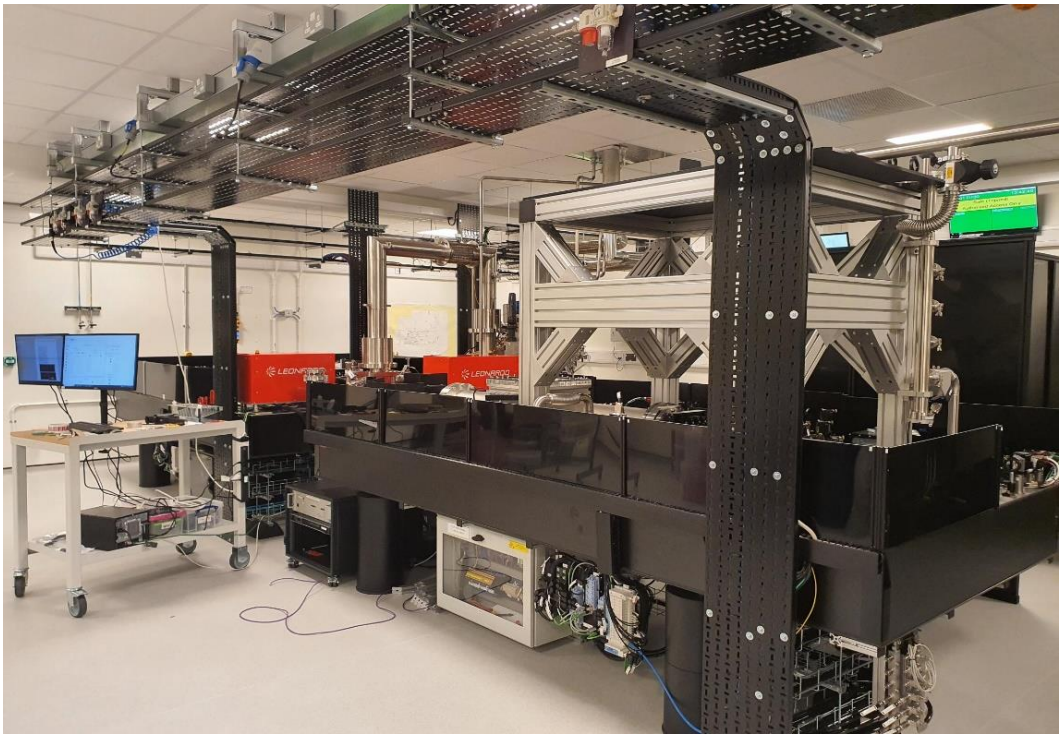

Figure 19: 10 J pumps, cryo-amplifier systems, and beam transport

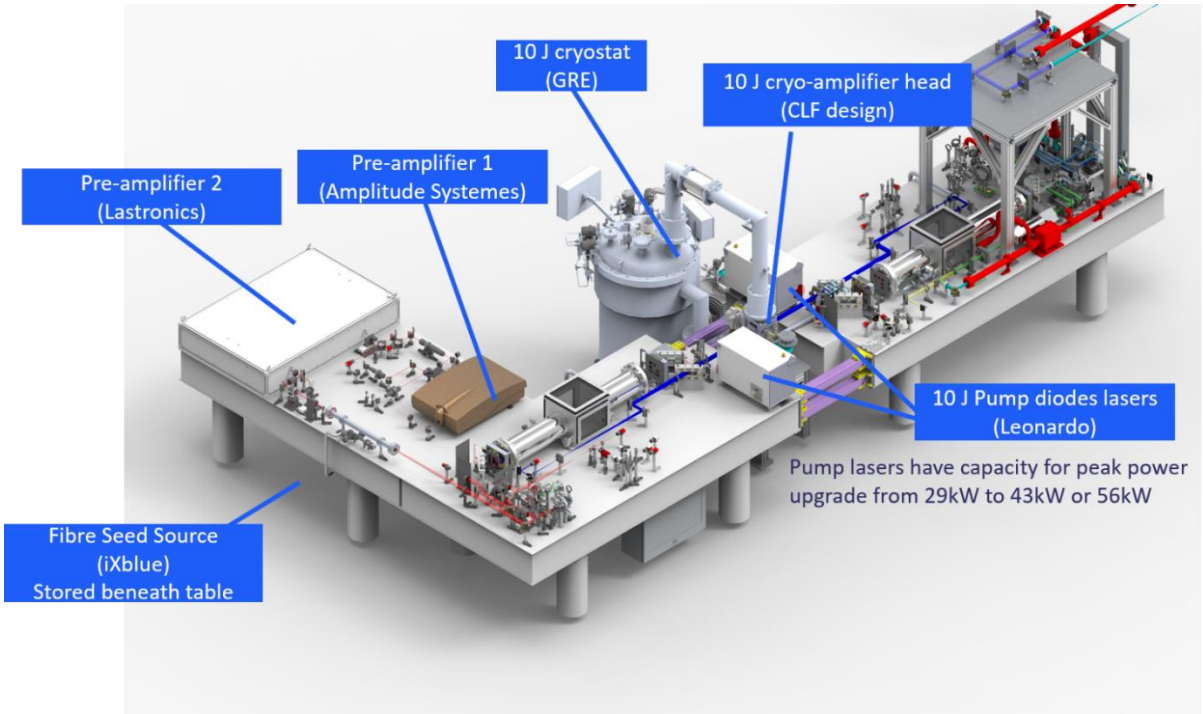

Figure 20: Isometric view of the pump laser Front End, 10 J cryo-amplifier and beam transport stages. The CAD design work for these sections is almost complete.

The optical tables have been fitted into the EPAC Pump room, and all opto-mechanics are now in place. Cameras and flippers have been installed and successfully integrated into the control software. The mirrors, lenses and fiducials for all passes have been fitted and aligned. In addition, all 10 J diagnostics opto-mechanics and optics are in place. Oscilloscopes have been installed in the adjacent rack room and have been incorporated into the control software.

The vacuum components and vacuum spatial filters (VSFs) have also been fitted on the tables, and function correctly. The component that will automatically let the vacuum to air still needs to be fitted as this has not yet been delivered.

The Adaptive Optics (AO) mirror has been tested, and the wavefront sensor (WFS) and computer were installed in the EPAC Pump room in February 2024.

The 10 J cryostat and 10 J amplifier head have been successfully installed and have been passed tests with dummy gain media. Both sets of 10 J gain media have now been coated, and the sapphire windows have been bonded and coated.

The SAT for the 10 J pump diode lasers was completed in February 2023, with the diodes in situ on the optical table. The debris shields have been manufactured and fitted on the optical table, and laser safety skirts have been added around the table.

The 10 J CW beam has been aligned through all the passes, and onto all seven diagnostic channels.

2.3.3 10 J to 120 J beam transport section

The design of the beam transport section, that will transfer and expand the beam from the 10 J cryo-amplifier stage to the 120 J cryo-amplifier stage, was described in the previous report. Most of the optics have been ordered, including waveplates, mirrors, polarisers, and filters, and have arrived at RAL.

All the opto-mechanics have now been installed, as well as the Faraday isolator and vacuum tubes, and all the optics in the beam line. Beam transport diagnostics have been installed and incorporated into the control software, and CW alignment of the beam transport has been completed.

The hardware required for the beam transport to the second 120 J amplifier is not included in the Project scope and so, although included in the design, will not be ordered.

2.3.4 120 J cryo-amplifier

The 120 J cryo-amplifier stage is the final part of the EPAC Pump laser. It must receive the expanded seed beam from the 10 J stage and amplify it to a nominal energy of 120 J output energy in four passes through the amplifier head. The last ISTAC report detailed the design of this section but, for completeness, an isometric view of the section is shown in **Figure 21**.

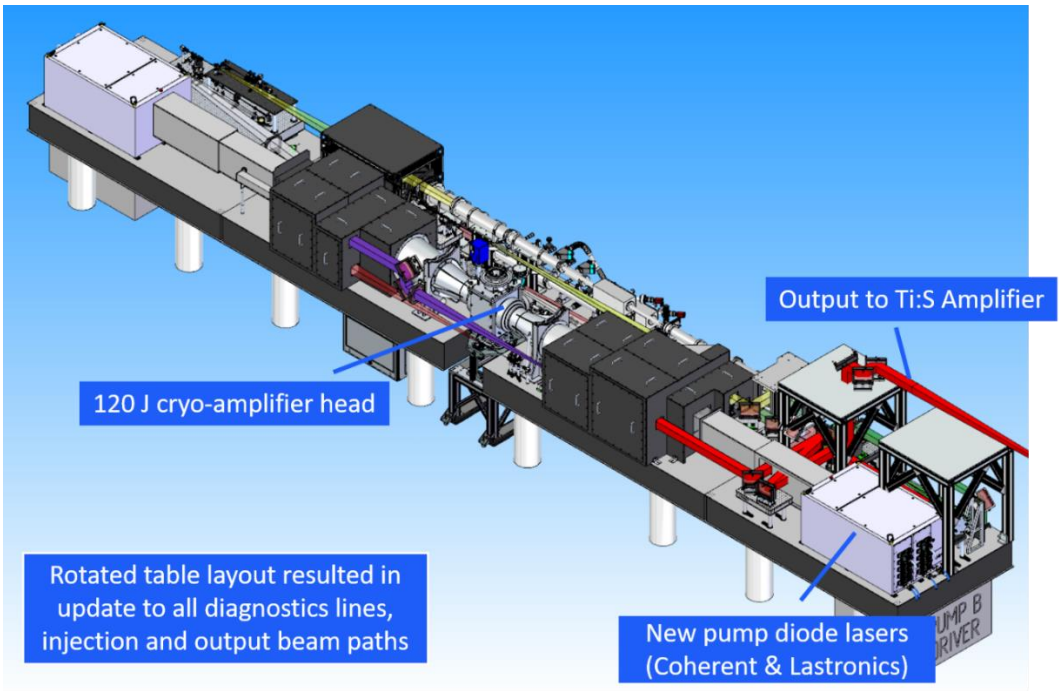

Figure 21: Isometric view of the 120 J amplifier stage. The outer tables have been rotated from the original design to make the best use of laboratory space. The new pump diodes are now in line with the amplifier head, and new shielding is still under development.

Figure 22: 100 J blast shields and amplifier head

Figure 23: The 100 J beam transport to the Ti:Sapphire room

The second set of gain media has arrived, and both sets of gain media have been coated and are being stored in an optical clean room.

Three large aperture sapphire windows have been bonded and AR coated. The fourth sapphire window did not bond well to the tungsten frame. An improvement to the process was evaluated and used to finish bonding this window.

All high energy mirrors have now been delivered, with a few selected for optimisation at 42.5 and 47.5 degrees.

The optical tables have been fitted in the EPAC Pump room, and all off-the-shelf opto-mechanics are in place and have been surveyed. All large aperture mirrors are in their opto-mechanical mounts. The large aperture AO mirror is on the 100 J optical table, with the control box and drive computer. The vacuum components and vacuum spatial filters (VSFs) have also been fitted on the optical table, and they have been tested and incorporated into the control software.

The 120 J amplifier head, comprising pressure and vacuum vessels, was fitted late in 2022 and the SAT was successfully completed in September 2022. Work has been started on alignment of the 100 J optics with the dummy gain media in the amplifier head. Blast shields have been fitted, and skirts for the operation of the pulsed / CW alignment beams have been added.

The 100 J pump diode lasers have now completed their FAT and are due to be shipped to the CLF before the end of April 2024. The SAT is now scheduled for late April / early May 2024.

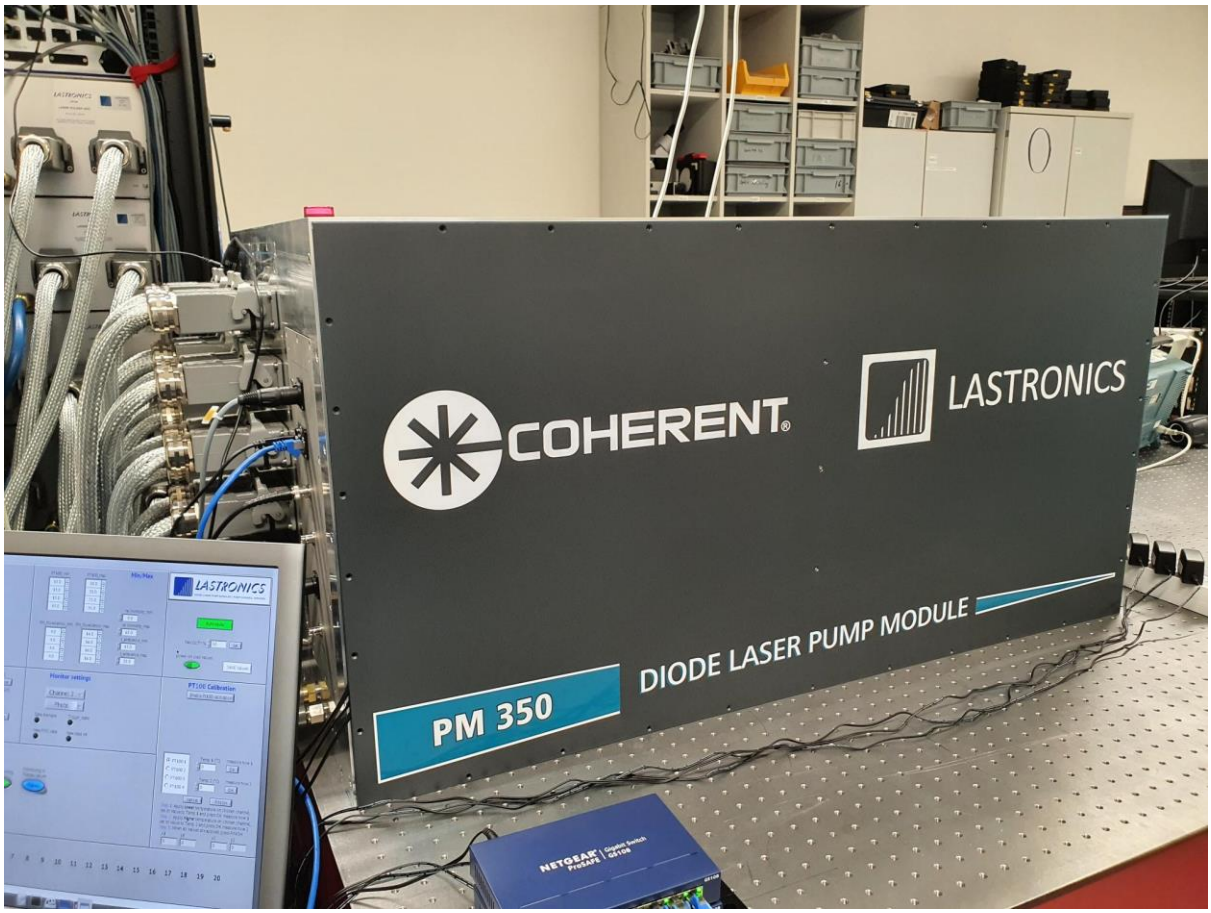

Figure 24: 100 J Pump diode PM2 at the FAT, February 2024

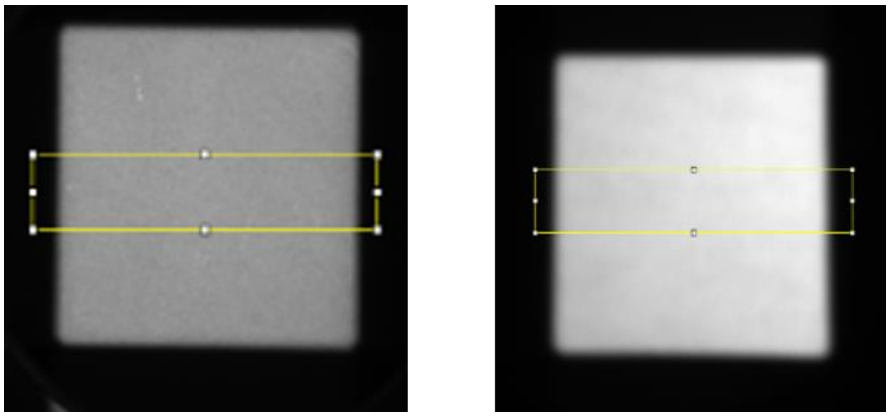

Figure 25: Beam profile for PM1 (left) and PM2 (right) at 350 kW

2.3.5 Services

The services systems have been installed and are all working, except for the helium gas supply: at present, bottled helium gas will be used when needed for the cryostats.

The systems, shown in **Figure 26** and **Figure 27**, provide water, vacuum, compressed air, liquid nitrogen (LN2), helium gas, data, and power to all areas of the Pump laser room as required. Many of the services are housed in the adjacent rack room, which also acts as the main entrance to the laser room. Services are delivered through wall penetrations at specific locations and routed along a triple-tiered gantry system, with drops at key locations around the optical tables. LN2 is delivered and vented through pipework in the ceiling, with individual interface panels for each cryostat.

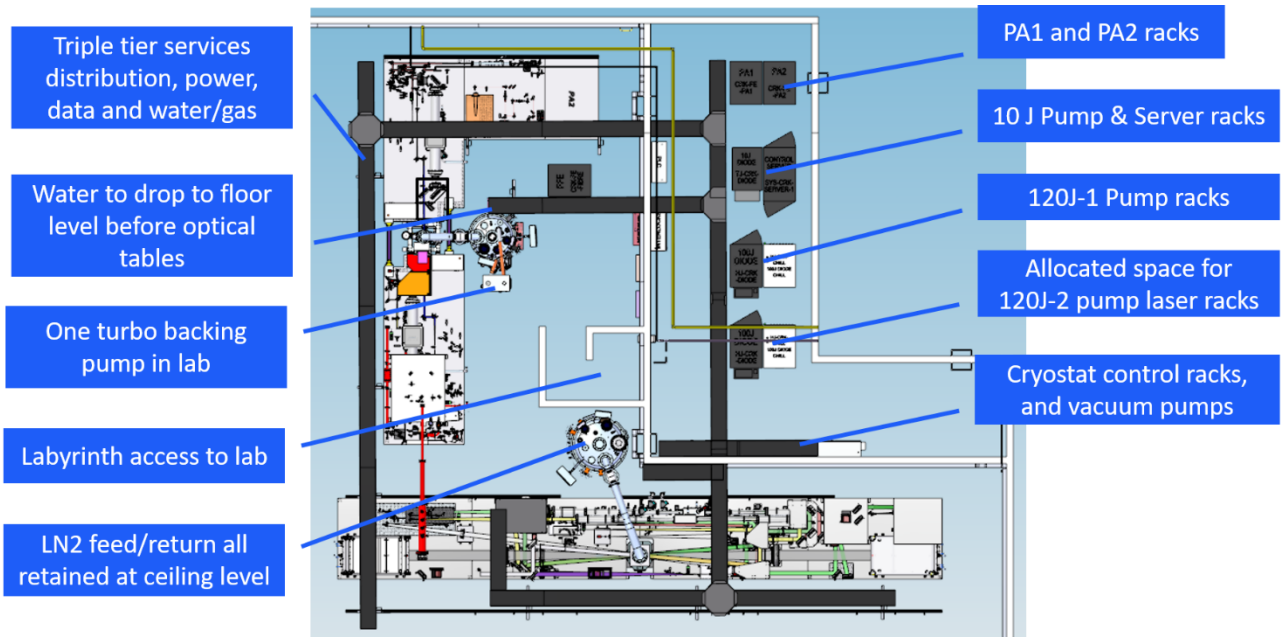

Figure 26: Plan view of the pump laser and associated rack room with racks and services highlighted

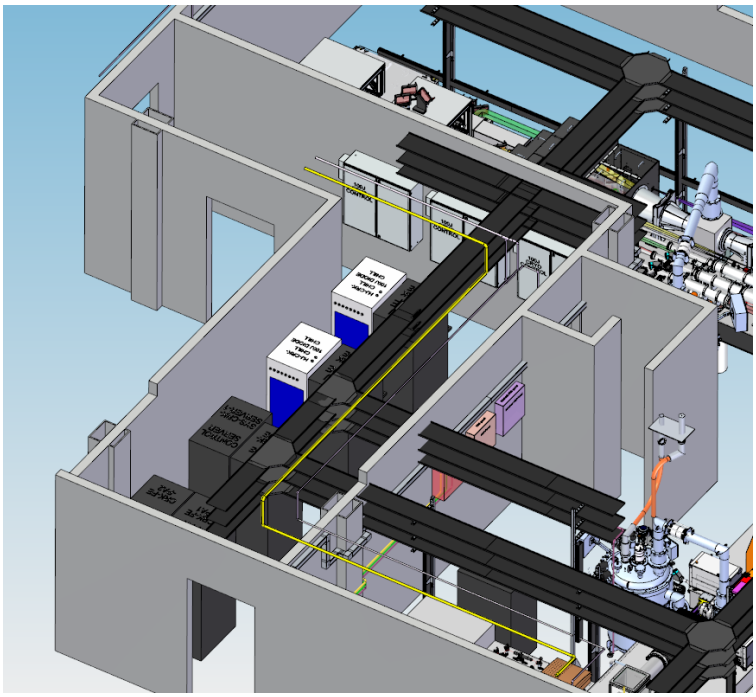

Figure 27: Isometric image of the pump laser and rack rooms showing the triple tiered services layout and wall penetrations

The services have been designed to minimise heat load in the laboratory, with all racks and vacuum pumps located in the rack room, apart from a single backing pump next to the 10 J section. **Figure 28** shows the oscilloscopes, timing systems, and the cooling systems for the Front End and the 10 J pump diodes. The photographs also show the pipework for the 100 J back water-cooling system.

Service cables and pipes have been fitted on the gantry, and service apertures in the wall have been sealed to fireproof standards. The water services are in place, as are nitrogen supplies for PA2 purging, and network cables for control software have been installed.

Figure 28: Rack room racks, displaying the Front-End chillers and the timing system (left) and the 10 J cooling system (right)

The cables for the cameras and flipper mounts are connected for the Front End, 10 J and 100 J sections, and alignment aids have been installed and connected to pressurised air for moving.

Installation of the interlock services for the lasers is now complete, with CW Alignment and Darkfield lasers, Front End lasers systems, Fibre, PA1 and PA2, 10 J Pump lasers all incorporated. In addition, provision has been made for the 100 J Pump lasers. Laser blinds for the window have also been installed and incorporated into the interlock system.

The 10 J and 100 J cryostats, with amplifier heads, have now completed their SATs.

2.3.6 Polarisation

There is no change to polarisation since the last report. CLF staff have used the Bivoj laser at the HiLASE Centre in Prague, Czech Republic[4], to measure depolarisation at 100 J. The input polarisation was optimised at the output of the 10 J amplifier with half-wave and quarter-wave plates, to reduce depolarisation losses at the output of the 100 J to 3%.

2.3.7 Future developments

Funding for an additional Pump laser has been secured, and we are currently investigating several options for the construction of this second pump source. The first option would involve using a two-amplifier head approach, in that the current 10 J would provide a seed for a second 100 J cryo amplifier. An alternative approach would be to have a Front End that has sufficient seed for one 100 J cryo-amplifier head (therefore not using the 10 J cryo head). This latter approach would present the opportunity for this system to be independent of the first pump system, which could open a distinct set of experimental conditions, i.e. it could be used as a pump source in synchronisation with a plasma generated x-ray source. For both options, we are researching the option of having a circular beam at the output of the 120 J pump.

2.4 Ti:Sa High Energy Amplifier

The EPAC Ti:Sa High Energy Amplifier (HEA) is used to amplify the ns-scale stretched broad bandwidth output pulses from the EPAC Front End (**Section 2.2**). The Ti:Sa HEA is based on a helium gas-cooled Ti:Sa amplifier head pumped from both sides by a high energy green (515 nm) beam generated from the EPAC Pump Source (**Section 2.3**). The Front End output beam is circulated through the amplifier head four times to extract the stored energy and is then expanded before being transported to the compressor (**Section 2.5**). The following sections describe progress on development of the Ti:Sa HEA system since the last ISTAC report, including: changes in the layout of the green conversion stage; demonstration of high energy wavelength conversion; initial test results for transforming the square green beam to a circle for pumping the Ti:Sa amplifier; manufacture, testing and installation of the Ti:Sa amplifier head and helium gas cooling system; solid-state cladding of low-doped Ti:Sa crystals, and an update on component installation in the EPAC laboratory. The specification for the output of the Ti:Sa HEA before propagation to the compressor is given in **Table 5**.

Table 5: Specification of the output from the Ti:Sa high energy amplifier

Parameter	Design requirement
Pulse energy	50 J with Pump A & B Day 1 = 30 J with Pump A only
Pulse duration	3.0 ± 0.5 ns FWHM
Central wavelength	800 nm (+10 nm, –5 nm)
Pulse repetition rate	10 Hz, 1 Hz
Amplification bandwidth	> 75 nm
Shot-to-shot pulse energy stability	< 2.5% RMS
Power contrast	10^{10}
Beam shape	Circular, super-Gaussian (N ≥ 8)
Beam size	72 ± 2 mm FWHM Day 1: 52 ± 2 mm FWHM
Beam spatial intensity modulation	< 10%
Beam pointing stability	< 5 µrad
Beam quality	2.0 x Diffraction Limited
Single shot capability	Yes
Polarisation	Vertical
Polarisation purity	100:1

2.4.1 Green conversion layout

Figure 29 shows a schematic layout (not to scale) of the finalised layout of the green pump conversion stage for the high energy Ti:Sa amplifier, highlighting the functionality of mirrors, and the positions of automated alignment fiducials and safety shutters.

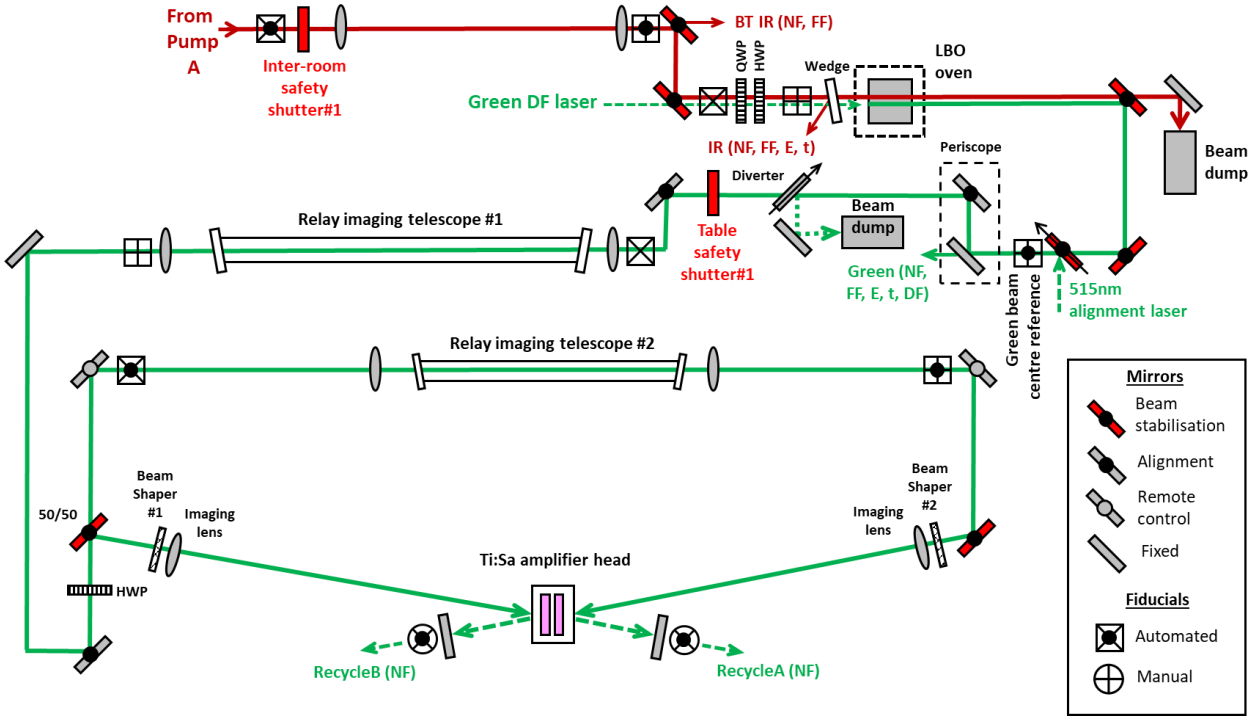

Figure 29: Schematic layout of EPAC green conversion stage. BT = Beam Transport, QWP = Quarter Wave Plate, HWP = Half Wave Plate, 50/50 = 50:50 beam splitter, DF = Dark Field, NF = Near Field, FF = Far Field, E = Energy, t = temporal.

The main change since the last ISTAC report has been the introduction of a pair of relay-imaging telescopes in the green beam. These have been added to ensure that the spatial beam quality of the green beam is maintained after propagation to the beam shaping optics (see **Section 2.4.3**). The first telescope images the beam generated at the LBO SHG crystal onto the first beam shaper over a propagation distance of approximately 10 m. The second telescope images the beam after the 50/50 splitter onto the second beam shaper after propagating a further 10 m.

A change has also been made to the method by which green pump energy is controlled. Rather than using a polariser and half-wave plate combination after the SHG crystal, energy control will now be carried out by adjusting the polarisation state of the infrared beam incident on the SHG crystal by rotating the first half-wave plate. This simplifies the optical set-up and reduces the number of components needed. **Figure 30** shows a CAD drawing of the green conversion stage, with the main system components labelled.

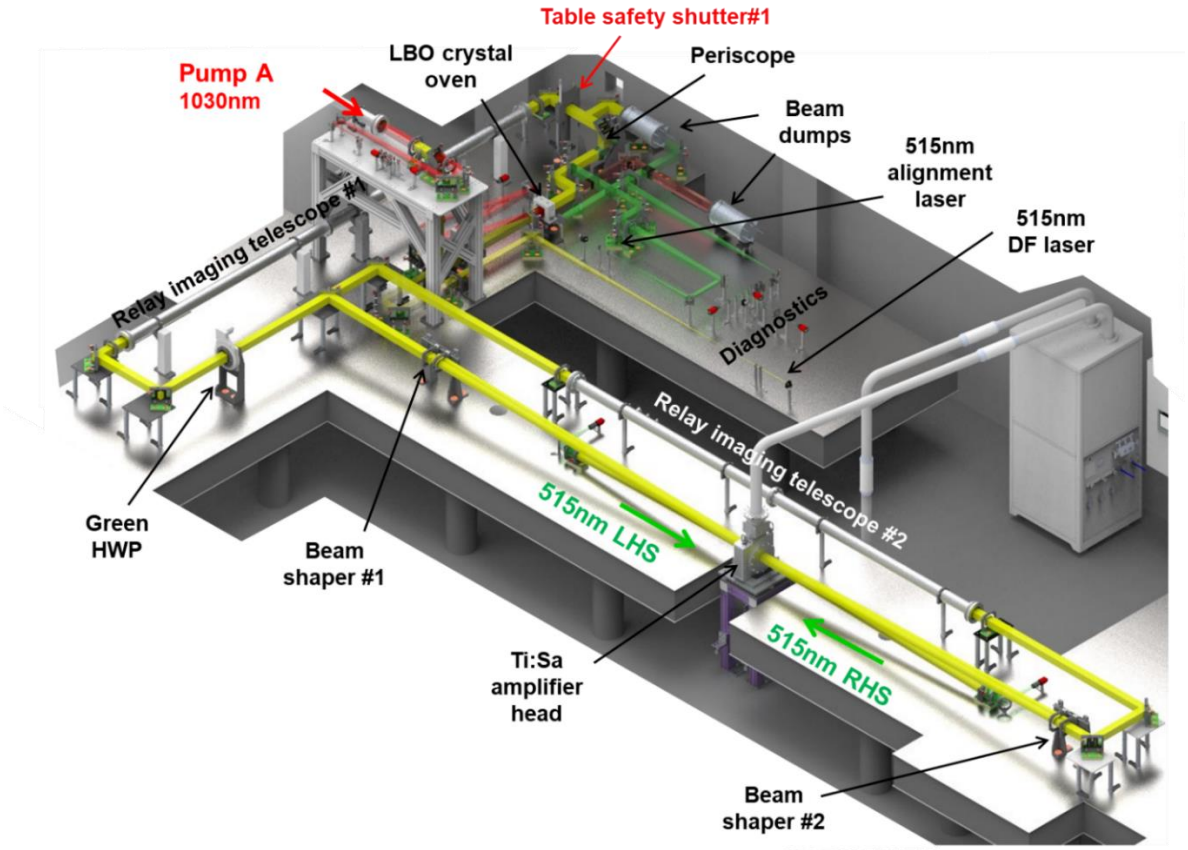

Figure 30: CAD drawing of the green conversion stage

2.4.2 High energy green conversion

Since the last report, further high energy green conversion tests at 10 Hz have been conducted in collaboration with the HiLASE Centre in Prague, Czech Republic[4], using the output from the first DiPOLE100 pump laser. By careful control of the input polarisation state to the main DiPOLE100 cryo-amplifier, an output 1030 nm polarisation purity of close to 97% was achieved when operated at 120 J and 10 Hz. Efficient wavelength conversion was then demonstrated in a 60 mm x 60 mm x 13 mm thick LBO crystal producing 95 J green pulses at 515 nm, corresponding to an average power of almost a kilowatt and a conversion efficiency of 75% (**Figure 31**). The re-alignment changes marked in **Figure 31b** correspond to points where the crystal phase matching angle was re-optimised as a result of thermally induced phase mismatch. These changes should not be necessary in the EPAC system, as this will utilise a new design of LBO crystal oven that minimises temperature gradients and has previously demonstrated stable wavelength conversion under similar thermal loading conditions to those planned for EPAC.[5]

These world-leading results were published in a recent paper by Divoky *et al*.[6] "*Kilowatt-class high energy frequency conversion to 95 J at 10 Hz at 515 nm*", and give confidence that the required level of green energy (80 J – see **Table 5**) will be obtainable over the full range of operating modes and thermal loads expected for the EPAC petawatt laser on Day 1.

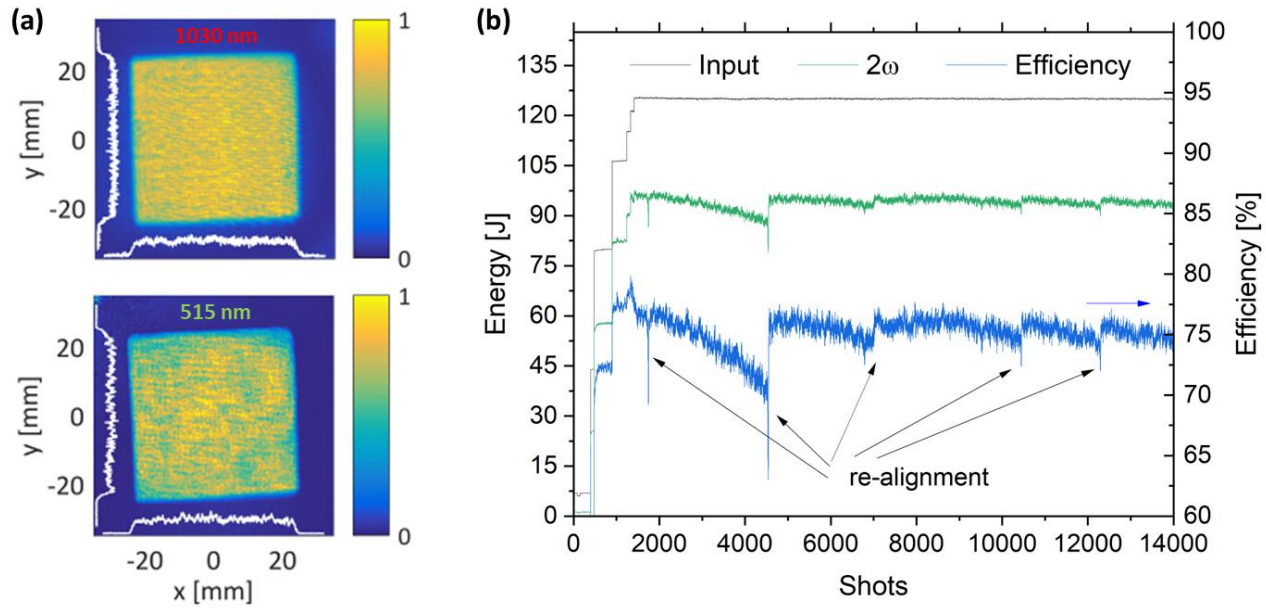

Figure 31: (a) Near-field profiles of input beam at 1030 nm (energy of 121 J) and converted second harmonic green beam at 515 nm (energy of 95 J) at 10 Hz pulse rate, and (b) measured energy conversion efficiency over approximately 25 minutes

2.4.3 Green beam shaping

In order to match the Front End beam size and shape in the Ti:Sa amplifier, the generated green beam needs to be reshaped from a square (65 mm width), high-order (N~20) super-Gaussian (SG), near single-mode (M^2 ~2.2) beam to a circular SG and resized, initially to 55 mm diameter (Day 1) and eventually to 75 mm diameter. Over the past year, a custom refractive field-mapper (or SQUIRCLE) has been developed in collaboration with an industrial partner[3]. This SQUIRCLE spatially remaps the intensity distribution in the original square beam onto a circular beam in the image plane of a conventional lens. A prototype beam shaper with a design matched to that required for EPAC on Day 1 has been manufactured. To test the performance of the prototype SQUIRCLE, the output beam from the EPAC green CW alignment laser[4] has been over-expanded, collimated, and then apertured to provide a 65 mm square beam with a near-uniform intensity profile.

Figure 32 shows a schematic of the test layout used to evaluate the prototype SQUIRCLE, with the inset showing the set-up used to measure the beam shape at various positions around the image plane of the 3.5 m lens that will be used in EPAC. To measure the propagated beam shape, a camera[5] is set-up at near-normal incidence to a scatter screen[6], and images of the backscatter from the screen are captured at the chosen measurement plane.

[3] The field-mapper is fabricated using a laser-based micro-structuring technique applied to the surface of a fused silica substrate producing a transmissive optical component that can then be AR coated at 515 nm.
[4] Fibre-coupled single-mode 520 nm diode laser.
[5] AVT Manta G158, 1456 x 1088, 3.45 µm pixel size.
[6] MACOR machinable ceramic screen that provides near Lambertian scatter.

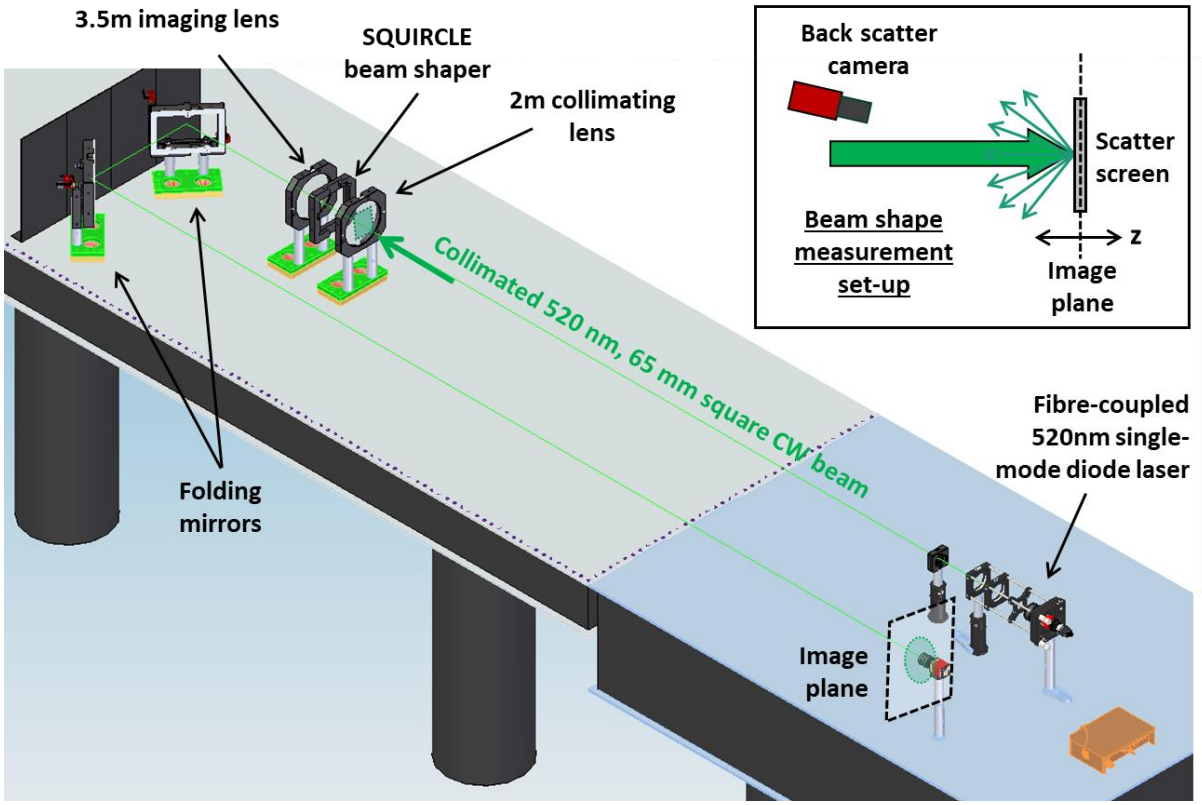

Figure 32: Schematic of test set-up for evaluating EPAC SQUIRCLE beam shaper, with inset showing the set-up for measuring beam shape at the image plane (not to scale). A similar approach is used to measure the input beam to the SQUIRCLE.

Beam shape measurements of the beam incident on the SQUIRCLE and at two propagation distances – 3020 mm and 3500 mm from the imaging lens – are shown in **Figure 33a**. These can be compared to the predicted performance of the SQUIRCLE calculated from a ZEMAX ray tracing code[7] shown in **Figure 33b**. The input beam is not a perfect flat-top SG, because it is cut from an expanded Gaussian beam, so a fit function[8] has been derived to provide a more accurate comparison of the ZEMAX predictions with experimental results. A separate noise function (10% amplitude) has been added to the ZEMAX input profile to simulate the level of amplitude modulation seen in beam shape measurements.

[7] ZEMAX code uses physical optics propagation where the SQUIRCLE is represented by a custom Grid Sag data file and a paraxial imaging lens is assumed.

[8] The fit function is the product of a TEM_{00} beam ($1/e^2$ width 150 mm) and a superGaussian beam (65.0 mm FWHM and order N_{SG}=40).

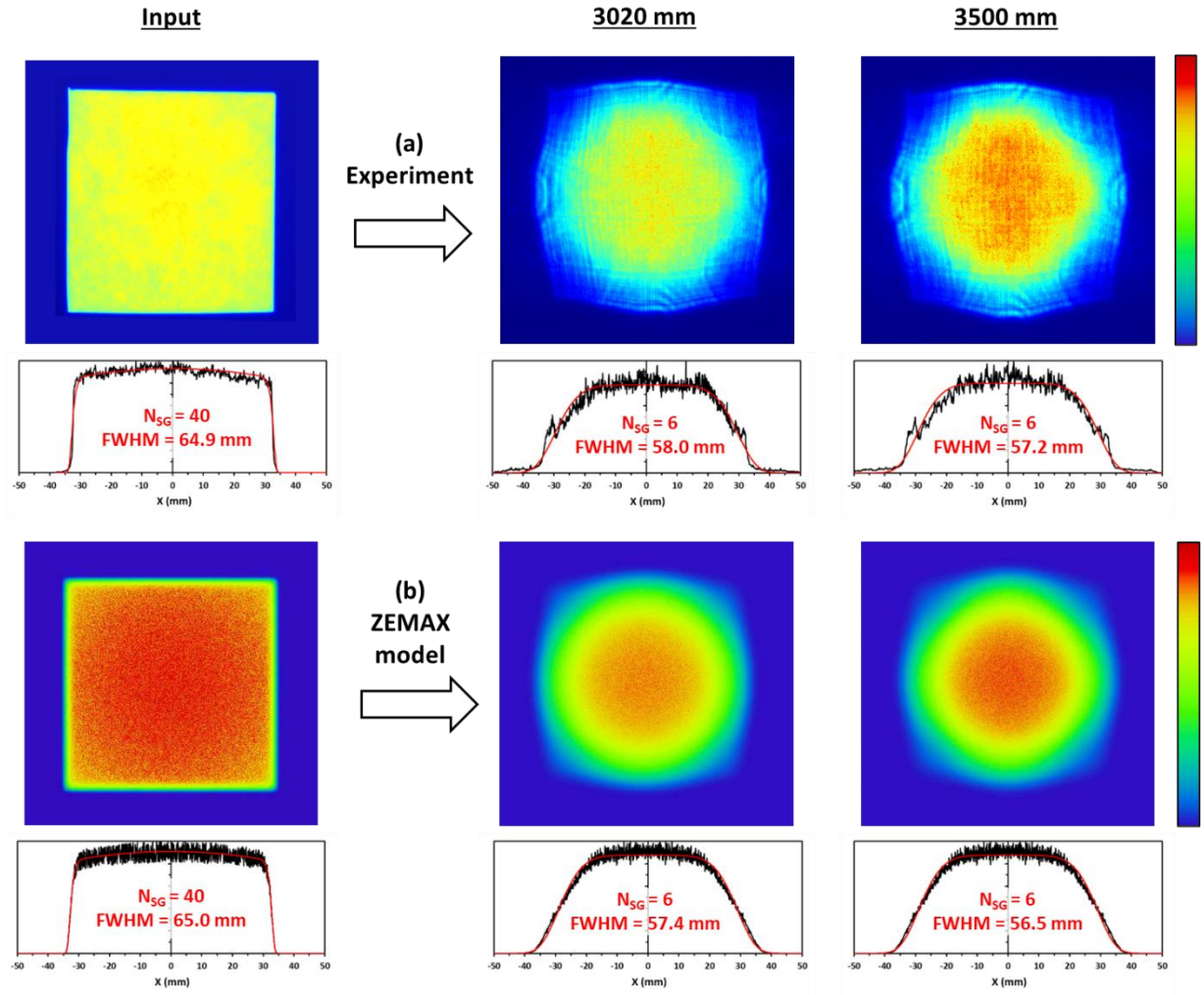

Figure 33: (a) Measured experimental and (b) ZEMAX predicted beam shape profiles of input beam and propagated beam 3020 mm and 3500 mm from the 3.5 m imaging lens. Cross-section profiles are measured through the centroid of the beam image (black) and are compared with best-fit super-Gaussian functions (red).

The measured beam shapes and dimensions for the prototype shaper are in reasonable agreement with the model predictions, although there are structural features evident in the measured profiles that are not seen in model predictions. These are thought to be due to a combination of manufacturing tolerances and the difference between SQUIRCLE design (N_{SG}=20) and experimental (N_{SG}=40) input beam parameters. To better assess the strength of amplitude modulations at the image plane (3500 mm), a separate evaluation was conducted using a higher resolution camera[9] placed directly in the beam with a 7 mm iris to capture a sub-aperture image. **Figure 34** compares the measured back-scatter beam profile measured at the image plane with the image measured directly on the camera chip, now with fluence calibrated assuming a 40 J green input beam. The average fluence across the plateau of the beam is ~ 2.5 J/cm²; however, the direct camera image clearly shows evidence of high frequency linear modulation features with a period of approximately 100 µm. These artefacts are believed to be caused by the manufacturing process, where a processing laser is raster scanned across the surface of the fused silica substrate. The increased depth of modulation evident suggests a peak fluence of ~4.5 J/cm², compared to 2.9 J/cm² measured from the

[9] AVT Manta G235, 1936 x 1216, 5.86 µm pixel size.

lower spatial resolution back-scatter camera. Although this is below the quoted damage threshold of the dual-band AR coating deposited on the fused silica amplifier pressure windows, and the planned coating for the Ti:Sa crystals, this is a concern for use of the SQUIRCLE beam shaper in EPAC. As the modulation period is short, and the pump beams propagate off-axis to each other and the multi-pass extraction beams, the modulation structure is not expected to be encoded on the amplified high energy Ti:Sa beam.

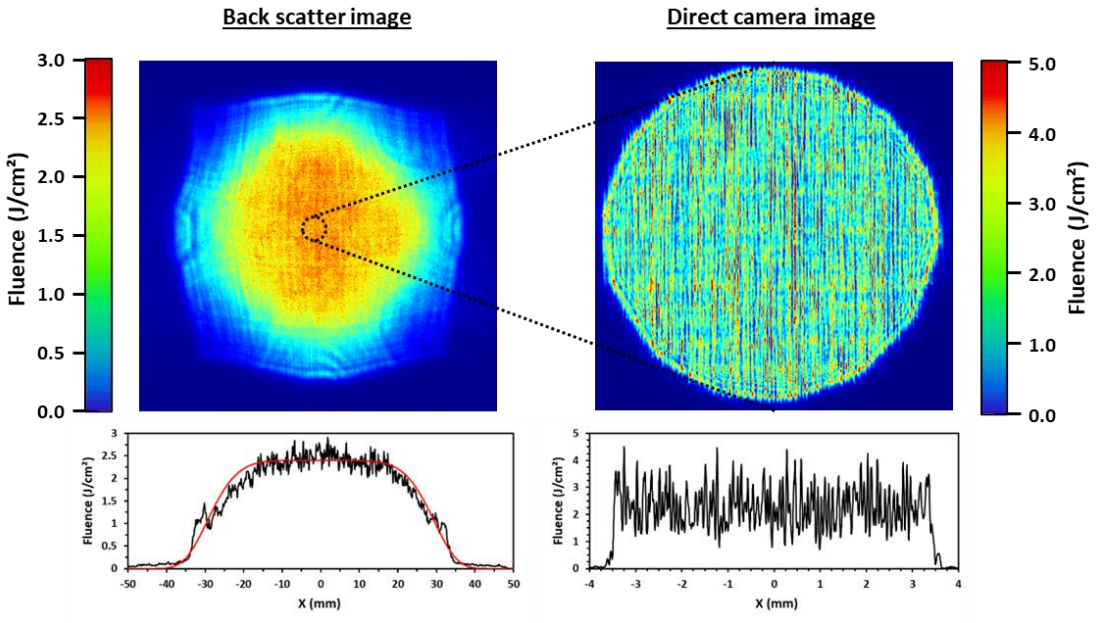

Figure 34: Comparison of back-scatter and direct camera images measured at the image plane of the 3.5 m lens

Further measurements of the 'power-in-bucket' at the image plane for the required Day 1 aperture size (55 mm), and the propagation characteristics of the beam beyond the image plane, are currently under evaluation. Assessment of beam propagation and re-imaging are important to confirm the design of our planned energy recycling scheme. Following these tests, a review of beam shaper design will be conducted and refinements will be made to improve performance. A second SQUIRCLE, with optimised design, is scheduled to be manufactured shortly. Once the EPAC green beam is available, further tests will be conducted on the optimised shaper before a final decision is made on the suitability of the SQUIRCLE for spatial beam shaping on EPAC.

2.4.4 Ti:Sa multi-pass layout

The concept of the Ti:Sa multi-pass extraction architecture remains unchanged since the last report. **Figure 35** shows a schematic layout (not to scale) of the finalised design of the multi-pass architecture, again highlighting the functionality of mirrors, and the positions of automated alignment fiducials and safety shutters. **Figure 36** shows a CAD drawing of the Ti:Sa HEA with the main system components labelled.

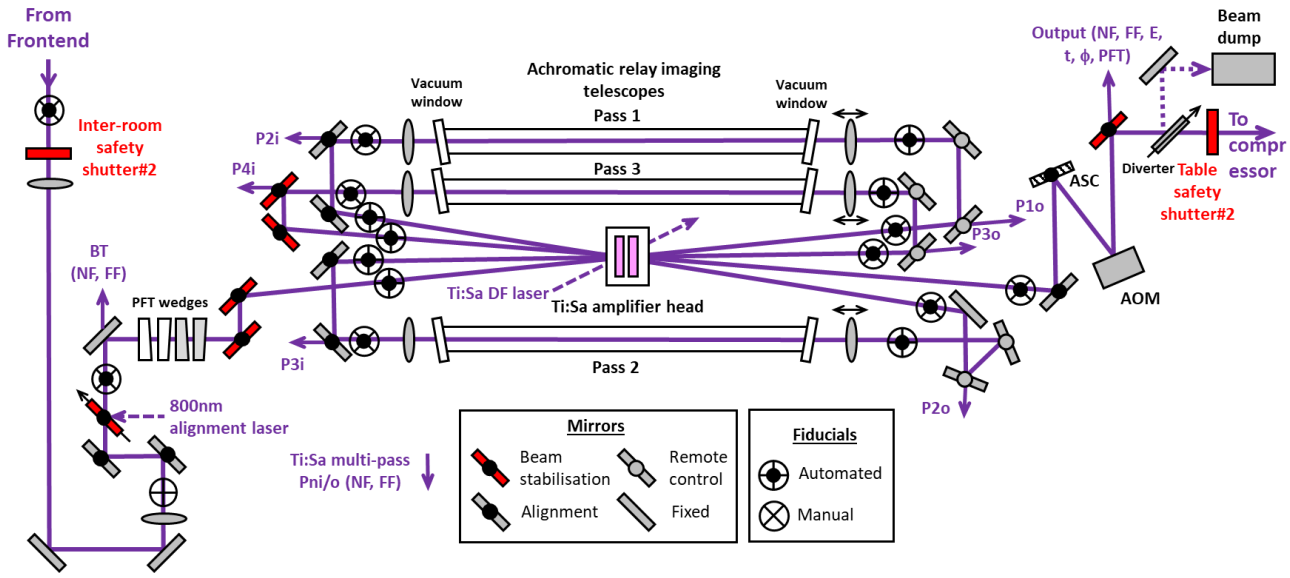

Figure 35: Schematic layout of EPAC Ti:Sa multi-pass extraction architecture. DF = Dark Field, NF = Near Field, FF = Far Field, E = Energy, t = temporal, ϕ = wave front, PFT = Pulse Front Tilt, AOM = Adaptive Optic Mirror, ASC = Astigmatism Corrector.

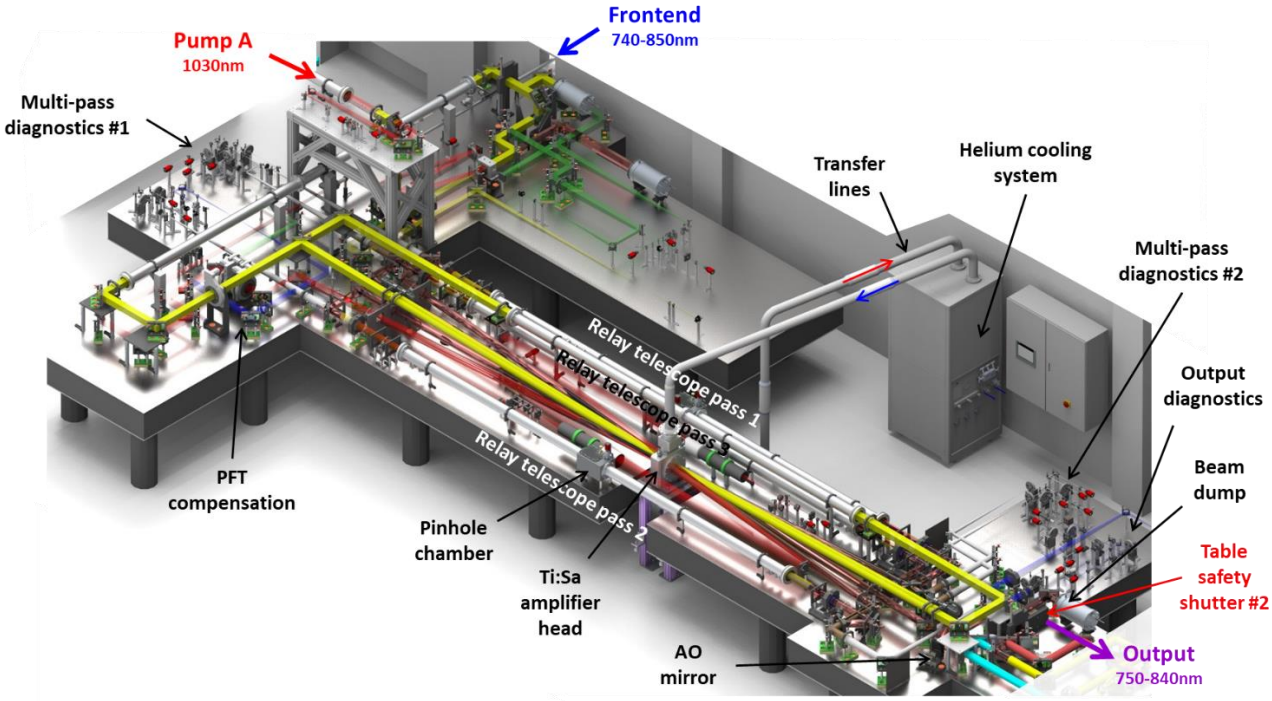

Figure 36: CAD drawing of EPAC Ti:Sa high energy amplifier

2.4.5 Amplifier head and helium gas cooling system

Manufacture of the Ti:Sa high energy amplifier head was completed in October 2023, and a pressure testing certificate to 7.2 barg (x 1.5 maximum working pressure) was issued in November 2023. The amplifier head has now been installed on its support table in EPAC and integrated with the cooling system. Photographs of the amplifier head during testing, and when installed in EPAC, are shown in **Figure 37**.

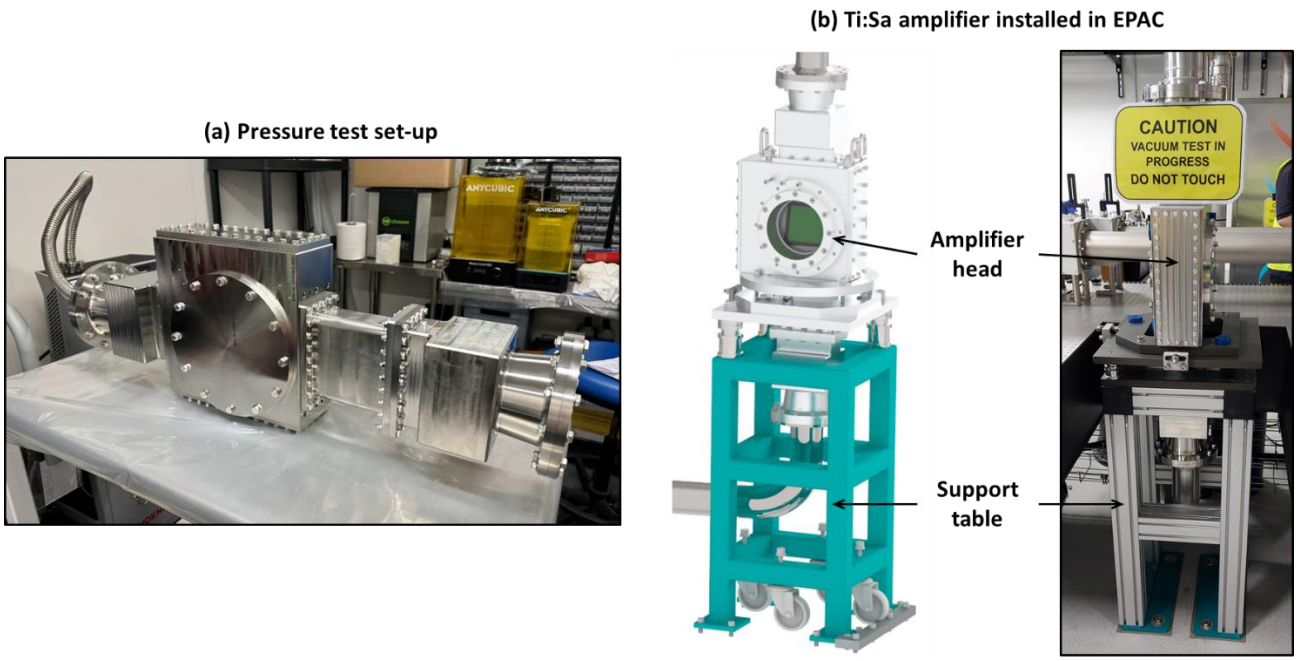

Figure 37: (a) Photograph of Ti:Sa amplifier head during pressure testing, and (b) schematic and photograph of amplifier head as installed in EPAC

Manufacture of the helium gas cooling system was completed in June 2023, with a FAT conducted in September 2023. The system was then delivered and installed in EPAC, with commissioning tests completed in December 2023. These tests were undertaken using a dummy amplifier pressure vessel simulating the predicted pressure drop in the Ti:Sa amplifier. **Figure 38** shows a photograph and CAD drawing of the cooling system installed in EPAC with the main system components labelled, including the transfer lines to and from the amplifier head.

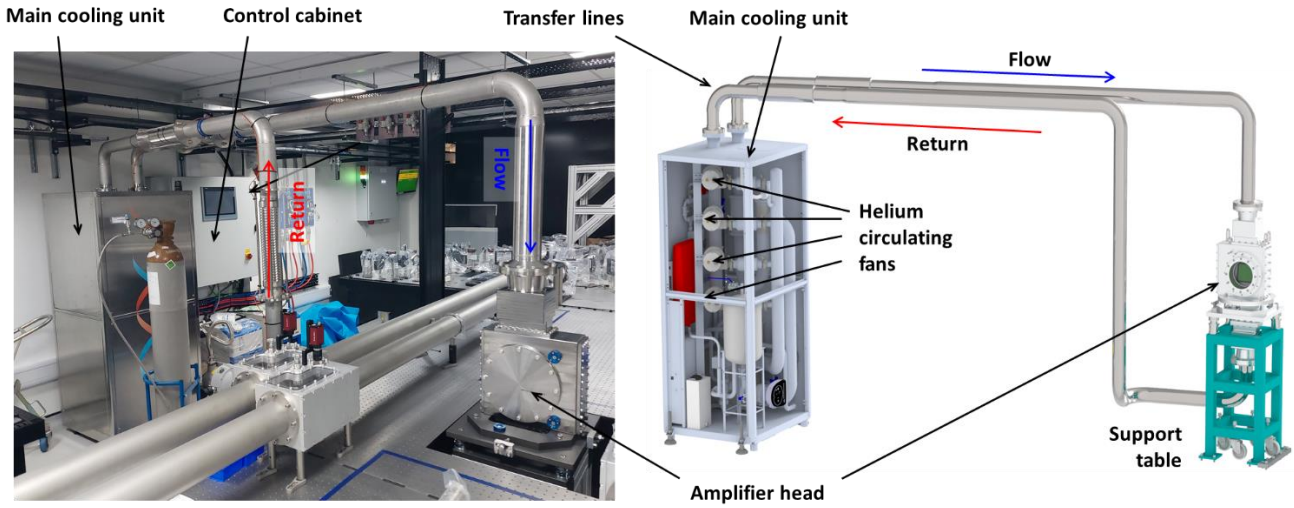

Figure 38: Photograph and CAD drawing of helium gas cooling system installed in EPAC

Commissioning tests have demonstrated that stable helium gas temperature control can be achieved at mass flow rates (MFRs) up to 100 g/s (design point 80 g/s), at a helium pressure of 4 bara, over a range of temperatures from 290 K (17°C) to 300 K (27°C), and heat loads from 0 to 1.4 kW. Thermal load was simulated using an internal heater within the main cooler unit, where 1.4 kW represents the worst case heat load (140 J at 10 Hz) that would be present

on Day *N* if no energy extraction were to take place within the Ti:Sa amplifier. Operation at the design MFR was achievable with only three of the four turbo circulating fans running, providing some contingency in the event of fan failure. **Figure 39** shows the measured temperature and MFR stability over a 14-hour period with the cooling system set at 295 K (22°C) and 80 g/s for a heat load of 800 W. These results give confidence that the system will provide the required cooling capacity and stability required for operation of EPAC over the full range of operating modes and thermal loads.

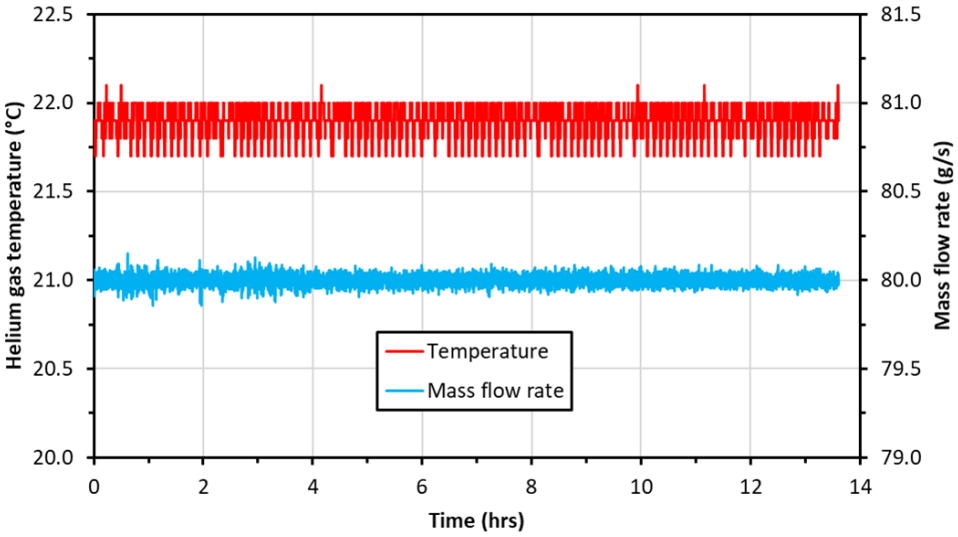

Figure 39: Measured helium temperature stability over a 14-hour period with the cooling system set at 295 K (22°C), MFR 80 g/s, He pressure 4 bara, and heat load 800 W

2.4.6 Solid-state cladding of low-doped Ti:Sa crystals

Further development of the two approaches for cladding EPAC large aperture Ti:Sa crystals with a near-index matched absorptive cladding[10] has continued over the past 18 months. This has involved production of a series of trial test samples, increasing in scale from small-size (25 mm undoped or Ti-doped sapphire core) to final full-size (100 mm sapphire core) clad composites, all with 10 mm depth cladding.

The first cladding approach is based on a customised adhesive free bonding (AFB) process developed in collaboration with a commercial supplier. An optimised procedure has been developed for cladding shaped sapphire with YAG[11] and **Figure 40a** shows a photograph of the first full-size test composite produced using this technique. This used a trapezoid shaped a-cut undoped sapphire crystal clad with undoped YAG. In parallel with this, an optimised procedure was developed for AFB-bonding a custom high index flint glass[12] to shaped sapphire. **Figure 40b** shows a photograph of the second full-size test composite produced from a similar shaped undoped sapphire crystal core, but this time clad with pieces of undoped high index flint glass.

[10] Absorptive cladding is important to minimise the impact of amplified spontaneous emission (ASE).
[11] Commercial availability of large single crystal pieces of Cr-doped YAG (n=1.82 at 800 nm) with the required absorption characteristics (≥ 2 cm^{-1} at 800 nm) has already been confirmed.
[12] Two large billets of copper-oxide (CuO) doped flint glass with the required absorption (≥ 2 cm^{-1} at 800 nm) and high refractive index (n=1.74 at 800 nm) have been produced, providing sufficient glass to clad two EPAC-sized Ti:Sa crystals.

The second cladding approach has been developed in-house and uses a near-index matched UV-curable optical resin to bond absorber cladding to Ti:Sa crystals. **Figure 40c** shows a photograph of a full-size test composite produced by the resin bonding approach, where pieces of an undoped high index flint glass (with a different composition to that used for AFB) are bonded to a similar shaped undoped sapphire crystal core.

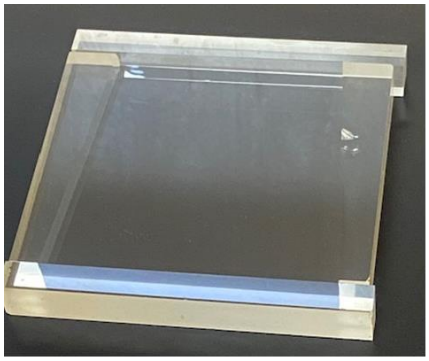

(a) Full-size AFB bonded sapphire/YAG test composite

(b) Full-size AFB-bonded sapphire/glass test composite

(c) Full-size resin-bonded sapphire/glass test composite

Figure 40: Photographs of: (a) full-size and shaped AFB-bonded undoped sapphire/YAG clad test composite; (b) full-size and shaped AFB-bonded undoped sapphire/glass clad test composite; and (c) full-size and shaped resin-bonded undoped sapphire/glass clad test composite. All test composites have internal centre line dimensions 100 mm x 100 mm with nominal 20 mm thickness.

Following a review of the test results from both cladding approaches and cladding material options, AFB bonding using a Cr-doped YAG absorber was chosen as the cladding approach for the first two Ti:Sa crystals for use in the EPAC high energy amplifier. Cr:YAG absorber was selected over the glass because its thermo-mechanical properties better matched those of sapphire, relaxing the requirements for thermal control during bonding, which resulted in an improved bond yield during trials. Development of both the AFB and the in-house resin bonding approaches using glass-based absorptive cladding is continuing, as both offer potential future benefits. The use of glass offers an advantage in terms of reduced cost and delivery time, and the resin bonding approach is more tolerant to cladding imperfections than AFB and does not require high quality surface preparation ahead of cladding.

Figure 41a shows a photograph of the first EPAC Ti:Sa crystal clad with Cr:YAG after the AFB bonding procedure. The composite is now undergoing final surface polishing prior to anti-reflection (AR) coating. The EPAC clad crystal will have outer dimensions of approximately 120 mm x 120 mm x 20 mm. Processing (shaping and polishing) of the second EPAC Ti:Sa crystal has been completed (**Figure 41b**) and Cr:YAG cladding is scheduled to commence shortly.

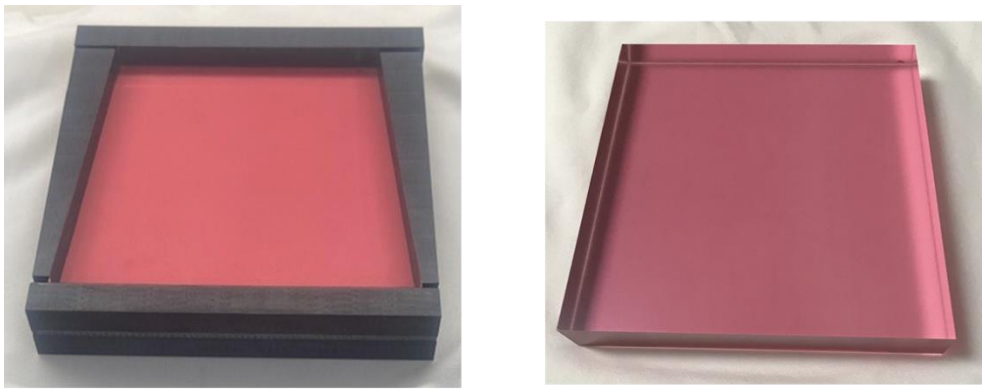

(a) EPAC Ti:Sa/Cr:YAG Crystal #1

(b) EPAC Ti:Sa Crystal #2

Figure 41: Photographs of (a) first EPAC Ti:Sa / Cr:YAG clad crystal prior to final surface polishing, and (b) second EPAC Ti:Sa crystal processed ready for Cr:YAG cladding. Both EPAC Ti:Sa crystals are a-cut low-doped HDS[13] grown and have internal centre line dimensions 100 mm x 100 mm with nominal 20 mm thickness after shaping.

2.4.7 Update on component installation

Installation of the main opto-mechanical components (mirror, lens, and waveplate mounts) for the infrared pump beam transport, green conversion stage, front end delivery, and the Ti:Sa multi-pass commenced in November 2023, and is almost complete. Installation includes the vacuum spatial filter (VSF) tubes for the front end beam expanding telescope, and multi-pass relay imaging telescopes with accompanying pinhole chambers. Installation of commercial-off-the-shelf (COTS) components for all the diagnostic channels, and both 515 nm and 808 nm CW alignment and dark-field beam lines, is also near completion. Progress can be seen in the various photographs shown in **Figure 42**.

Manufacture of all large aperture custom optics has been completed (apart from the large aperture green half-wave plate), and all COTS diagnostic optics have been procured ready for commissioning to commence. Design of the blast-shield safety enclosure for the amplifier head is underway, with ballistic calculations being completed by an external contractor. A number of separate environmental enclosures are also being designed to protect the remainder of the system. Commissioning of the high energy Ti:Sa amplifier system is scheduled to commence within the next month, starting with optic installation and followed by low power CW alignment.

[13] Horizontal Directional Solidification (HDS)

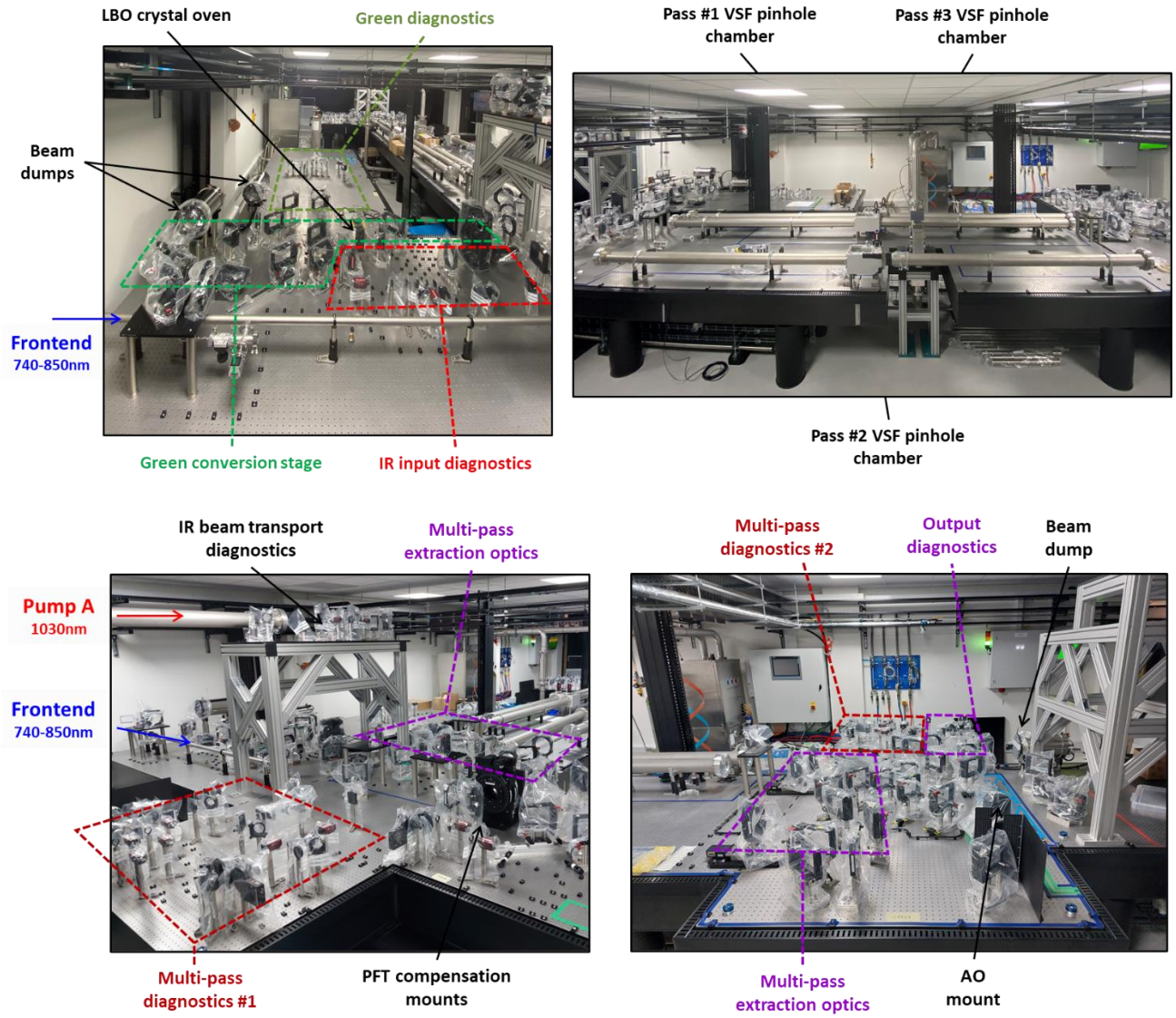

Figure 42: Photographs showing progress of component installation for Ti:Sa HEA system in EPAC laboratory.

2.5 Compressor

The EPAC compressor will shorten the duration of the high-energy laser pulses from 3 ns to ≤ 30 fs FWHM. It will be stationed on the upper level of the EPAC building, next to the laser amplification areas. The specification for the compressor is shown in **Table** 6.

Table 6: Specification of the EPAC Compressor

Parameter	Design requirement
Pulse energy	30 J; Day 1 = 20 J [14]
Pulse duration	≤ 30 fs FWHM
Peak power	1 PW; Day 1 = 0.67 PW
Central wavelength	800 ± 10 nm
Pulse repetition rate	10 Hz, 1 Hz, Shot on demand
Transmission bandwidth	110 nm (750-860 nm)
Output pulse bandwidth	> 75 nm FWHM
Power contrast	@ -100 ps > 10^{12}; @ -20 ps > 10^{9}; @ -2 ps > 10^{5}
Grating Aperture	G1, G4: 300 x 300 mm; G2, G3: 760 x 300 mm
Grating Line Density	1480 lines / mm
Grating Incidence Angle	In diffraction plane: 37.24° (Littrow); 10° out-of-plane.
Grating Peak Fluence @ 1PW	G1 (3 ns): 105 mJ / cm^2; Day 1: 65 mJ / cm^2 G4 (30 fs): 65 mJ / cm^2; Day 1 = 42 mJ / cm^2

Over the past year, compressor works have largely focused on procurement of the chambers, diffraction gratings and optic mount hardware. Over the next year, a large amount of hardware installation is planned, with the aim of starting initial compressor alignment, grating contamination countermeasures and RF cleaning, finalising compressor diagnostics capability, and operation and continuing investigations into alternative diffraction grating technologies.

2.5.1 Chamber

The compressor chambers have been manufactured and are being delivered to EPAC in April 2024. All specifications were met during the FAT, with 5 x 10^{-7} mbar vacuum achieved.

The alignment of the four-grating plus one mirror compressor optical setup requires very high precision measurements and adjustments that are typically performed when the chamber is let-up to atmosphere. It is therefore imperative that the alignment of the compressor is maintained between air and vacuum. These optics will be mounted onto a breadboard, the legs and feet of which are designed to be isolated from any movement and vibrations on the chamber. The isolated optic breadboard contract was awarded to the chamber manufacturer, AVS. This has greatly simplified installation and assembly as it was pre-installed at the factory.

[14] Day 1 corresponds to initial operations where output will be reduced whilst de-risking high peak / average power operation.

Combining the vacuum mechanical analysis between the chambers and breadboards also delivered technical advantages, confirming isolation can be achieved. Vacuum load on the chambers leads to an upwards deflection of the chamber floor by up to 2 mm, moving the chamber feet, which can exert large forces on the baseplate that is connected to the breadboard feet. A small modification to the way that the chamber feet were locked in position removed much of this transferral of forces. Additionally, a uniform distribution of baseplate anchoring bolts constrained any residual movement of the baseplate near the breadboard feet positions. As a result, there is less than 1 micron of deflection in the breadboard when vacuum load is applied. This is also seen as a worst case, as the analysis ignored effect of epoxy resin that fills the voids between the concrete and baseplate, which will further support the baseplates.

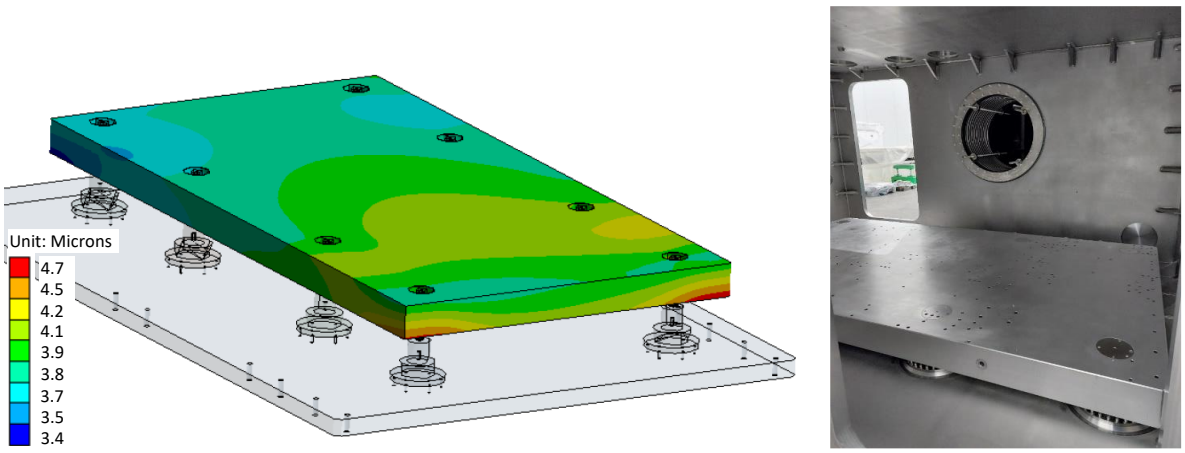

Figure 43: (Left) Chamber breadboard operational load case when a vacuum is applied. Breadboard shows less than 1 micron displacement due to vacuum action. (Right) Compressor breadboard completed at factory.

2.5.2 Grating mounts

In addition to breadboard stability, the optic mounts for the compressor optics must remain stable, with less than 1 µrad pointing instability, to minimise pulse durations maintain and the focal spot position stability target in experimental areas. In previous reports, we have documented the Vulcan OPPEL grating mount design, achieving better than 0.5 µrad stability during standalone testing of the mount. Since then, we have addressed some disadvantages of this design that may not be applicable to EPAC:

- The pitch motion of the mount is unbalanced, requiring significant torque from the motor to drive the weight of the optic. For the larger EPAC G2G3 (300 x 760 mm) gratings, this creates significant mechanical fatigue and possible failure of drives.
- With roll adjustment location behind the optic, there is little to no access to the rear of the optic for possible water connections for a cooled grating optic.
- A vertical translation on the gratings, in addition to the two horizontal translations, would aid alignment, especially for G1,G4 (see **Figure 44**) where there is less alignment tolerance onto the centre of the grating.

A three-point base kinematic mount design was chosen to address all of the above points. These use three lifters at the base of the mount, two linear translation axes, and a yaw rotation drive to provide all degrees of movement and the range of freedom necessary for grating installation, precise alignment and cooling access. Absolute optical encoders will be used for closed loop motion control of the optic mount.

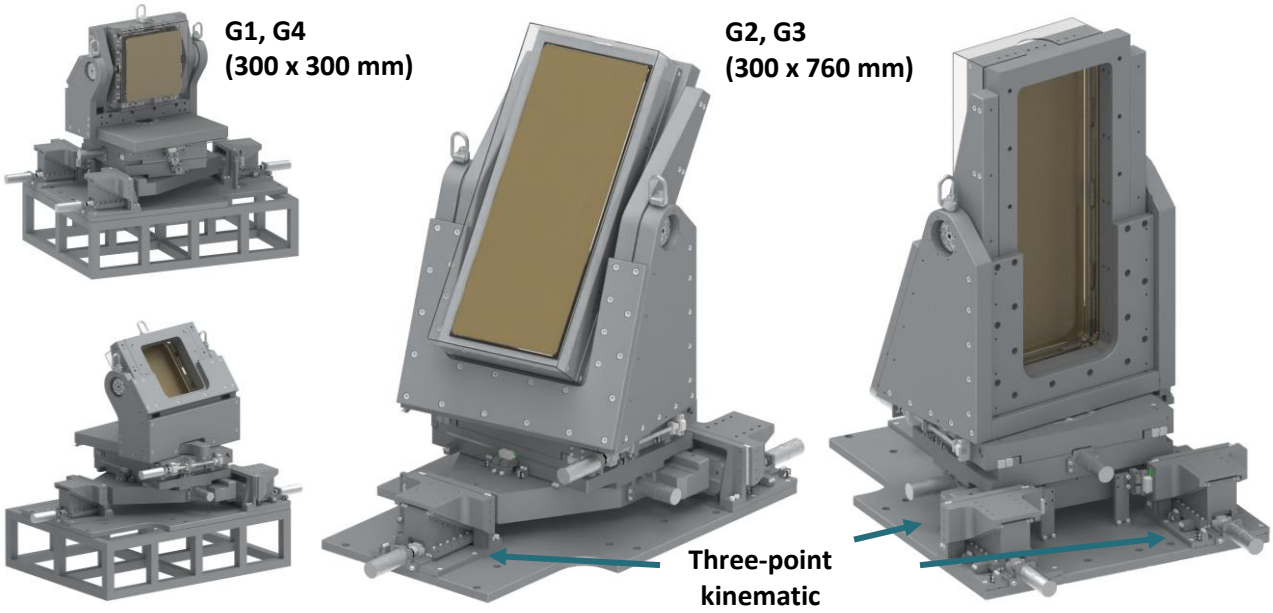

Figure 44: CAD images of the new EPAC grating mount designs. (Left) G1,G4 mount front and back. (Centre, Right) G2,G3 mount front and back respectively. Optics can be manually moved to upright position, e.g. optic loading.

A modal analysis of the mounts' resonance frequencies versus the known, measured vibration spectral amplitudes of the building, estimates that the new EPAC mount design will be at least twice as stable as the Vulcan OPPEL mount (<0.1 µrad pointing stability), with fewer resonance modes in the 0 – 100 Hz range, and no resonance at near 50 Hz.

Table 7: Calculated angular stability of the new EPAC grating mount design compared to the Vulcan OPPEL design and build

Angular Stability	VOPPEL	EPAC
RX, pitch (nrad)	167.7	58.7
RY, roll (nrad)	145.6	79.5
RZ, yaw (nrad)	477.8	22.3

2.5.3 Grating choice

Since the last report to the ISTAC committee and the recommendations that came out of the meeting, the Project has taken a decision to send the first EPAC full-sized diffraction grating substates to the Lawrence Livermore National Laboratory (LLNL) Advanced Optical Technologies Program, to have the 1480 lines/mm gratings written with their proprietary dielectric + Au overcoat method. The UKRI-supplied, polished Clearceram-Z substrates arrived at LLNL in March 2024, with the earliest estimated delivery of the final gratings to the CLF being March 2025 for. At the same time, the Project has continued to investigate and invest in alternative grating technologies with potential to scale to high average power operation: multilayer-dielectric (MLD) coated gratings and water-cooled gratings.

The first gold grating set from LLNL will allow facility commissioning experiments to run at either reduced (1 Hz) repetition rate or reduced energy 10 Hz pulse campaigns, with confidence that the damage threshold (>200 mJ/cm^2, likely >400 mJ/cm^2 [7]) will not be exceeded during commissioning and the first user experiments. The ~5% absorption of each

gold coating layer on the reflective diffraction gratings will lead to more heat being transferred into the grating structure, optical substrate and mounting mechanics of the optics. This heat will act to deform the optic and slowly degrade the compression performance of the optical system.

2.5.3.1 Cooled grating solution

We have used external support from Demcon physics and engineering consultants to model the thermal impacts of operating 1 PW @ 10Hz on gold gratings in greater detail. The modelling so far has identified a range of sources that may deform the optics, and has identified which gratings will see most benefit from the water-cooled grating solution.

Laminar water flow was modelled inside cooling channels to avoid turbulence induced vibrations onto the optic. The profile and length of the cooling channel has been optimised to balance cooling of the grating surface versus water pressure deformation. The optic holder and mount play a key part in managing heat outflow; the optic clamps are an interface for conductive cooling to the mount. Temperature gradients and highly constrained clamps will exert significant deformation contribution on the optic substrate.

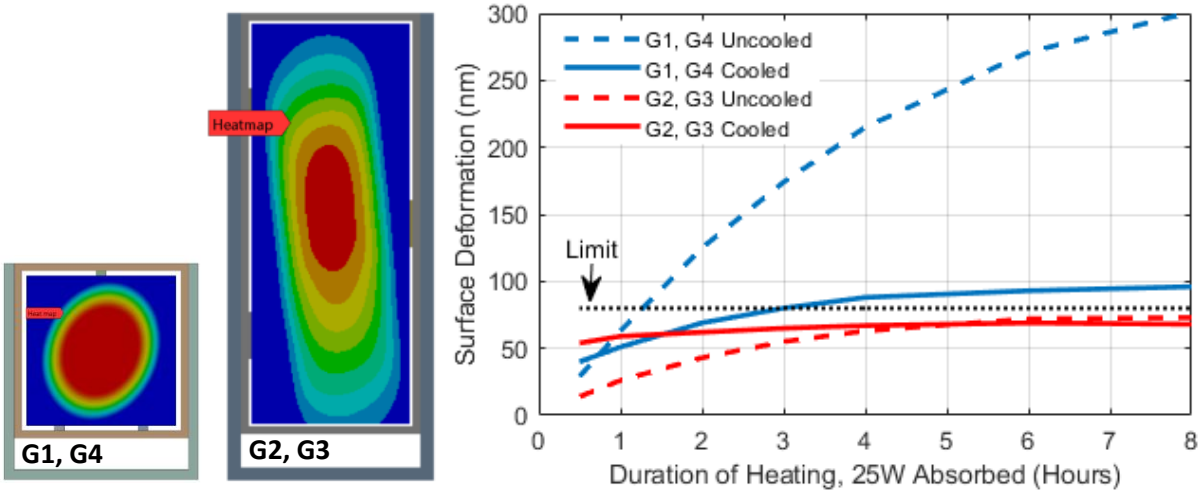

Figure 45: (Left) Modelled heatmap of cooled grating simulations, with 25 W absorbed heat into each substrate size. (Right) Calculated peak-to-valley deformations over time, comparing uncooled versus cooled solution G1,G4 and G2,G3.

Additional work is being planned, in four key areas:

- Continuation of the work to optimise the design of the optic holder (bezel and clamps) and cooling channels with the final EPAC grating mount design. This will also include gravitational sag analysis and optic clamping optimisation.
- Modelling of uncooled substrates, utilising the optimised optic holder design from above and additional feasibility studies into retrofitted cooling solutions that may assist reducing deformations.
- Modelling of the 75 x 75 mm cooled grating prototype in cooled/uncooled gold configurations, as a benchmarking exercise against experimental test data.
- Investigations into the future scalability of the cooling solution to higher average power, >1 PW, lasers.

The feasibility and costing of a full-sized G1,G4 cooled prototype is being actively investigated. This will address the practical challenges, such as larger-scale bonding of the front and back sections of cooled grating substrate, as well as methods to safely connect and route the water connections in vacuum.

2.5.3.2 Gemini TA2 compressor grating tests

An investigation in the near-future reality of 1 PW operation at 10 Hz in EPAC has been recently explored in the CLF Gemini laser facility, from operation of gold gratings (Jobin Yvon) and MLD gratings (Plymouth Grating Laboratory) at EPAC compressor fluence and repetition rate, with a 40 - 55 mm diameter beam at <20 TW peak-power.

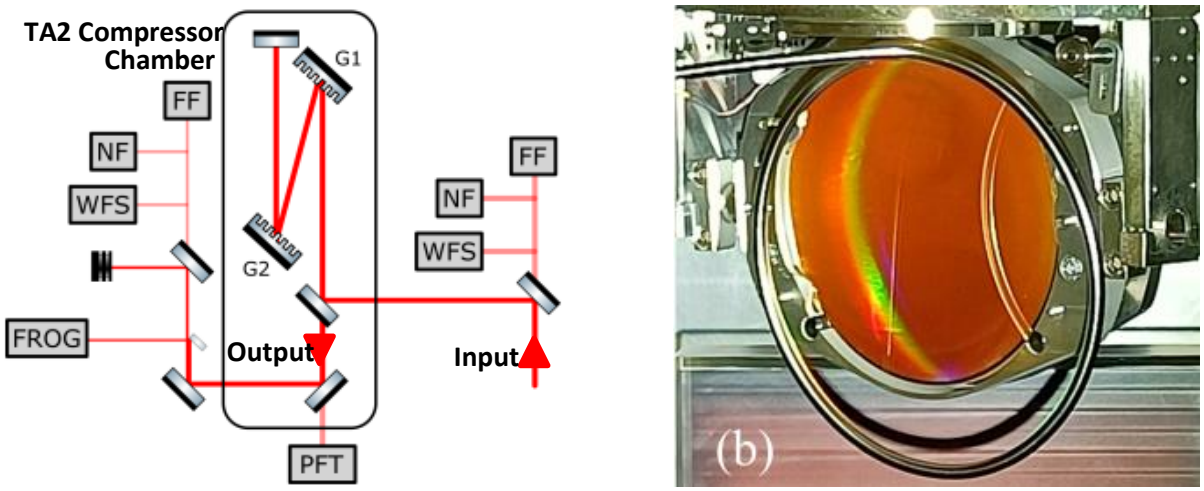

Figure 46: (Left) Schematic of Gemini TA2 compressor setup and diagnostics. WFS = wavefront sensor, PFT = pulse-front tilt diagnostic. (Right) Photo of G1 with 70 W RF antennae in front.

The total compressor energy throughput was measured over time and found to fall by up to 8% after four hours at 60 mJ/cm^2 input laser fluence (similar to EPAC Day 1 operation of 65 mJ/cm^2). This operation required RF cleaning cycles of up to four hours to recover energy transmission, removing a black carbon contamination layer from the surface of the optic. It should be noted that these gratings are not fully comparable to EPAC (different manufacturing processes), and the chamber environment and cleanliness will be different. However, these observations illustrate the importance of an RF cleaning setup and regular – possibly daily – cleaning cycles will be needed for the EPAC gratings.

The impact on pulse duration and wavefront at 10 Hz for MLD and gold grating types was investigated. Thermal deformation of the gold gratings was observed, where the pulse broadened over 10 minutes before stabilising at ~90 fs. No pulse broadening was observed when using MLD gratings, even at higher pulse fluence.

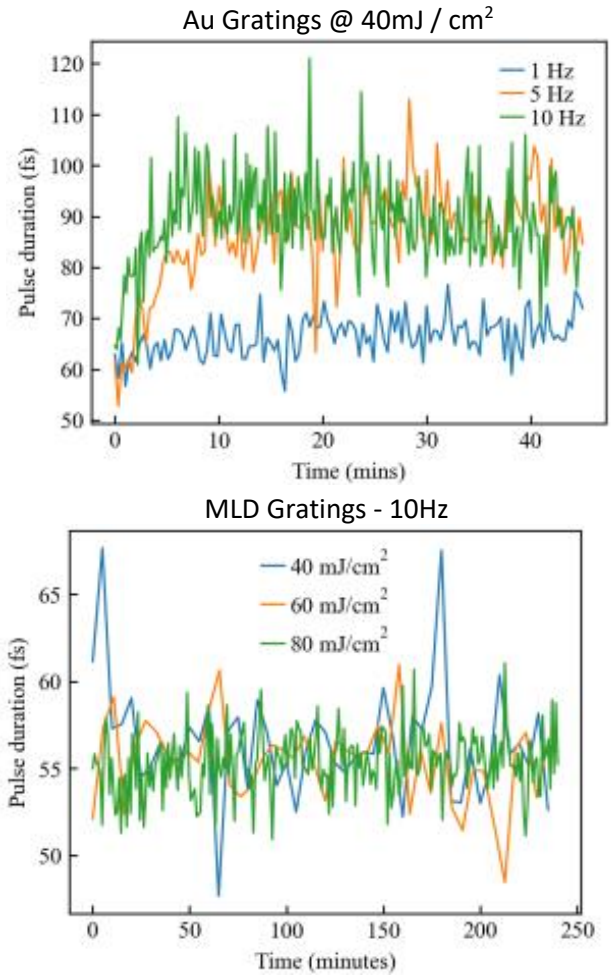

Figure 47: TA2 pulse duration over four hours for (top) gold gratings and (bottom) MLD gratings

While the pulse duration remained constant for all measurements with MLD gratings, we observed a slow-building wavefront distortion that became more severe with increasing laser energy. As the wavefront distortion was observed to scale with energy rather than fluence, it is difficult to extend predictions to the much higher energies of EPAC, but the data points towards possible thermal effects in MLD gratings.

2.6 Beam transport

Since the last ISTAC report, progress has been made on the design and manufacture of many of the components of the beam transport pre- and post-compressor. The riser pipework and supporting infrastructure has been manufactured, and is in the process of being installed. The turning mirror chambers, EA1 and EA2 double turning mirror chamber, and switchyard chambers have been designed and are in manufacture. Other components are at various stages of the design process.

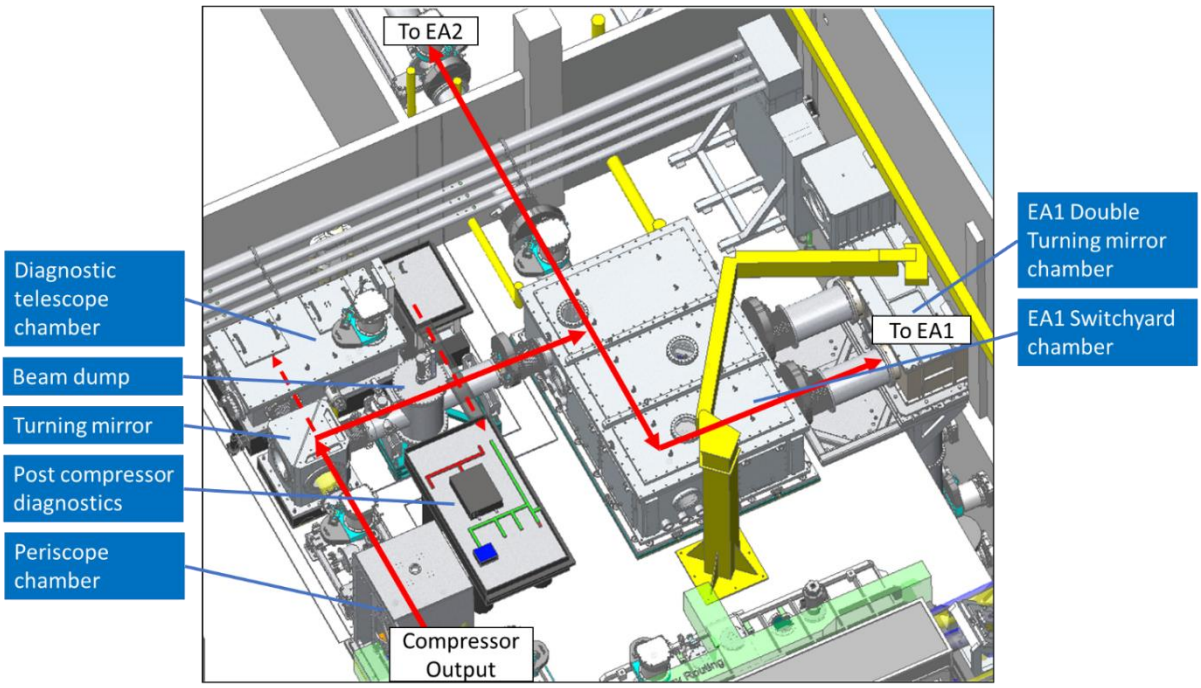

Figure 48: CAD model of the post-compressor beam transport and switchyard

The pre-compressor beam expander and post-compressor diagnostics telescope are discussed below. The post-compressor periscope chamber has gone through several iterations and is being optimised for stability. The EA2 switchyard chamber, which in concept is identical to the EA1 switchyard chamber, will not be procured until required by the future laser system. The initial layout will consist of a single turning chamber, with pipework connecting it to the EA1 switchyard chamber and the EA2 double turning chamber.

2.6.1 Pre-compressor 220 mm beam expander telescope

The laser beam profile image propagation starts with the beam expander after the Ti:Sa multi-pass amplifier. Its primary function is to increase the diameter of the beam from 52 mm to 220 mm, to reduce the fluence on the compressor and beam transport optics. The design of the telescope also considers the achromatic image relay of the super-Gaussian amplified beam, and the alignment tolerance to maintain the wavefront within expected alignment instabilities. We have settled on an optical design that is a combination of refractive and reflective optics. A refractive VSF is made of a low index glass meniscus input lens and a compensating Flint glass meniscus output lens. This creates an achromatic diverging beam that is then collimated by a 2.5° off-axis parabolic mirror. The telescope will be mounted above the compressor chambers at 2.3 m off the floor.

The telescope length was maximised within the constraints of the available footprint, resulting in an optically folded design. The optical design took into consideration effective locations for mounting the optics with high stability whilst maintaining good access. This led to a requirement for two stable platforms to support the optics. The first platform is on the main optical table of the Ti:Sa multi-pass amplifier on which the input periscope, VSF input lens and parabola are located, with a second structure mounted next to the compressor input that supports the VSF output lens, fold mirrors and output periscope.

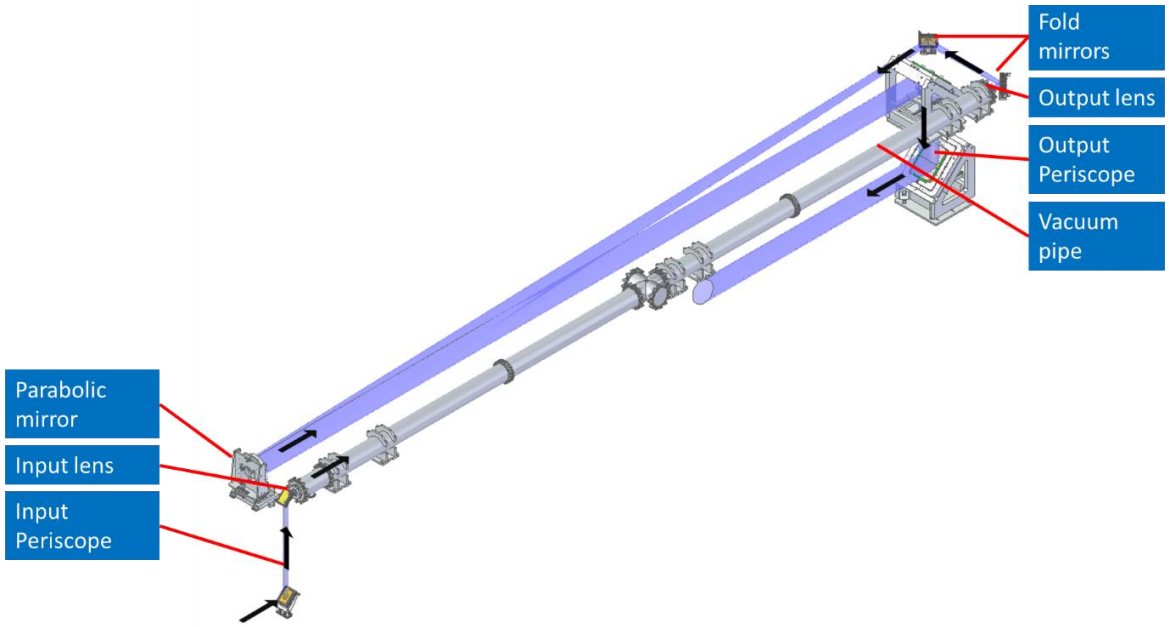

Figure 49: Beam path of the Pre-Compressor Expander Telescope

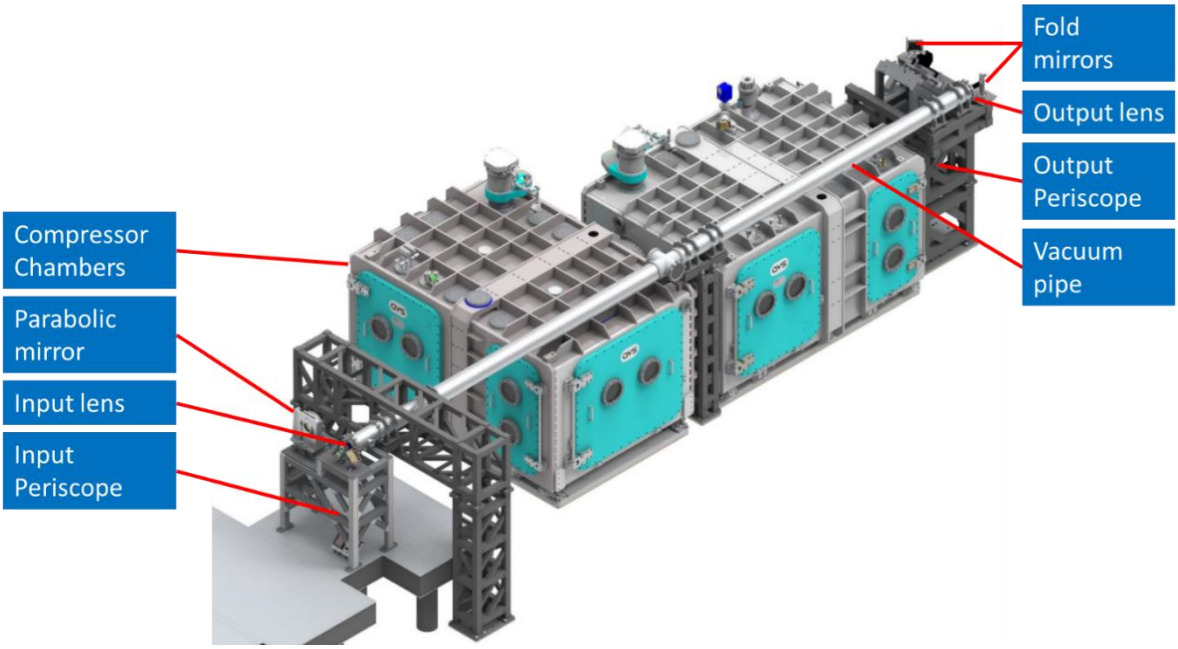

Figure 50: CAD model of the Pre-compressor expander telescope and the Compressor Chambers

The distance from the Ti:Sa amplifier to the input lens was minimised to 7.3 m, with an input lens of 5 m focal length to enable a real image plane at the input of the compressor. The low angle of incidence of the parabola results in a setup that is relatively insensitive to alignment errors. The beam is then propagated back above the compressor and directed down the output periscope into the compressor. The two 380 x 270 mm mirrors of the periscope allow for precise alignment of the compressor input, independent of the telescope alignment. The near-field image of the beam propagates ~60 m to the focusing parabola in the experimental areas: this has been identified as being acceptable in maintaining the high-order super-Gaussian beam profile.

2.6.2 Post-compressor diagnostic telescope

The post-compressor diagnostic telescope has undergone significant development from the concept presented in the second ISTAC report. The main drivers for the changes were the need to reduce the footprint and complexity, and improve the stability of the diagnostics. The chamber design has been shortened to allow a small breadboard to be mounted beside for alignment diagnostics. The telescope is based around a f/4 parabola mirror, and has eliminated the need for folding mirrors within the telescope. Having two output levels, as in the previous design, has been retained: one output level has high attenuation for use with the highest energy modes, and the second has low attenuation for use with lower energy modes.

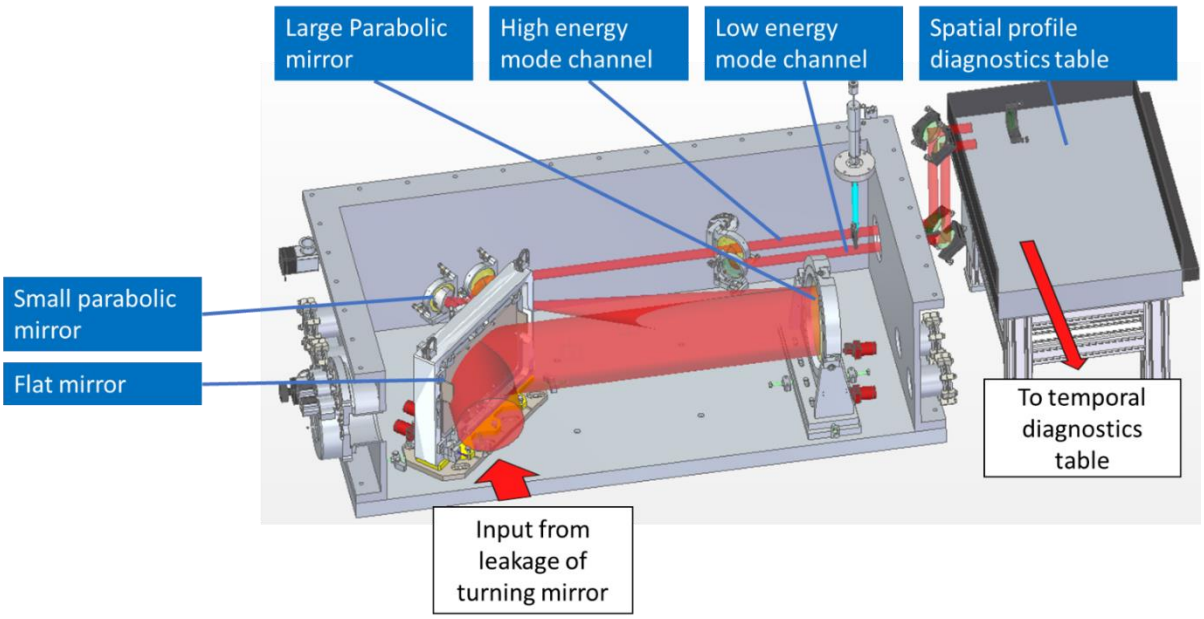

Figure 51: CAD model of the post-compressor diagnostics telescope

3. Experimental areas

3.1 Overview of Experimental Areas 1 and 2 (EA1 and EA2)

EPAC has two experimental areas:

- EA1 has a fixed configuration, delivering a long-focus laser beamline, predominantly for driving a laser-wakefield accelerator. Sources derived from the accelerator will be used for experiments and industrial applications in the 20 m x 9 m applications area (EA1-A).
- EA2 contains a large vacuum chamber that can be configured in a flexible way with short, medium, and long focus beamline options. Multiple diagnostic arrangements can be provided depending on experimental requirements.

The core design work for the laser and accelerator beamline in EA1 has now been completed, and the large components have been delivered or are on order. Focus has now shifted to consideration of how we can meet the requirements of a wide range of experiments, including MoD and industrial users. Several applications beamlines are being designed as part of the project – the timescale for provision of these capabilities will be dependent on available resources. For EA2, design work on the major components is progressing well and procurement has begun on some of the large-scale beam transport infrastructure. With additional funding made available to EA2, other aspects of the beam transport, optics and associated engineering kit are now entering the procurement phase. Research and development continue across several areas relating to high repetition rate operations, and these activities are closely linked to collaboration with the user community.

3.2 Collaborative input

Over the last 18 months, we have continued to engage with our CLF academic user community through user forums and collaborative design projects spanning a range of technologies, as well as through involvement in wider programmes, such as EuPRAXIA and development of the European Particle Physics Roadmap.

In addition to engaging with stakeholders at larger meetings and workshops, we have continued to meet individual groups to get updates on particular scientific requirements, and to talk about new developments that might influence how the experimental areas are configured in the first years of operation. These meetings are also proving valuable in helping to determine the prioritisation of capabilities past Day 1. We have also collaborated with industry, to ensure designs will meet the needs for industrial use.

3.2.1 Particle diagnostics and beam transport

3.2.1.1 Diagnostic development

To further benchmark the performance of scintillators and phosphors that could be used as detectors for a number of ion diagnostics, we have worked with the University of Strathclyde, Imperial College and Queen's University Belfast (QUB) to achieve a common goal of establishing the best candidates at a number of MeV ion source facilities. In the past year we have deployed diagnostics on Vulcan, Gemini and ELI-NP experiments and we plan to continue similar collaborative experiments this coming year. Our collaboration with ELI-NP is especially productive as it allows us to test a range of diagnostics in conditions similar to EA2[8].

Within the (H2020) MULTISCAN 3D project[9], the CLF is collaborating with University of Szeged and other partners to develop efficient neutron sources using high-power lasers. The CLF is contributing by developing diagnostics to characterise the neutron spectra in Time of Flight (ToF) arrangement, and we expect the development of a heavy liquid water target to overlap with our existing targetry research.

3.2.1.2 Beamline design

We have recently agreed joint funding on a PhD studentship at QUB, to work on developing a compact ion beam transport system[12] that could be deployed in EPAC EA2. Together with experts in magnet development from ASTeC[15] within STFC, the plan is to design a modular system that can efficiently capture a large fraction of the laser-generated ion beam and refocus it onto a second interaction point for secondary source experiments. The scale of the system would be 1 – 3 m and would allow beam focusing/collimation and some energy selection over an expected range of 30 – 50 MeV.

The design of application beamlines is continuing in parallel with EA1 design and implementation. A jointly-funded postdoctoral researcher at QUB is working on positron generation and transport. A meeting held at STFC-DL established the requirements for magnetic modelling and the expected positron beam properties onto samples. This work is closely aligned with EuPRAXIA objectives as outlined in their CDR. Following several campaigns led by Imperial College London proving the capabilities of single-shot x-ray absorption spectroscopy (XAS) using femtosecond betatron x-ray pulses, we are developing a beamline design that can access higher photon energies and superior time resolutions than synchrotron sources. A joint PhD studentship is dedicated to laser-driven XAS and will work closely with Johnson Matthey to consider ultrafast industrial applications in catalysis R&D.

3.2.2 Engagement on targetry systems

3.2.2.1 Liquid targets

While the CLF has extensive in-house expertise for deploying solid targetry on high power laser experiments, in order to progress R&D on liquid targetry we have been engaged in two collaborative projects.

The first project is on liquid jet targetry with Stanford Linear Accelerator Center (SLAC) and QUB. Over the past year, this has involved working together to both update the jet design, and then manufacture and characterise working prototypes on site at the CLF.

The second project is working with Ohio State University (OSU) on liquid crystal technology[10],[11] that would be of primary relevance to the production of high repetition rate plasma mirrors, but also relevant to ultra-thin targetry. This project is expected to commence shortly, after lengthy legal hold-ups.

3.2.2.2 Gas target development

As part of target development for EPAC, we designed and purchased a set of precision engineered gas jet nozzles, of 20, 30, and 40 mm lengths. The gas densities have been characterised with double-pass interferometry in Gemini Target Area 1, and with plasma

[15] Accelerator Science and Technology Centre (ASTeC) is based at STFC Daresbury Laboratory (STFC-DL). It is a Centre of Excellence for study of the production, acceleration and delivery of charged particle beams.

fluorescence at the Oxford Plasma Accelerator Laboratory. The nozzles have been successfully deployed by our user groups in experiments on Gemini, ELI, and CoReLS. Using this design, we plan to scale the acceleration length to of order 200 mm while maintaining a well-controlled density profile.

3.2.3 Simulations

3.2.3.1 Solid target interaction modelling

We currently have two jointly funded PhD positions looking at how to apply machine learning techniques to optimise laser-matter interactions in EA2, and help us understand aspects of the complex plasma physics involved. The first, with the University of Strathclyde, centres on using Bayesian optimisation to use guided feedback from a large number of simulations to optimise secondary sources on EPAC and Gemini[13]. The second, from the University of York, focuses on optimising the EPOCH particle-in-cell (PIC) code[14] to integrate into such a system. The ultimate aim of these studies is to be able to provide guided feedback to the user during an experiment as to what is happening with the underlying physics, as well as how to better optimise desired parameters.

3.2.3.2 Gas modelling

In order to co-ordinate laser wakefield accelerator (LWFA) simulation efforts within PWASC[15], we have established a working group to carry out PIC simulations using EPAC parameters. Three regimes of interest are being pursued: (1) highest beam quality (characterised by 6D brightness) in unguided LWFA; (2) highest beam quality in guided LWFA (in hydrodynamic optical-field-ionised (HOFI) channels); (3) highest beam charge in unguided LWFA. These beams are tracked through beamline components, using magnet tracking codes to predict bunch properties at diagnostic and sample locations.

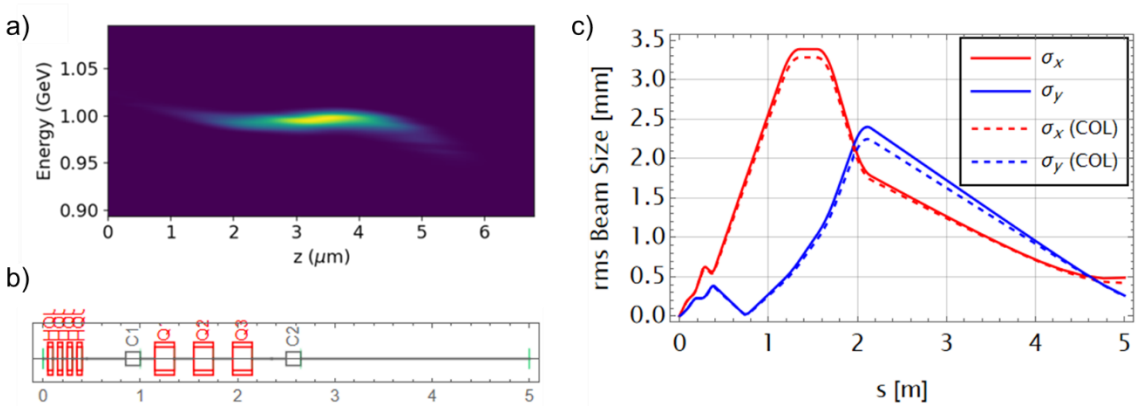

Figure 52: (a) Longitudinal phase space of a simulated 1 GeV electron bunch using machine-learning optimisation; (b) series of quadrupole and corrector magnets used to control the beam profile; (c) electron beam size in horizontal (red) and vertical (blue) plane as a function of distance along the beamline

3.2.4 Engagement with industry

A number of collaborations are ongoing to explore the feasibility of industrial applications employing the radiation sources generated using EPAC. Our first priority will be to achieve the good source quality and stability that is necessary over extended periods for industrial use.

We have a long-term collaboration, including a joint PhD studentship, with the Warwick Manufacturing Group (WMG). They have a wealth of experience in assessing image quality

and creating operational protocols with conventional scanners. Translating these methods to LWFA sources will standardise our validation procedures and give us credibility within the XCT community.

One benefit of EPAC-driven x-rays is the ability to produce small source size MeV x-rays. We have an ongoing collaboration with Rolls Royce to develop high resolution penetrative radiography, and have expanded our network in this area by engaging with the Nuclear Advanced Manufacturing Research Centre (AMRC) and starting discussions with Los Alamos National Laboratory (LANL). LANL and the Atomic Weapons Establishment (AWE) have an interest in multi-modal, multi-scale imaging that will be well suited to EPAC capabilities.

We work closely with the Advanced X-ray Imaging (AXIm) group at UCL to develop new techniques using LWFA-driven x-rays. An experiment using betatron radiation at the Advanced Laser Light Source (ALLS) laboratory demonstrated the potential of edge illumination phase contrast imaging for battery studies, and we aim to attempt ptychography in future experiments. XAS at the femtosecond level has been explored in collaboration with Johnson Matthey, and they have highlighted several research areas where this would have a significant impact. Our next step will be to design proof-of-concept experiments that can be carried out on the EA1 beamline to prove the capabilities of EPAC for fs-XAS applications.

In June 2024, the CLF will host the 8th Dimensional X-ray Computed Tomography (dXCT) conference at STFC-RAL. We have been chosen to host because of the long-term interest from the National Physical Laboratory (NPL) in the future inspection capabilities that will be offered by EPAC. This conference is an ideal opportunity to showcase our technology to a range of experts from all sectors, particularly advanced manufacturing, who require accurate XCT metrology. At previous dXCT conferences, we have already discussed proof-of-concept studies with various interested parties.

3.3 EA1 update

3.3.1 Progress updates

3.3.1.1 Laser beamline

The major components of the EA1 beamline have now all been delivered or are on order.

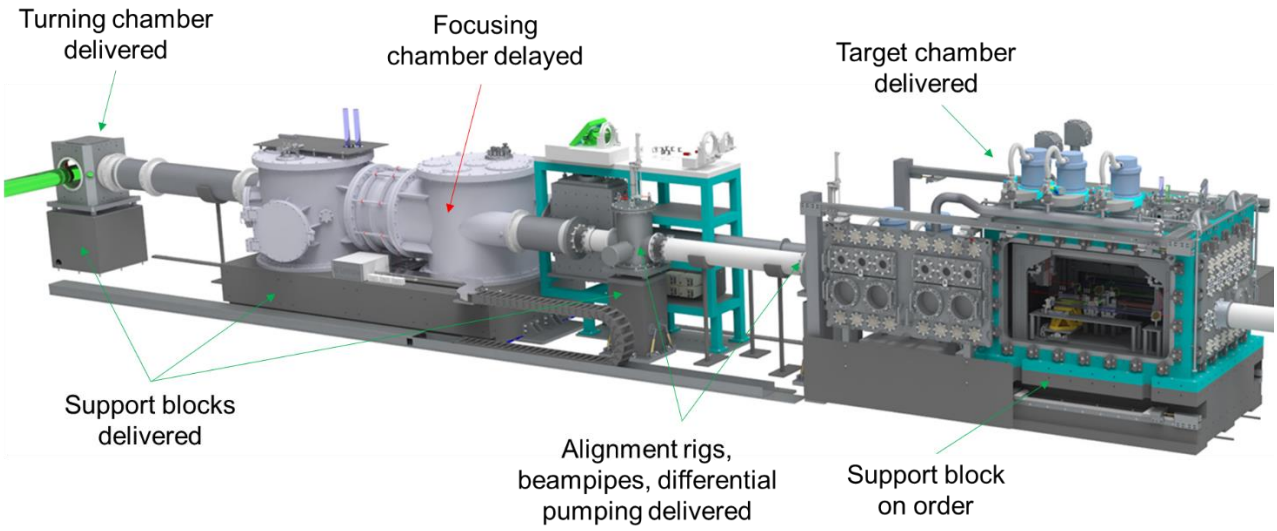

Figure 53: Status of EA1 beamline components

- **Granite bases** for the focusing chamber, turning chambers, and alignment rigs are in the area; the granite base for the target chamber is due to be delivered in July 2024.
- **Vacuum chambers** for the turning mirrors and alignment rigs have been delivered. The **focusing chamber** has been held up by welding failures, but is expected to be complete by summer 2024. The **target chamber** is in the area and has passed the Site Acceptance Test.
- The **vacuum chamber, mounts, and large optics** for the exit mode characterisation have been ordered and are due for delivery within the next three months.
- The **internal components for the target chamber** are finished or are being assembled and we aim to install these after the chamber has been lifted onto the granite support block. The sliding door mechanism can then be added.
- All **beam pipes and equipment for differential pumping** at the entrance to the target chamber have been procured.

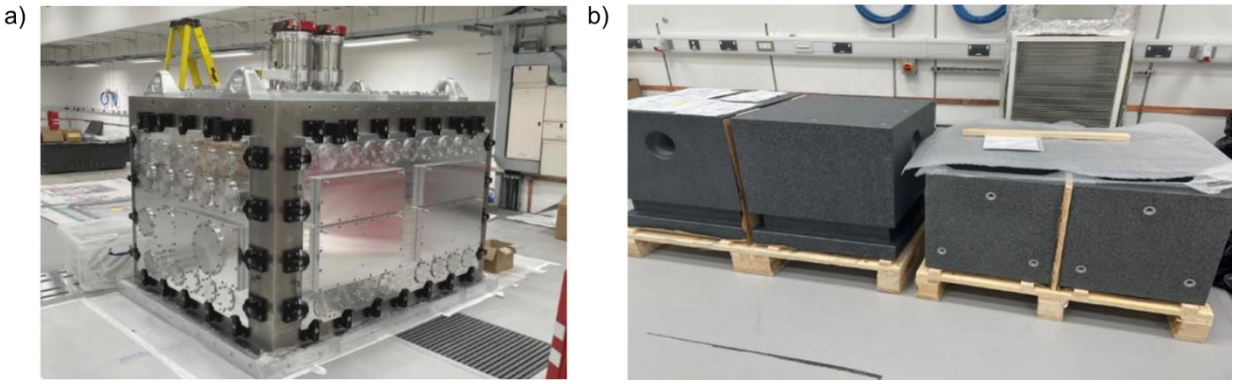

Figure 54: Delivery of EA1 target chamber and granite support blocks

3.3.1.2 Magnets

A set of four permanent magnet quadrupoles (PMQs) has been designed by the ASTeC group to act as the initial capture array at the exit of the LWFA. Each PMQ has a physical length of 50 mm, an internal diameter of 8 mm, and a peak gradient of 500 T m^{-1}. The magnet pieces have been purchased commercially but, because the suppliers could not guarantee our magnetic field requirements, the magnet assembly is taking place at STFC-DL.

A preliminary design for an electromagnet quadrupole triplet has also been completed, but is currently not funded within the Project. This will be necessary for producing an electron beam waist at a specific location – for example on a diagnostic screen, or on a sample.

A double-dipole electromagnet has been designed to act as a spectrometer, and also to allow energy selection for a conditioned electron beamline. This will work over a range of 100 MeV to 10 GeV energies, with an operational procedure such that the target energy should always emerge at 120 mm below the laser beamline. Used in combination with focusing quadrupoles, this spectrometer is expected to achieve 1% resolution at 6 GeV. Production of these magnets is currently out for tender.

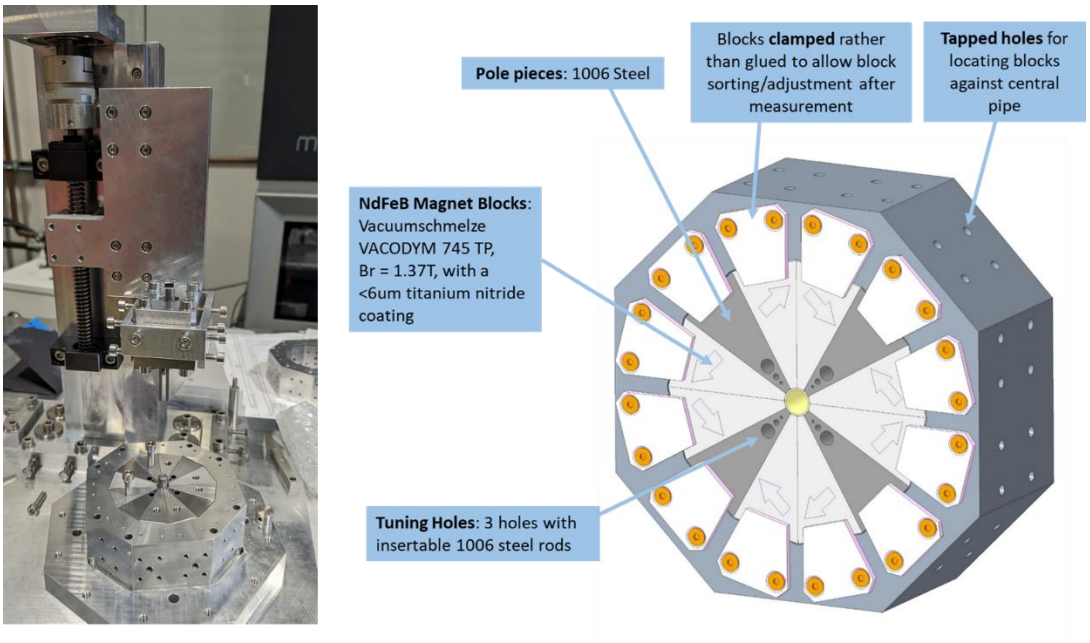

Figure 55: Design and assembly of permanent magnet quadrupoles at STFC-DL

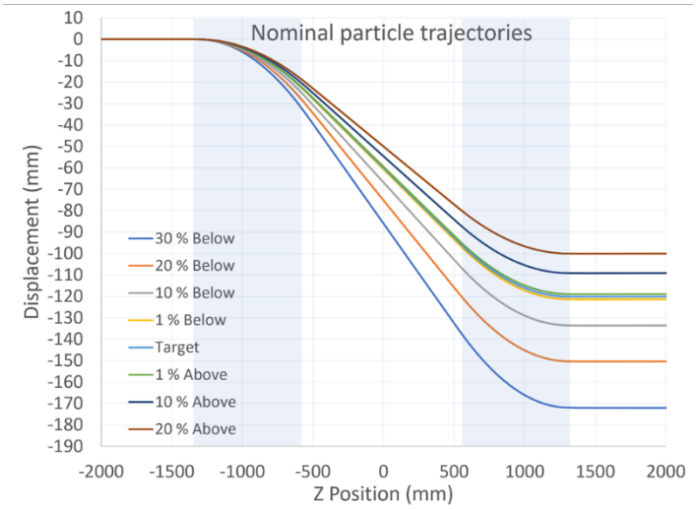

Figure 56: Simulated flight paths showing the relation between electrons of the target energy and electrons of certain percentages above and below the target, assuming the field is chosen such that the target always lands at 120 mm displacement.
The shaded areas show the longitudinal positions of the magnets.

3.3.1.3 Beamline design

Several beamline configurations have been designed, using the output of PIC simulations to predict the electron source properties, and tracking codes to design the magnetic components. We used up to 12 PMQs, up to six electromagnet quadrupoles (EMQs), and the double dipole spectrometer. This will allow flexible delivery of 1 GeV and 5 GeV beams for the experiments we expect in the first phase of operations.

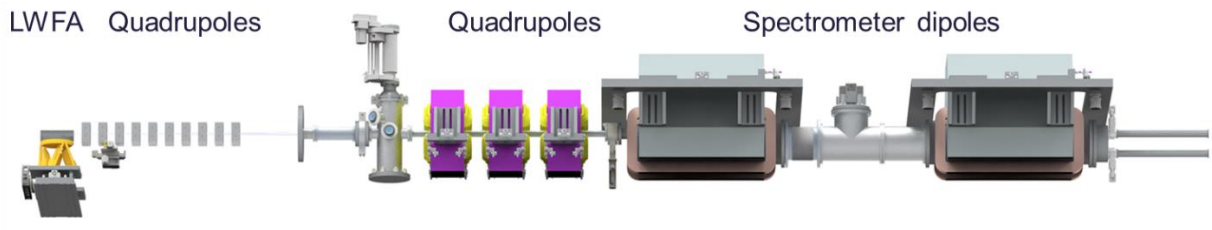

Figure 57: Components of EA1 electron beamline

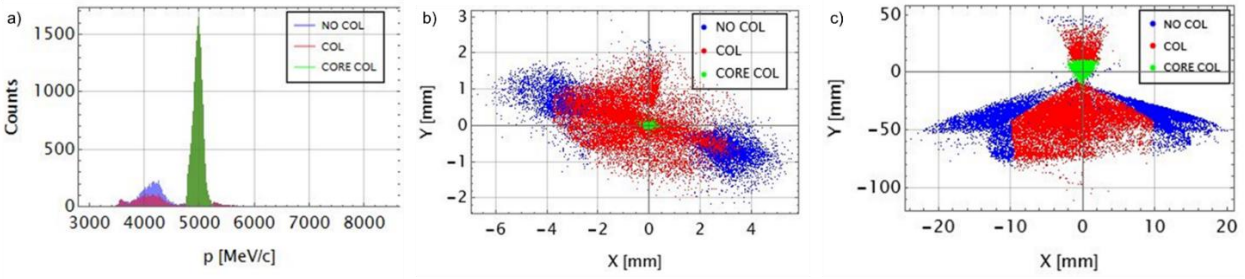

Figure 58: (a) LWFA electron spectrum from PIC simulation; (b) focus formed by 12 PMQ array with core electrons shown in green; (c) electron distribution on the spectrometer screen using 8 PMQs and 6 EMQs

Figure 58 shows results from modelling with a 5 GeV electron beam. We define a core of the electron beam – those within the narrow band peak at the target energy. These electrons can be well controlled by the magnetic beamline. Using an array of 12 PMQ modules, we can deliver a 10 x 40 micron spot containing 99.92 % of these core electrons. This would be of interest, for example, to produce an inverse Compton scattering x-ray source, where the collision laser interacts only with the central spot of on-target energy electrons. To diagnose the electron spectrum, we would use eight PMQs and six EMQs to form a focus on the spectrometer screen. This improves resolution and also creates the bowtie shape that can be used to determine beam emittance. Alternative focal planes can be selected by tuning the EMQs, and we find good transmission and sub-mm spots at 10 m and 15 m from the source.

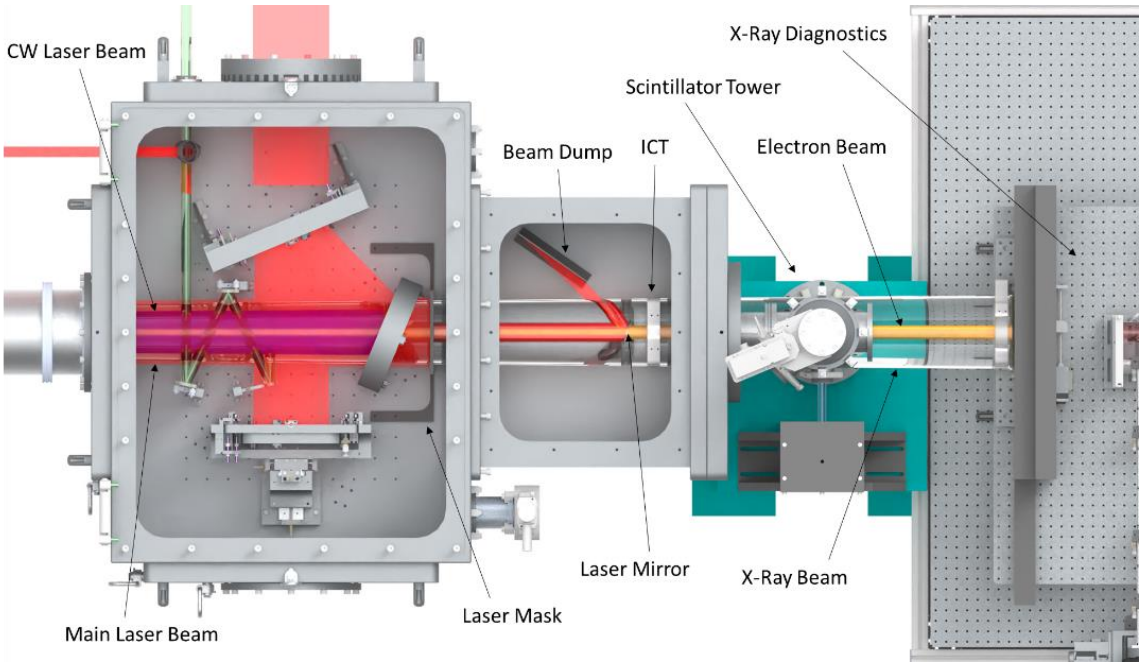

Figure 59: Diagnostic arrangement at the end of the EA1 beamline

At the end of the beamline the laser is directed into the exit mode diagnostic suite to measure the beam profile, wavefront, and spectrum. We will have an integrating current transformer (turbo-ICT) and second scintillator screen here for the electron beam when the electromagnetic spectrometer is turned off. X-ray emission will be detected on direct-detection or scintillator-based cameras.

3.3.2 EA1 source optimisation experiments

3.3.2.1 Objectives

The first set of experiments using EA1 needs to confirm our readiness for full facility operations. The work will be performed in collaboration with user groups, with a focus on essential facility deliverables. Our approach is first to establish multi-GeV LWFA performance, using a set of diagnostics already used extensively on Gemini experiments. We aim to explore the capabilities of EPAC by implementing automated and machine-learning guided LWFA optimisation, and demonstrating beam stability over extended periods. Following this, we plan to prove the suitability of LWFA sources for industrial, biomedical, and security applications, by conducting a set of proof-of-principle x-ray scans in collaboration with x-ray tomography end-users. At this point, the facility can enter the fully operational phase and be opened for user applications to conduct industrial and scientific experiments.

The delivery plan for EA1 can be split into three phases, shown below.

Delivered within the project
• Laser beamline and monitoring diagnostics • Confirmation of laser specifications, alignment procedures, and laser stabilisation • Target and interaction region preparation and testing, high repetition rate gas handling, plasma imaging diagnostics • Experimental control and data acquisition at high repetition rate.
LWFA source optimisation
• Electron and x-ray beamline diagnostics • Confirmation of LWFA performance, operating regimes, and beam stabilisation • Automation of LWFA optimisation • Proof-of-concept demonstrations of x-ray tomography in 50 keV and MeV ranges • Installation of electron beamline components – electromagnets, quadrupoles, diagnostics (time and resource dependent) • Ultrafast (< 10 fs) imaging capability (time and resource dependent).
Operations
• Experiments submitted through the peer-reviewed proposal system • MoD experiments • Commercial experiments carried out through either academic collaboration or proprietary access • Source development to improve secondary source quality and/or implement new techniques and diagnostics.

3.3.2.2 Energy ramp with gas target

The first experiments will use slot nozzle gas targets of 20, 30 and 40 mm length, with a tuneable backing pressure of helium and helium mixes (nitrogen dopant values of 1%, 2%,

5%). After the interaction, the drive laser pulse will propagate into the standard direct exit-mode diagnostic configuration. An independent probe beam will be compressed within EA1 and directed orthogonally through the plasma, to provide a measurement of the average electron density profile. In addition, we plan to monitor the neutral gas density with a CW backlighter in a double-pass interferometer arrangement. We will place two retractable scintillator screens in the beamline to check the direction, profile, and divergence of the electron beam. An in-vacuum ICT will also be used to measure the beam charge. At first, the spectrometer – using Gemini permanent magnet dipoles – will be placed inside the main target chamber to make initial optimisation easier. Once electron beams have been established, the diagnostics can be moved out of the chamber into a beamline configuration.

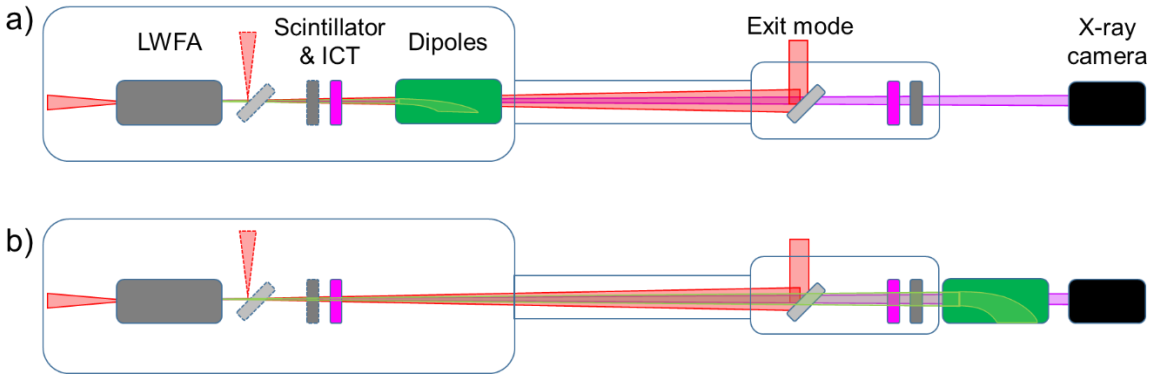

Figure 60: Diagnostic arrangement for initial LWFA experiments using a) Gemini-style configuration, b) Bella-style configuration. Both arrangements use a direct vacuum beamline for exit mode characterisation.

When we have found suitable operating conditions, we will test the accelerator stability by running continuously at 10 Hz for several hours. This will allow us to determine correlations between fluctuations in the electron beam and laser and target parameters, as was achieved with stability tests at DESY[16]. Active stabilisation systems can then be implemented to correct for any machine drifts. Ideally, we will also be able to test machine-learning optimisation and tuning of the electron beam properties, but this will depend on progress with control code development.

3.3.2.3 Tomographic imaging

In order to demonstrate tomographic x-ray imaging (XCT), we need to install a reflective exit mode diagnostic using two plasma mirrors, which will remove the laser from the beampath. Initially this will use tape drives, with a view to switching to ultrathin (200 nm) liquid sheets in the future. The electrons will be swept off axis using the dipole magnet, and the x-ray beam will exit vacuum through a low density (polyimide) window. The first XCT experiments will use betatron radiation in the 10 – 50 keV region to image centimetre-scale samples. This has already been done using Gemini, and EPAC will produce superior datasets (higher quality, more projections) for comparison. For these small samples, a standard XYZ stage and rotation stage (Newport URS100) can be used. Depending on the nature of the sample, it can be placed directly on the stage, or be glued or held in foam on a manipulation stage (e.g. Huber 1005).

[16] Germany's largest accelerator centre - Deutsches Elektronen-Synchrotron DESY

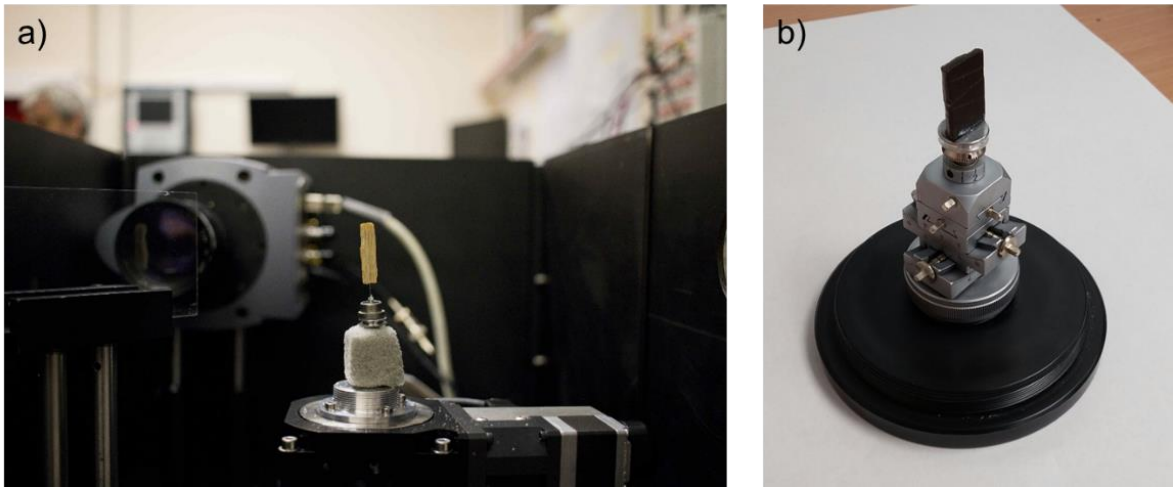

Figure 61: Centimetre-scale samples mounted for XCT scanning. The manipulation stage (Huber 1005) allows fine tuning of the sample orientation relative to the x-ray beam (defined with a CW laser).

The second XCT demonstration will use MeV radiation to image large, dense samples. We have proven the penetrating power of LWFA-based high energy x-ray sources, but these experiments were not optimised in terms of radiation spectrum or detector operation to yield the best quality images. In advance of EPAC commissioning, we will use Geant to produce simulated radiographs and tomograms, to determine the optimum configuration for each test sample. We can produce MeV radiation by generating bremsstrahlung in a convertor material, or ICS radiation using the self-reflection scheme in which the LWFA drive laser is reflected from a plasma mirror onto the electron bunch. Small samples can be mounted on the same stage as used for betatron imaging, while larger samples can use existing stages either in CLF stock or on loan from other STFC facilities. When the XCT performance has been verified, we can specify several stages for procurement, suitable for the expected range of samples.

Images will be detected using a flat panel detector, a scintillator fibre-coupled camera, or a camera imaging a scintillator, as have been used on previous experiments. The amount of shielding required around the detector, to reduce background from the electron beam dump on the floor, will need to be determined experimentally: this will be guided by Geant simulations.

3.3.2.4 Electron beamline

The previous experiments are designed to optimise and validate EPAC performance in producing stable, high-quality electron and x-ray beams. The next step will be to translate experimental demonstrations into a reliable accelerator beamline. This involves: (a) the addition of magnets to condition and control the electron beam; and (b) an improvement in diagnostics, ideally the installation of non-invasive devices.

- Replacement of the permanent magnet dipoles with the bespoke double-dipole electromagnet will provide a superior measurement of the electron spectrum, and the ability to freely tune across the different energy ranges required on EPAC.
- The addition of permanent and electromagnet quadrupoles to the beamline will provide focusing capability onto diagnostics and samples. This will enable an increased flux for electron irradiation experiments, such as radiobiology and electronic disruption, and preliminary studies of undulator/FEL radiation generation.

- The installation of transition radiation monitors and a dielectric streaker will allow characterisation of the longitudinal (temporal) profile of the bunch. Cavity beam-position-monitors could also be installed, to enable non-invasive monitoring and correction of electron beam position.

3.4 EA2 update

3.4.1 Progress updates

3.4.1.1 Design update

For EA2, the original Project deliverables focused on fully designing the area and procuring large-scale beam transport infrastructure. Following additional investment into the Project, it will now be possible to deliver significantly more of the hardware required to deliver first light to EA2.

The overall design for the experimental area (**Figure 62**) has not changed significantly since the last report. However, one noticeable change in the beam transport is the addition of a periscope chamber after the beam exits the pit in the corner of the room. This has replaced one of the standard turning chambers, in order to change the polarisation of the beam on target to a default horizontal polarisation (**Figure 63**) following confirmation of the grating choice in the compressor (see **Section 2.5.3**).

The required services for EA2 (electrical, vacuum, data etc.) are now entering the design phase, with some installation work already underway. Although selected work will be carried out in parallel with EA1, most major services, such as vacuum, gas lines and motion control, are scheduled for design and installation later this year and into early 2025.

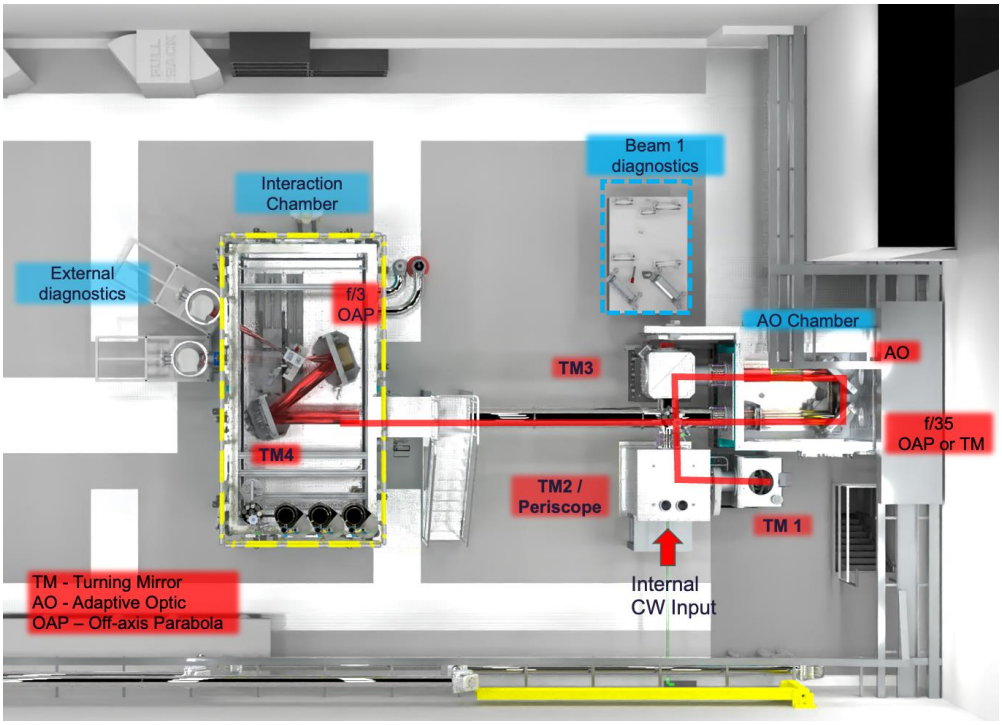

Figure 62: Overview of Experimental Area 2 in a standard (short focus) configuration

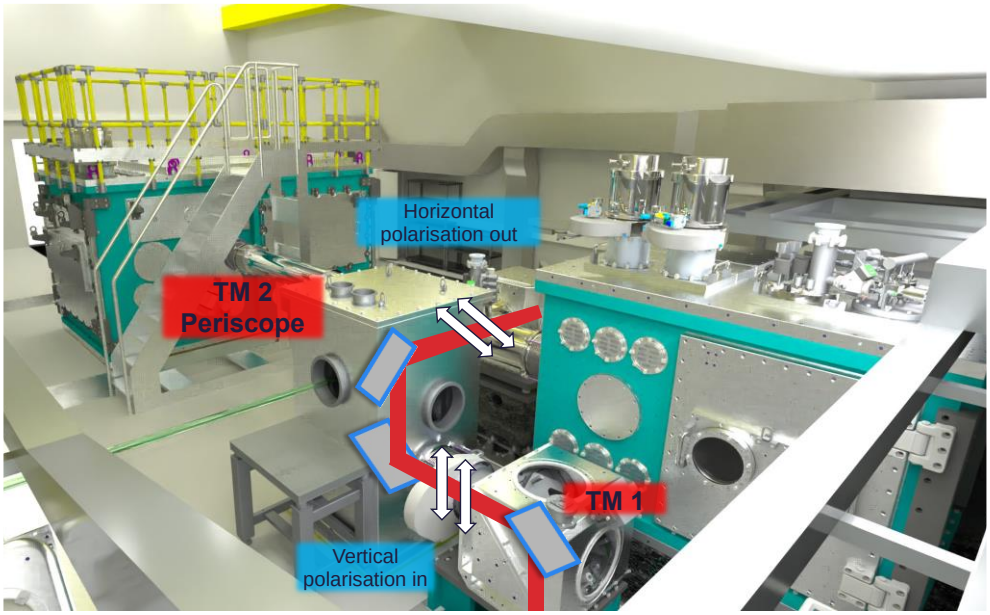

Figure 63: Turning mirror chamber 2 (TM2) has been replaced with a periscope chamber with a low-level beam input in order to switch the default polarisation at target to horizontal

Design work has begun on laying out the beam transport for two optical probes and a long pulse beam, in order to inform the final detailed design for the interaction chamber, even if these capabilities are not available on Day 1. **Figure 64** illustrates the draft beam transport for each beam along the wall of EA2, leading to a diagnostic area near the back of the room. Provision is being made for a 50 mm optical probe, an 85 mm auxiliary beam, and an ~85 mm long pulse beam to be propagated from the pit to the large optical table. This optical table needs be two-tiered, to enable sufficient space for beam diagnostics, compression (for optical probe), and frequency conversion. Each beam will likely propagate above head height from the diagnostics table in order to enter the interaction chamber through the permanent roof ports (see below).

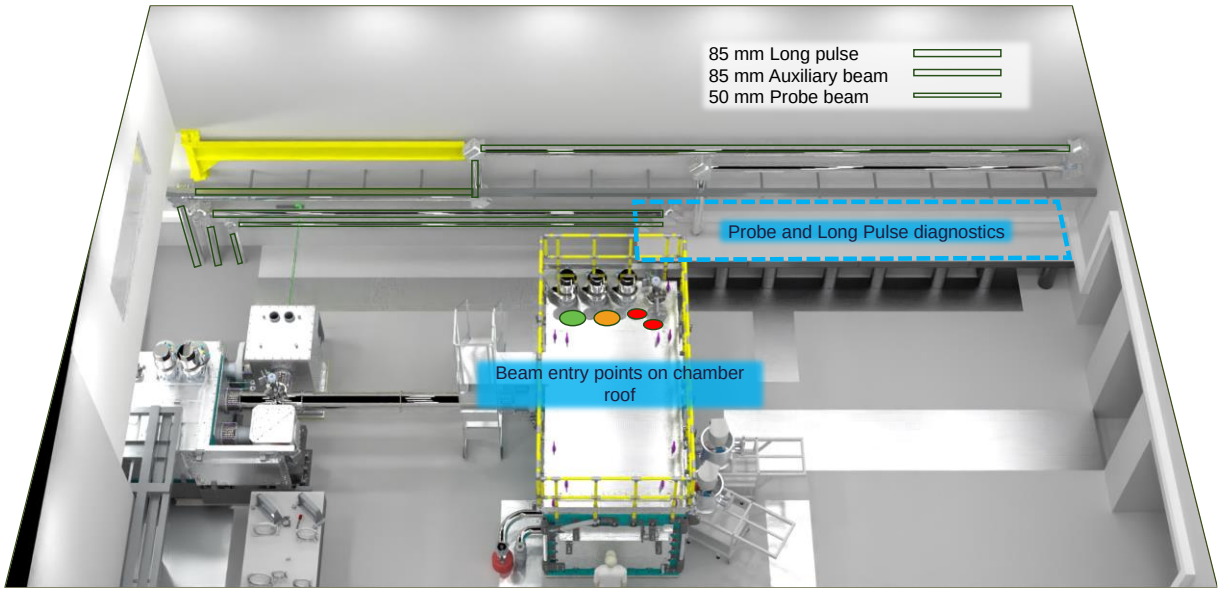

Figure 64: Early layouts for beam transport for auxiliary and long pulse beams in EA2

3.4.1.2 Interaction chamber

Since the last ISTAC meeting, significant progress has been made on the design of the EA2 interaction chamber. The default interaction point for short focus experiments has been moved closer to the centre of the chamber, to improve user and diagnostic access around the target. The new setup is shown in **Figure 65**. Illustrated is a typical F/3 experiment, with the solid targetry array system and two external diagnostic chambers.

As it is envisioned that many early experiments will utilise either a solid targetry array or a tape drive, a long translation stage has been added to allow users to exchange targets at the side access door without having to enter the chamber. Similarly, several internal diagnostics have the option of being mounted on a second long stage, should any filters or detectors need to be replaced between data runs. The capability to mount adjustable rails and optics at height has been added, in order to propagate these smaller secondary beams in such a way that there is minimal interference with the main PW beam's path in the chamber.

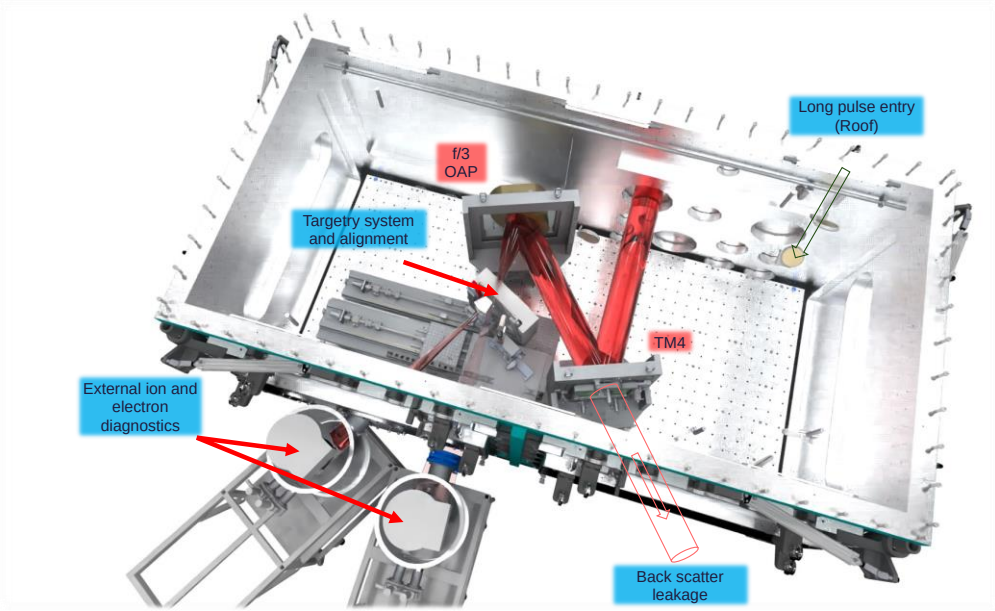

Figure 65: Open view of the EA2 Interaction Chamber

Access to the chamber is maintained through five doors in total, with the large roof area being accessible via a semi-permanent ladder on the side of the chamber where the main beam enters. The roof aperture has been enlarged to permit full crane access to the section of the chamber where most experiments will take place. A suite of permanent ports on the roof have now been populated with relevant vacuum services. Several of these ports will also be used to transport the optical probes and long pulse beams into the chamber.

Detailed design work is entering its final stages, with a focus on analysing the current breadboard design, finalising support and operation of the large doors, and planning how the chamber will be installed in EA2. It is expected that the chamber will go out for tender this summer, for delivery in mid-2025.

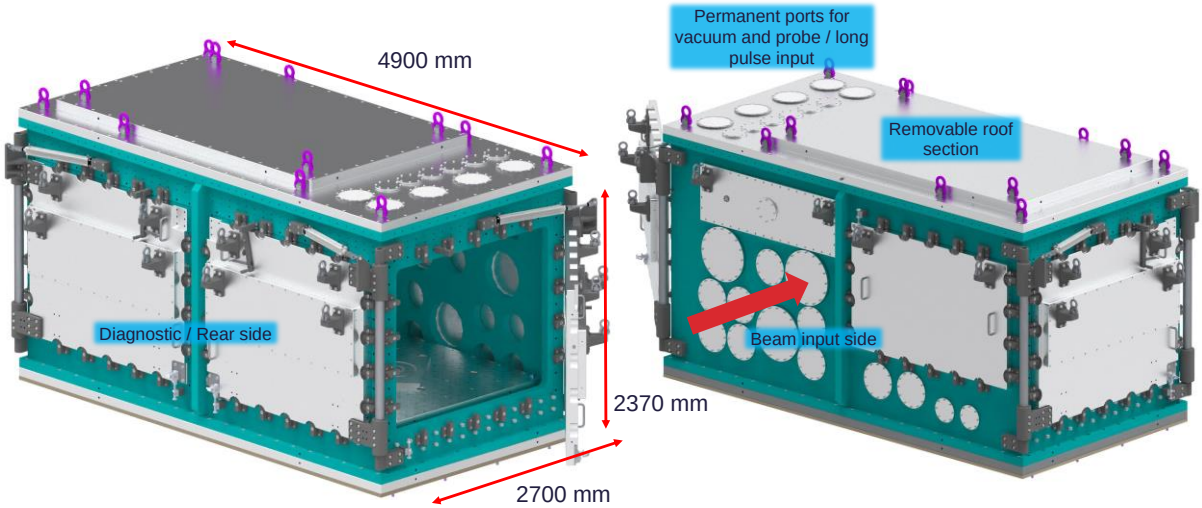

Figure 66: External views of the EA2 interaction chamber

3.4.1.3 EA2 Procurement

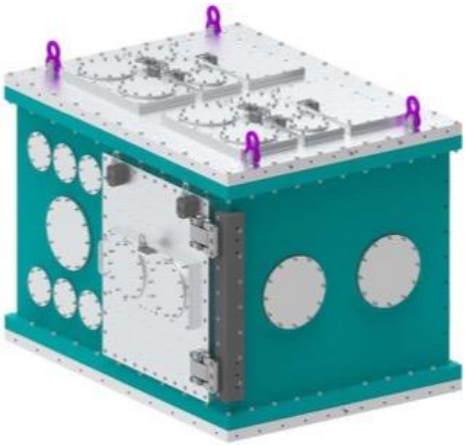

Figure 67: Adaptive Optic (AO) chamber awarded to AVS for manufacture

Since the last ISTAC report, procurement has begun on some of the large-scale beam transport for EA2. Where possible, some engineering equipment (in particular, vacuum equipment) has been also procured in parallel with work in other areas. The tender for the AO chamber has been awarded to AVS (Added Value Solutions), following detailed specification work. This chamber is expected to be delivered to EPAC early in the first quarter of 2025.

All of the components for the large optics mounts inside the AO and interaction chambers have been delivered. Each of these mounts will be assembled on site by our engineering team, and will be fully cleaned and tested before being moved to EPAC ready for installation. The large transport mirror substrates have been ordered, although the specification for the final coating has still to be finalised. The 90-degree AO has been delivered and fully tested offline. Before EA2 is commissioned, a second AO substrate with a higher damage threshold coating will be ordered, to mitigate the risk of the first getting damaged during initial test shots.

With the recently upgraded budget for EA2, is it expected that additional orders will be placed for the remaining beam transport infrastructure in FY2024/25, and for some of the supporting engineering services once these have been fully designed. One longer term item for procurement is the short focus parabola, which should be out for tender later this year once the coating specification has been finalised (see **Section 3.4.1.5**).

3.4.1.4 Ion Diagnostic development

In the past year, we have continued to develop concepts for high repetition-rate ion diagnostics, which will be central to operating EA2 for both fundamental science and secondary source applications.

Our focus remains on developing a number of solutions for both spectrally and spatially resolving laser-generated ion beams. The first will be an updated 1D/2D Thomson spectrometer, with an active detector based on either a microchannel plate (MCP) or phosphor/scintillator, combined with an efficient optical read-out. The second will be a two or three colour, high resolution scintillator imager, capable of imaging the ion beam at two or three discrete energy ranges[16]. To accelerate these developments, we have recently hired a post-doctoral researcher to lead on several aspects of the R&D, and work towards final diagnostic designs in the next 12-18 months.

In collaboration with several UK user groups and the Detector work for EPAC (see **Section 4**), we have continued to assess the suitability of various scintillators and phosphors in terms of signal response, by performing offline tests at the Birmingham Cyclotron facility. For Thomson spectrometers with a small acceptance angle (and strong energy dispersion by electric and magnetic fields), the low flux at the detector indicates that a phosphor screen or MCP would be most suitable. However, due to some issues with afterglow during testing of our default choice (P43 phosphor), we will be testing alternative phosphors as well as some crystal scintillators (e.g. YAG) in upcoming campaigns over the next six months. We are also exploring the options of improving the light collection efficiency to camera by either using fibre tapers or directly coupling the scintillating screen to a camera. As the 2D ion beam profiler is typically deployed at a few centimetres from the interaction, the signal flux has been found to be sufficient to use multi-colour plastic scintillators as planned.

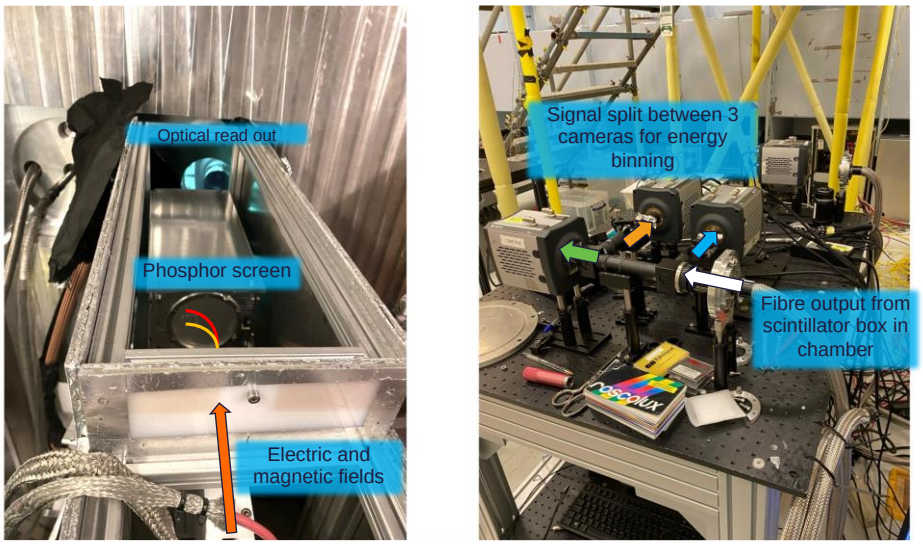

Figure 68: Active ion diagnostic testing in Vulcan and Gemini at the CLF. (Left) Phosphor-based Thomson ion spectrometer. (Right) 2D proton beam profiler in 3-channel mode.

3.4.1.5 Debris and LIDT testing

Since the last ISTAC report, we have continued to assess the risk of debris from operating at high repetition rates (≥1 Hz) in EA2. This work has focused on studying debris emission processes on current generation laser systems, as well as working out how best to design our large optic beam transport to prevent damage that might stop operations after a relatively short period.

The coating for the main focusing optic (40 degree f/3 off-axis parabola (OAP)) is being chosen on its ability both to reflect the full bandwidth of the EPAC beam with a sufficient damage threshold (at least 200 mJ/cm^2), and to resist rapid degradation when exposed to target debris.

Several candidate two-inch coated optic samples have been ordered, that will be partly exposed to some ballistic debris and then subjected to LIDT tests on the Gemini facility to determine which is more susceptible to early damage onset following debris build up. We plan to decide on the best coating following these tests in June this year.

We have also gathered quantitative data on debris from a several high power, high repetition rate laser experiments using glass witness plates. For one Gemini experiment, data was taken from ~1000 shots on 15 µm copper tape using six witness plates around the interaction (see **Figure 69**). Unsurprisingly, the largest build-up of copper (~50 nm) was seen on the plates facing the target front surface (close to the focusing optic). At 1 Hz for eight hours a day, this would scale to almost 1 µm of copper coating. While the tape drive was not affected by some of the local debris, this data emphasises the need to prevent debris propagating beyond the interaction region where possible. Further measurements are planned on other experiments using both passive witness places and active monitors, including a new high-speed camera purchased by our Target Fabrication group. A placement student from the University of York will be working with the CLF to help set this up for several upcoming experiments.

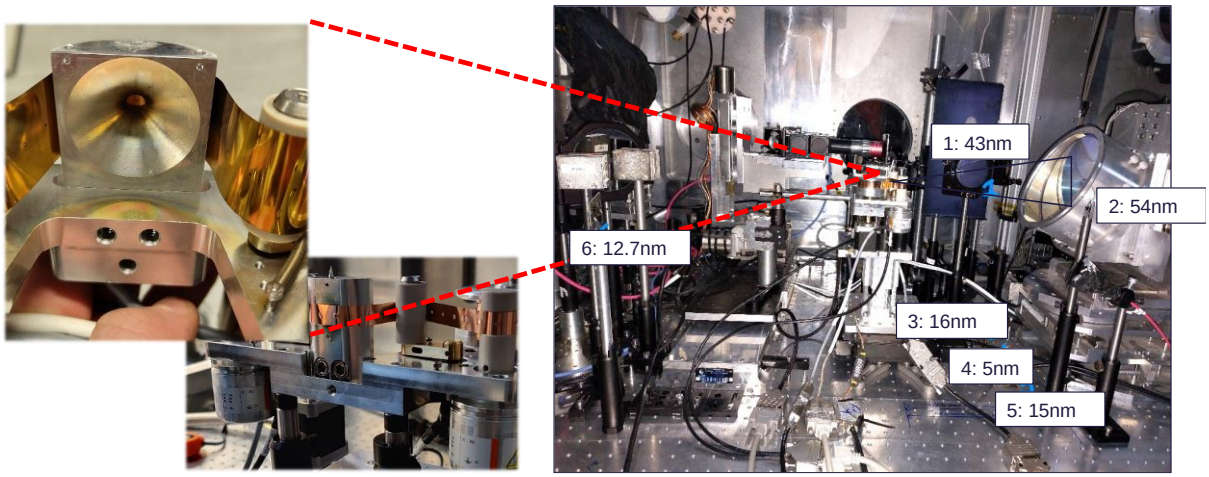

Figure 69: Debris measurements from an ion acceleration experiment in 2023

3.4.2 Day 1 deliverables

The scope of EA2 is to field a wide range of experiments covering fundamental plasma physics as well as the production of secondary sources for science and applications. In order to reach a point of readiness for regular EA2 operations, following first light, there will be a programme of internal commissioning and source optimisation, the latter in close collaboration with the user community. The priority for EA2 source optimisation will be the stable production of ion beams, and bright Bremsstrahlung x-rays for large area imaging.

It is expected that when it is possible to deliver the first full power beam to EA2 (estimated late 2025), the beam parameters will be 20 J in 30 fs, with a maximum repetition rate of 1 Hz. Initial commissioning in EA2 will start with significantly lower energies in a single shot mode before ramping up to the full power of 20 J. The f/3 f = 660 mm OAP (40 degree off-axis angle) will produce a focal spot close to 4 µm ($1/e^2$), yielding a focused intensity of ~2 x 10^{21} Wcm^{-2}.

3.4.2.1 Commissioning

With successful beamline installation, the main beam will be aligned together with the internal CW beam, and focused to the nominal interaction point using the f/3 short focus parabola. A staged approach will be taken in the commissioning period, covering testing of engineering

services (mainly vacuum and motion control), data acquisition and triggering, target positioning and alignment, and characterisation of beam alignment and stability at low powers. With initial alignment and testing complete, the laser pulse energy will be ramped up, initially without focusing to target, to fully optimise laser diagnostic filtering and data acquisition at up to 1 Hz, whilst ensuring all relevant transport optics are free of damage after a period of extended operation.

The final step in internal commissioning will be a repeat energy ramp but focused to target. During this time, a number of tests will be undertaken with a range of laser and target parameters:

- Radiological commissioning using standardised dosimetry methods
- Operation and in situ alignment of targetry systems
- Commissioning of a suite of plasma diagnostics to characterise laser absorption (and reflectivity) at full power
- Measurements of relativistic electron and ion beams to understand EPAC's baseline performance in the context of commonly used intensity scalings
- Assessing the ability of EA2 to perform experiments where relatively high native laser contrast is required, e.g. shooting of ultra-thin targetry
- Characterisation of debris emission and the effects of electromagnetic pulses (EMP) on diagnostic and control systems.

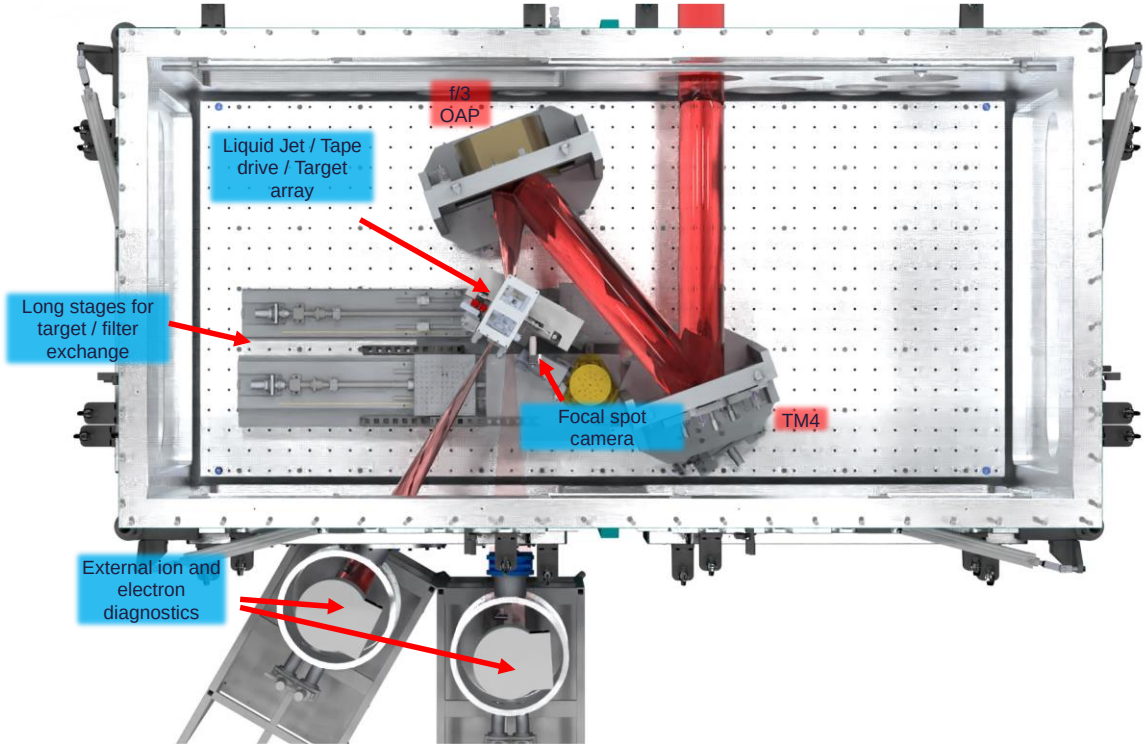

Figure 70: Standard F/3 set-up expected for Day 1 source optimisation experiments. (Additional internal and external diagnostics not shown)

3.4.2.2 EA2 Source optimisation experiments

Following the initial commissioning of all the main systems in EA2, the primary goal will be to achieve the production of a stable, tuneable ion beam at up to 1Hz. This phase of source optimisation will be carried out in close partnership with a number of our regular academic users, who will be able to assist with diagnostic and target set-up along with full power

operations and automated control and optimisation[17]. Compared to the previous phase of commissioning, more emphasis will be placed on operating the beamline in a stable mode for extended periods, using feedback systems to change laser and target parameters to achieve desired optimisation of ion beam properties.

In order to operate for longer periods (and at up to 1 Hz) without breaking vacuum, it is planned that these initial optimisation experiments will use either a tape drive or liquid jet target (see **Section 3.5**). Liquid jet targets are particularly well-placed to operate for extended periods, whilst also minimising some types of target debris associated with solid targetry. Initially the target interaction angle will be limited to 30-45° from target normal, to minimise both the risk of debris damage to the OAP and the backscattered energy propagating back down the laser chain.

A range of active diagnostics will be available for data collection, although it is expected that some passive media (such as Image Plate or Radiochromic Film) will be used to cross-calibrate and benchmark high repetition rate diagnostic performance. It is expected that most diagnostics will be those developed and optimised by the CLF, although we will not preclude user-developed diagnostics if they can be easily integrated into our data acquisition systems. The diagnostics we expect to have available are:

- Thomson parabola ion spectrometers
- High resolution 2D ion beam profiler
- Electron spectrometers
- X-ray Linear Absorption Spectrometers (see **Section 4**)
- X-ray MeV Tiled Imager (see **Section 4**)
- X-ray Large Area X-ray Panel (see **Section 4**)
- Laser reflectivity / backscatter spatial and spectral characterisation
- Opitcal Transmission Radiation
- Transverse/reflective optical probing (*may not be available Day 1*).

The second objective for the EA2 source optimisation period will be to optimise the production of bright x-ray bremsstrahlung, mainly for imaging applications. The target type for this activity is likely to be thicker and have a higher Z compared to those used for high repetition rate ion beams, so will primarily be delivered by tape drive. While the goal will be to optimise X-ray beam quality and tunability, there will also be significant emphasis on monitoring and minimising debris production, to assess the suitability of operating with thicker targets for extended periods.

3.4.2.3 EA2 user operations

While the final operational model for EPAC has yet to be agreed, it is anticipated that following user-assisted source optimisation regular calls will be issued for users to submit proposals for experimental time in EA2. It is likely that, for initial calls, expressions of interest are sought that align with areas of development in which the facility is interested, e.g. neutron generation from a high repetition rate ion source. Operating in a semi-configured access mode for experimental blocks will maximise the chance of these initial experiments yielding valuable results for the CLF and the user community, whilst minimising downtime between runs.

As additional facility developments come online, e.g. dedicated optical probe (if not available Day 1), or a long focus capability in EA2, these could also become a combination of an initial internal commissioning period followed by themed user-driven proposals.

3.5 Prototyping

Targetry prototyping to supply well-characterised targets at up to 10 Hz is ongoing for EPAC. Some technologies, such as the tape drive, are now developed to a level where they can be deployed on user experiments, to gain an understanding of their performance in EPAC-relevant conditions. In other areas, several targetry technologies remain under development. There has been significant progress on the liquid jet target and engineering designs for array-based targetry that will be utilised in EA2, where there is a requirement to field multiple targetry systems to meet a wide range of scientific and application requirements.

Several R&D projects are underway (see below), including further development of several larger collaborative efforts with UK and international institutions, such as the University of Strathclyde, QUB, the ELI Pillars, and an upcoming collaborative presence on an experiment at SLAC[17] to test liquid nozzle technology.

Commercial exploitation of the tape target system through licencing agreements has led to discussions with LLNL and the European XFEL to supply systems for their programmes, which will further progress refinements for final EPAC deployment.

3.5.1 Tape drive and tape targetry for high rep rate operations

The CLF tape drive system has been fielded on experiments both in the CLF and internationally. First shots have been taken using the system on the European XFEL for laser only time, with further experiments planned in 2024/25. The system survived the laser interaction with no negative effects; debris production was noted as an issue that needs to be addressed (see **Section 3.4.1.5**). The drive is being further developed to add shielding for EMP, x-rays and debris, and an initial set of shields has been provided to the University of Strathclyde and ELI-NP for testing.

Enhancements have also been provided to the University of Strathclyde's system to allow the system to be shot at a wider angle, and the focal spot camera system to be used. These enhancements have been tested and will also be implemented on upcoming experiments on Gemini, to give confidence in a greater flexibility for EA2 in EPAC. We have also implemented systems where the drive system can be triggered: this allows synchronisation with the laser systems and provides a more automated way of moving after the shot, which can be useful if users do not want to run in a continuous mode.

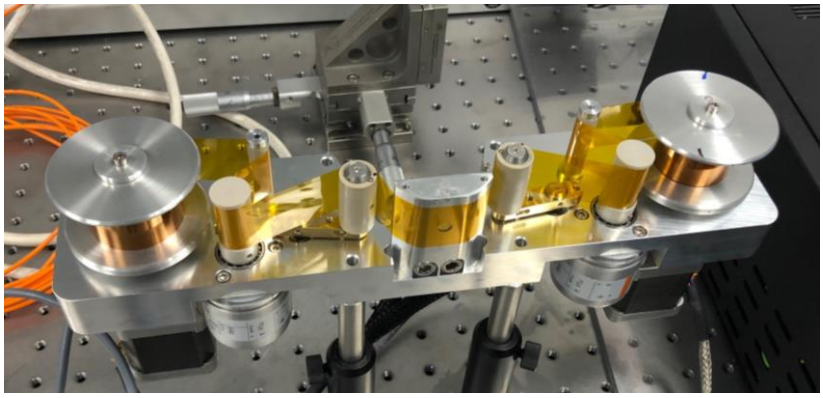

Figure 71: An extended tape drive for off axis shots

[17] SLAC National Accelerator Laboratory | Bold People. Visionary Science. Real Impact. (stanford.edu)

Through the EPIC[18] collaboration, work has continued to develop the target solutions to be fielded onto the tape drive; specifically this will develop a coating system to deposit metallic dots onto the tape. The project in India is focusing on two characterisation systems to measure the thickness of this coating, using both optical transmission and x-ray transmission/ fluorescence measurements.

Tape coating provision has been identified as a critical capability and has therefore been brought in house to the Target Fabrication group. A tender is currently out to provide a commercial coating system that will integrate with the CLF-designed 'coating plant tape drive'. The coating plant drive is an enhanced and elongated tape drive that will run a masking tape and a substrate tape in contact with each other in vacuum, to allow dots to be coated on the tape. The tender is for a system that will coat 250 m of tape in eight hours.

3.5.2 Liquid crystal technology

Liquid crystal technology is a promising medium to enable high repetition rate plasma mirror operation in EA2. Further meetings between the CLF and the Ohio State University (OSU) have progressed to enable a non-disclosure agreement (NDA) to be signed. A material transfer agreement will allow the CLF to access drawings and to host a demonstration system, to progress work to develop a system for EPAC. UKRI legal is working with OSU legal to complete this process. As part of the agreement, we will attempt to refine certain parts of the system to improve film formation, repetition rate and pointing stability, as these are key concerns for plasma mirror use.

3.5.3 Liquid jet technology

A significant amount of work has been carried out in the CLF to develop liquid targetry, specifically the development of a liquid leaf target. The collaboration with QUB is ongoing, with a PhD student regularly visiting the CLF to work on the system and to design future experiments based on its geometry. The CLF is working with a team from SLAC and as reported before, has a system in place for liquid delivery based on a SLAC system. We have developed new nozzles manufactured from metal using the unique capabilities of the Precision Development Facility (PDF) in STFC RAL Space, and have also used novel 3D printing techniques to produce cheap, high specification nozzles. This has enabled us to test many designs in a short period of time at limited cost.

A new room has been kitted out in EPAC to be a targetry development laboratory. This room has the required vacuum, power, and gas systems to enable the liquid target system to be fielded in a vacuum environment. Pumps have been procured and a target chamber has been installed into the laboratory. In the coming months, the first experiments under vacuum will be carried out to test the performance of the target system, with the aim of being able to field the RAL system in a Gemini target area within a year.

Diagnostics are being developed to characterise the system and initial measurements have been carried out with a high frame rate camera, to try to understand the formation mechanism of the jet. This diagnostic may become critical in understanding any ice formation that may inhibit the performance of the system. In collaboration with QUB, we are investigating

[18] https://epic-innovation.org/

interferometry systems to measure the thickness of the liquid leaf, and the designs for this are being integrated within the chamber design for the target test system.

Stages for the movement of the jet under vacuum have also been purchased and installed into the chamber, ready for testing under vacuum.

Simulation work that was funded by IMPULSE has been ongoing and, recently, access to the SCARF cluster (STFC) was obtained to reduce the processing time for the simulations. We aim to be able to test nozzle geometries before printing/ machining them, to be able to drive development quicker for experimental campaigns.

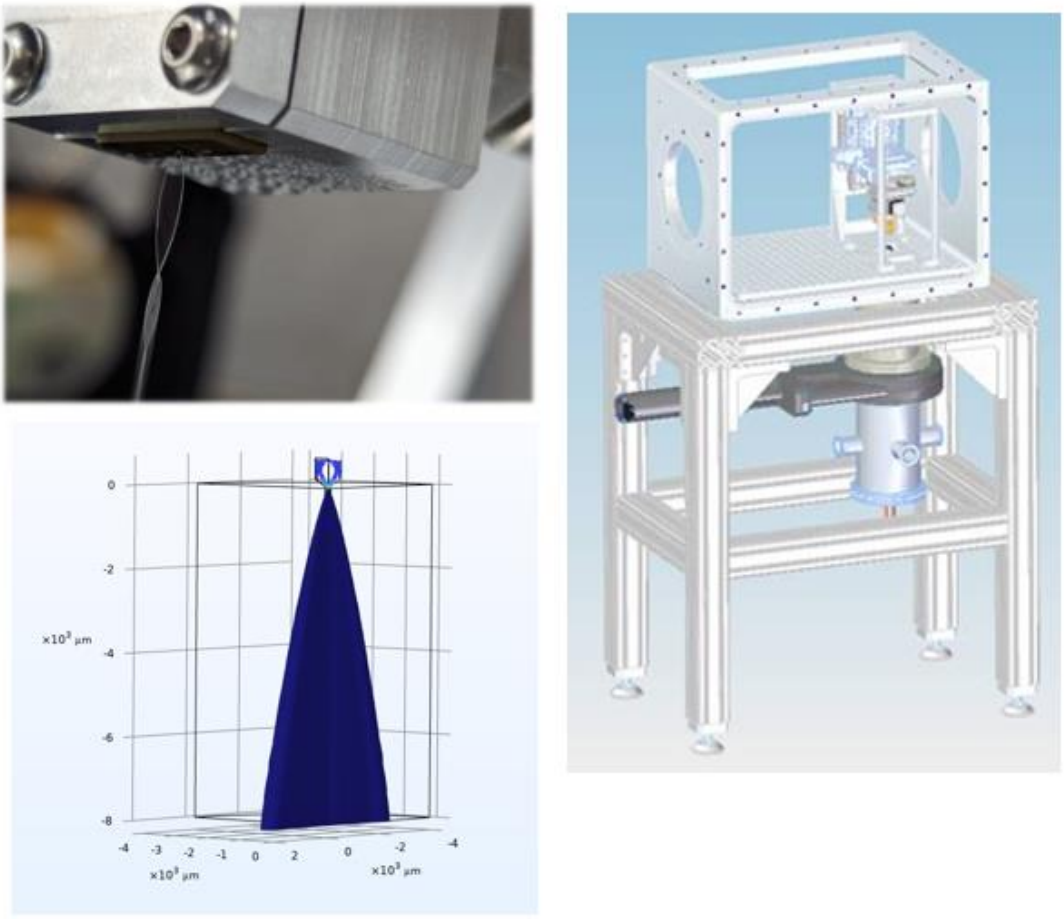

Figure 72: Liquid jet targetry developments. (Top left) A plastic/metal nozzle assembly creating a thin liquid leaf target; (Right) design for the target chamber installed in the EPAC test laboratory; (Bottom left) COMSOL simulation of a liquid jet from a custom nozzle

3.5.4 Solid targets

Alongside tape targetry, solid target systems will need to be developed that will field array-based targets. These will be medium repetition rate targets that will be supported on ‘pucks’ or smaller arrays within a larger holder. This technology is already being used on the Linac Coherent Light Source (LCLS) at SLAC and the European XFEL, and we have designed a target system to position this in the EA2 chamber. This target system is ready to be purchased when funding becomes available, and is suitable for use in the EA2 area.

A number of technologies will be able to provide targets to be mounted on these small arrays. One critical technology is Micro-Electro-Mechanical System (MEMS) targetry. The CLF DRIE

system is fully commissioned and operational, and has already been used to batch produce silicon-based targets. These targets can be fielded either on the array systems or on the High Accuracy Microtargetry System (HAMS) target wheel[18].

To provide many target arrays, it is clearly not possible to hand assemble targets, even for 1 Hz shot rates, so development has continued with the robotic assembly project. Further upgrades to the system, to include vision recognition and selection of good/bad targets, have improved the accuracy and the repeatability of the process. Targets have been assembled on the system and have been fielded on experiments on the European XFEL for the user commissioning of the DiPOLE laser system, and also on LCLS in the Matter in Extreme Conditions area. We plan to refine the system to work on multilayer targets as well as simple single layer foils, and to develop the user interface to make the system robust as well as flexible to different target array sizes.

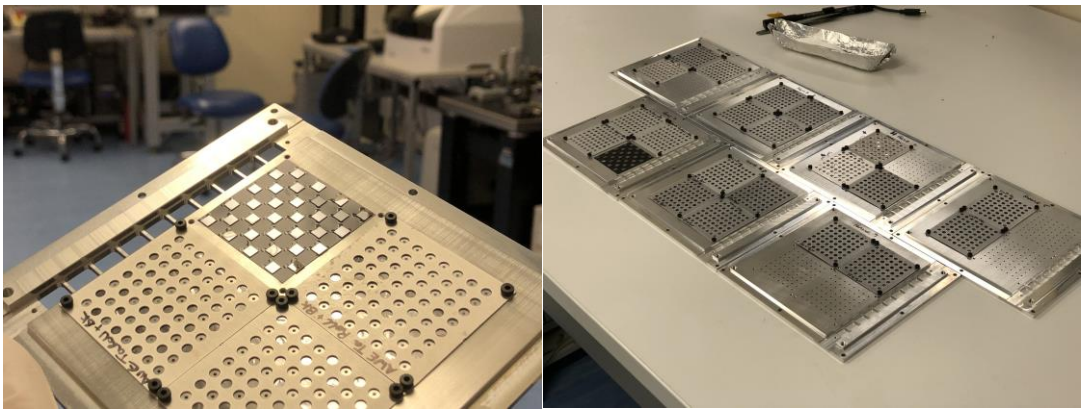

Figure 73: (left) Four small target arrays on the XFEL holder and (right) a set of seven target holders for the DiPOLE user commissioning experiment.

3.5.5 Developing Gemini TA2 as a test beamline for LWFA

In collaboration with our user groups, we are developing Gemini Target Area 2 as a prototype high repetition rate LWFA beamline. We have installed dielectric gratings in the compressor and confirmed that no significant damage or distortion occurs during full energy 5 Hz operation. We have also installed active drift stabilisation on the pointing of the laser beam exiting the compressor. The next steps will be to stabilise the wavefront of the beam on target, and ramp up to 5 Hz electron beams at ~ 100 MeV energy. When we have achieved stable performance, we will develop robust control routines for automated and machine-learning guided scanning, that can be directly translated to EPAC operations.

3.6 Future developments

3.6.1 EPAC long pulse capability

With the planned procurement of an additional pump laser in EPAC (see **Section 2.3.7**), the plan is to propagate this to one or more of the experimental areas. While these areas were always designed to operate with several additional beams, many of the initial user consultations focused on pump-probe set-ups with a future additional petawatt-class beam or lower energy auxiliary beam. The potential of EPAC to offer a 10 Hz petawatt beam in combination with high energy long pulse beam has garnered significant interest from the user community, including those who are starting to get the first results out of the similar D-100X capability on the European XFEL[19][20].

In recent months, potential users of such a setup have been approached to gain a better understanding of their requirements for addressing a range of scientific challenges. This information will be compiled in the coming months to influence the specifications of the new pump beam, as well as the requirements for beam transport and delivery down in the experimental areas. Areas of discussion have included pulse length (and shape), frequency conversion[21] and maximum energy deliverable at shorter (1 - 2 ns) pulse durations (c.f. EPAC's pump duration of 15 ns). The range of experimental setups requested will determine whether the long pulse setup could be initially delivered to just one experimental area, or whether an additional switchyard would be required to offer the capability to both.

3.6.2 High contrast laser operations

Whilst not currently funded for EA2, we have further explored options for improving the laser contrast for certain user experiments that require the lowest level of pre-pulses. Whilst high repetition rate plasma mirror substrate development is an active part of our targetry programme (see **Section 3.5.2**), the easiest route to higher contrast operations remains frequency doubling using a large area, thin KDP crystal[22].

As well as participating in experimental time on laser facilities that already have such a capability (for example, the Colorado State University's Laboratory for Advanced Lasers and Extreme Photonics), we are currently looking at whether it would be possible to procure a smaller area crystal for testing on Gemini and other similar systems. This latter approach would permit more in-depth testing with a range of our users, and a comparison with previous results from Gemini obtained with plasma mirrors. So far, through ongoing user consultations, it has been possible to identify groups interested in higher contrast operations, including those looking at hybrid ion acceleration schemes, high harmonic generation, plasma photonics and fundamental plasma physics.

4. Detectors

4.1 Scope and Overview of Progress

This chapter summarises the progress on detector and diagnostic designs, builds, and testing for the EPAC project. As with last year's report, a summary of the expected radiation characteristics for each radiation type is provided, together with an outline of the diagnostic projects planned or underway.

4.1.1 Scope

The detectors will be tailored to the emissions we expect from the EPAC facility, and designed to facilitate high repetition environments where possible. Whilst the exact emission will vary, depending on the experimental setup, we broadly know the regions of emission that we will need to address – x-ray, neutron, ion, electron, and THz. The energy of the emission is summarised in **Figure 74**, broken down by radiation type and mechanism.

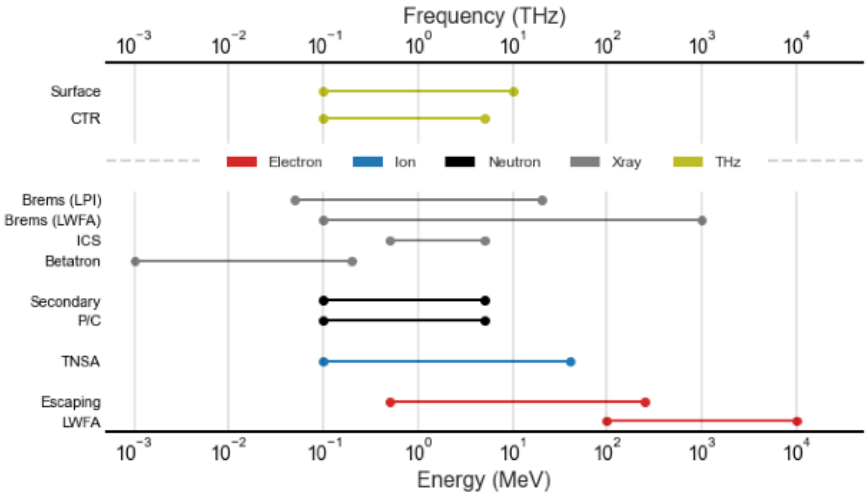

Figure 74: Approximate spectral characteristics expected from different mechanisms using the EPAC laser system

The primary focus of this year's developments has been on the x-ray diagnostics, and a paper summarising the expected characteristics from each mechanism shown in **Figure 74** was published late last year. The paper[23] focused on x-ray detectors for laser-plasma sources in general, but uses the expected parameters from EPAC to provide context to the discussion. **Figure 75** shows the expected scaling from each mechanism, with more detail in [23].

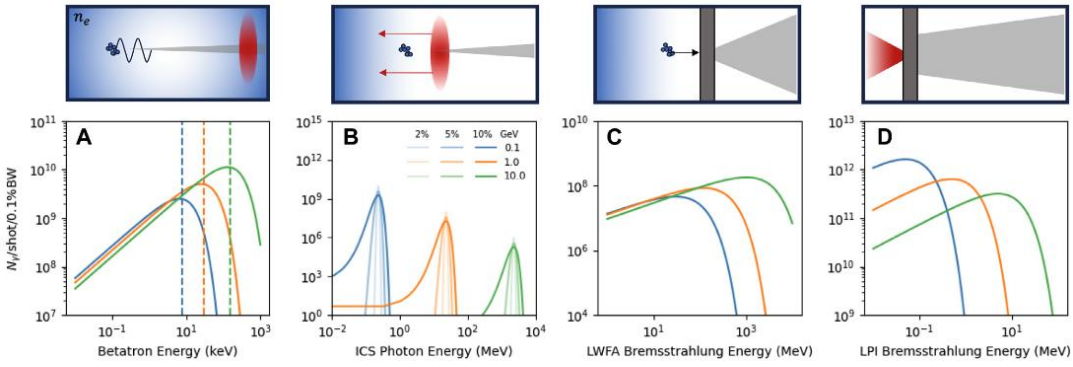

Figure 75: Schematic representation and example emission spectra for each x-ray generation mechanism by laser-plasma acceleration. (A) Betatron radiation, (B) inverse Compton scattering, (C) LWFA bremsstrahlung, and (D) direct target bremsstrahlung.

As a summary, the detector priorities have been split into two main categories:

- Imaging:
  - Sub-micron x-ray imaging (**SMXI**) for Betatron emission
  - Large-area-panel (**LAX**) for high sensitivity x-ray imaging
  - MeV detector (**MXI**) for ICS and Bremsstrahlung x-rays
  - Multi-Modal Imager (**MMI**) for simultaneous x-ray and neutron imaging

- Spectroscopy:
  - A Ross-pair Bayer pixelated array (**BKS**) for <100 keV narrow band spectroscopy
  - A linear-absorption-spectrometer (**LAS**) for spectral deconvolution over a broad set of energy and radiation types
  - Pixellated CZT detectors for direct x-ray spectroscopy (**Hex**)
  - Time of flight characterisation (**nTOF**) of fast neutrons
  - THz spectral characterisation with broad response (**THz**).

The radiation areas identified in **Figure 74** that are not directly covered by these detectors are being covered as part of the experimental area projects (Electrons/Ions) and EPIC consortium with TIFR (Electrons, X-ray, Ions).[19]

4.1.2 Progress

The primary milestones achieved this year are discussed in **Section 4.2**.

In addition, we have had the opportunity to test and develop diagnostic processes with help from the user community and wider projects, which is covered in **Section 4.3**.

4.2 Diagnostic updates

4.2.1 Pixelated spectroscopic CZT detector

HEXITEC is a fully spectroscopic hard x-ray detector developed by STFC, that delivers 1 keV energy resolution and operates from 5 to 600 keV. Each HEXITEC detector module comprises a CdZnTe detector with 80 x 80 pixels on a 250 µm pitch, bump bonded to the HEXITEC ASIC[24]. The detector modules have wire bonds on one edge and can be tiles into single 2 x N arrays[25].

Two 2 x 6 arrays are being produced for EPAC. They will each have 76,800 spectroscopic pixels that will be combined to provide an energy spectrum with up to ~10k photons per shot of the facility, and which can be operated in a 10 - 100 Hz frame rate, to keep the data bandwidth at a minimum. The detector can operate up to 10 kHz frame rate to monitor emissions during decay processes.

A prototype detector has been manufactured and used to develop the firmware and the software for the detector. All parts have been delivered to assemble the final systems to EPAC in 2024. The prototype highlighted some problems in the 10G data output signal integrity, but these have been solved, and a new assembly method has been developed to maintain a ~150 µm gap between modules to give a more continuous area for potential imaging applications.

[19] https://epic-innovation.org/

In **Figure 76(a)**, the inside of the prototype system with the readout board and the 2 x 6 array of HEXITEC modules is shown, with the EPAC 2 x 6 system shown on the right. **Figure 76(b)** shows the flat field images of the exposed detectors as an example of the performance/yield. Pixel yields of 99% are anticipated. The final deliverable detector modules for EPAC are in production and will be tested individually in a one channel system before assembly.

(a)

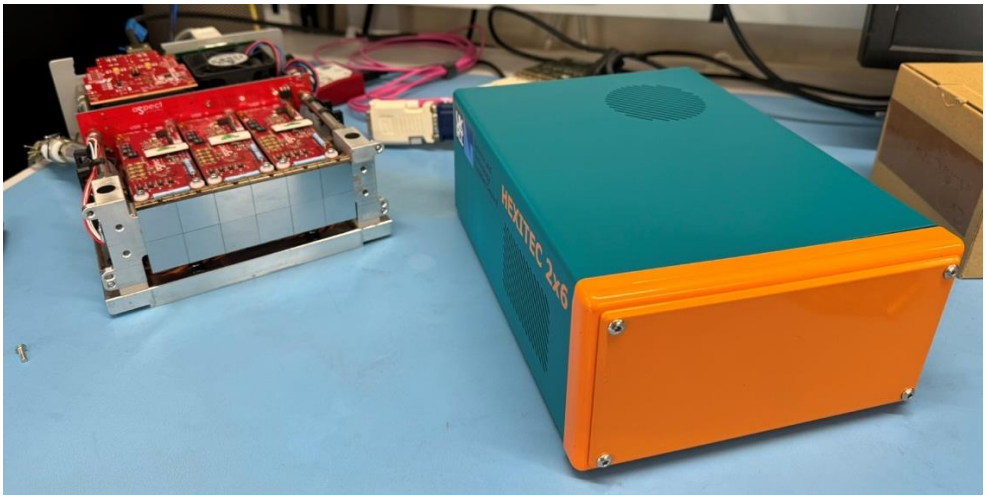

(b)

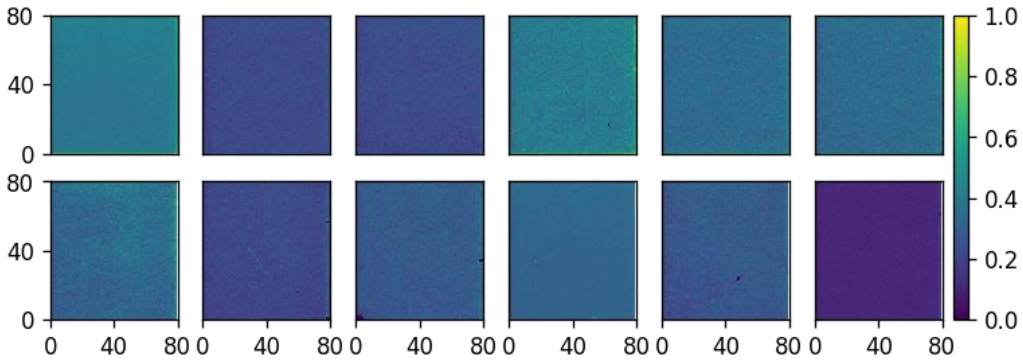

Figure 76: EPAC 2 x 6 Hexitec Build. (a) Shows the interior electronics and finished box; (b) shows the pixel-by-pixel flatfield for each of the sensors – final calibrations will be done after build is completed, to account for changes due to the readout electronics

4.2.2 Tiled MeV imaging (MXI)

4.2.2.1 Expanding the tiled build

Following the 2 x 2 prototype built last year, we established that the tiling method worked to increase the surface area of the detector, but that both the bezel and the lack of physical separation between tiles caused issues. To address these issues together, we have opted for a “lateral pinch” support structure to hold each scintillator, as shown in **Figure 77**. The interior walls are curved, high-grade aluminium, to give a deformable region that extends into the scintillator pocket. Scintillator tiles are inserted into these pockets; the walls deform and exert a lateral force to hold the scintillators in place. When each of the nine pockets is filled, the remaining separation between each tile is approximately 250 µm, significantly smaller than the optical bleed region measured in the 2 x 2 prototype. This wall shape also minimises the outer bezel size required, as no moving parts are needed to clamp the scintillators in place.

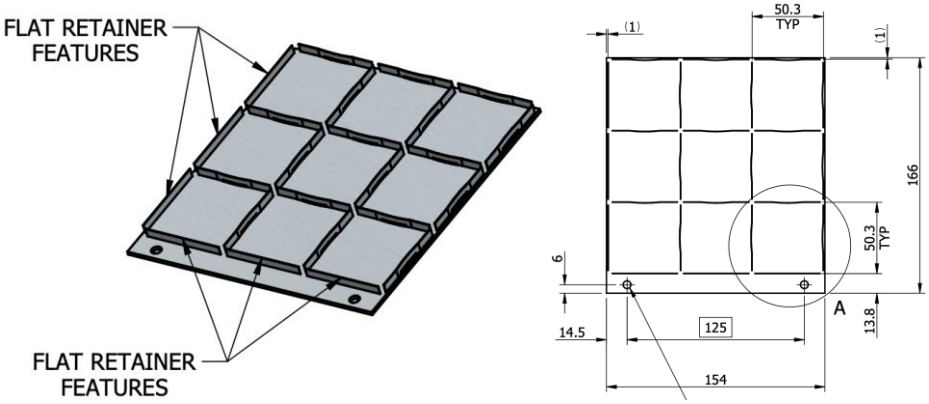

Figure 77: 3x3 Tiled scintillator design: images show schematic of frame and highlight the curved retaining wall that keeps the scintillators in position

The frame is machined from a single piece of 7000 series aluminium. This introduces one key difference between the prototype and this redesign, in that the back sheet of aluminium can no longer be removed to provide an optical line of sight from the x-ray side of the device. This makes it harder to minimise the reflection from the surface, and so the surfaces have been anodised to kill any stray reflection and sharpen the imaging quality. This design has higher tolerance requirements than the scintillators, with (+ 50 / -250 µm) lateral width limit on being able to support the scintillator screens.

4.2.2.2 Synthetic imaging results

While waiting for the scintillators to be produced, a thorough simulation study into the deposition profile and behaviour of x-ray distributions has been conducted. **Figure 78** presents the sensitivity and PSF curves expected for the energy deposition, calculated for monoenergetic energies up to 5 MeV. These simulations include the scatter induced by the backplate, and demonstrate the variation in energy deposition as a function of depth. For lower energy x-rays the deposition profile is non-linear, with significantly more energy deposited close to the x-ray side. This profile, in combination with the high numerical aperture lens system we are using, results in a non-uniform spatial resolution as a function of energy, which must be accounted for when considering the performance of the device.

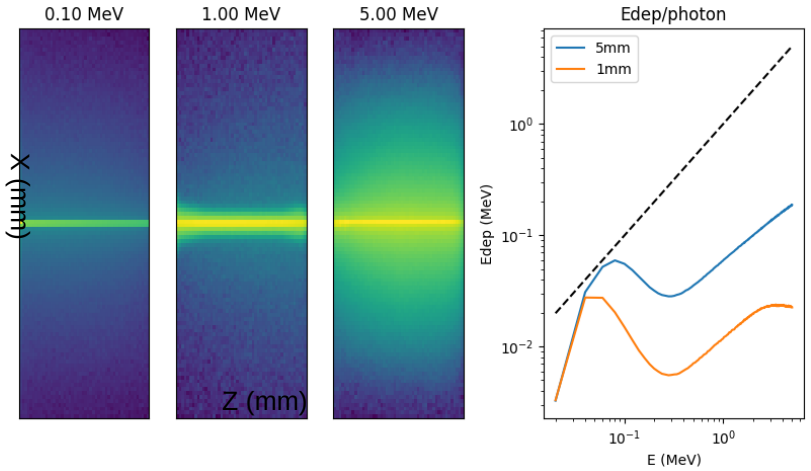

Figure 78: Deposition profile in the 1 and 5 mm YAG:Ce screens. The left panels demonstrate the spatial energy deposition for increasing energies of incident x-rays. The right panel shows the total absorbed energy fraction – at 1 MeV and above, the 5 mm screen has a stopping efficiency >10%.

Full synthetic images can also be produced using the same GEANT4 simulation toolkit, as shown in **Figure 79**. Here, a 5 MeV Boltzmann distribution is simulated with 10^7 photons incident on the frame in an isotropic distribution, resulting in approximately 10 - 100 photons per pixel – far below the expected signal in EPAC conditions. The signal-to-noise at these fluences is already reasonable, so we expect improvements to the contrast and signal-to-noise from EPAC parameters, albeit with a reduction in resolution when the effect of the optics is included.

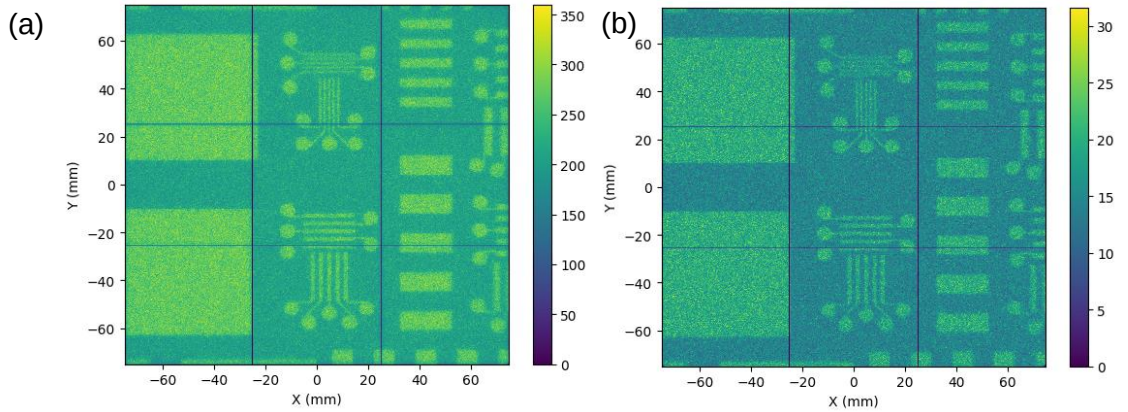

Figure 79: Modelled radiographs of a tungsten testgrid, showing the intrinsic resolution and relative contrast for a 5 MeV Boltzmann distribution incident on the a) 5 mm and b) 1 mm YAG:Ce screens

4.2.3 Linear absorption spectrometer (LAS) designs

Linear-absorption spectrometers[26][27][28] are the chosen method for broadband x-ray spectroscopy. These devices generally have a series of active layers, one behind the other, and each layer absorbs a fraction of the incident signal and transmits the rest. The attenuation in each layer is energy dependent, resulting in a variation in the layer-to-layer deposition. Knowing the attenuation profile of the linear absorption spectrometer, and the form of the incident radiation, it is possible to reconstruct the incident profile to high resolutions[27][29].

Here we present the finalised design for the EPAC Linear Absorption Spectrometers, presenting the crystal patterns for the initial Betatron, MeV Bremsstrahlung, and 100 MeV spectrometers. By default, the scintillators will be run with YAG:Ce scintillators, due to the concern of afterglow building and impacting data measurements; however, we have also procured CH and LYSO:Ce scintillators to provide flexibility in the response profile.

4.2.3.1 Shielding and housing design

The shielding and housing design for all the rail systems is provided below. The key requirement for the shielding is that the incident radiation coming in from other angles is minimised. As such, the lead is 20 mm in each direction (bar the viewing angle), with a narrow aperture (15 – 5 mm) that subtends a small solid angle from target. For 100 MeV spectroscopy, the collimator front plate can be extended, to increase the attenuation further.

The shielding is designed to maximise the field of view (FOV) of the camera and lens system, providing space for three full channels stacked vertically (with respect to the camera system). These channels correspond to a minor angular offset from the source and could be used to measure angular variations in the emitted spectra or, at a distance where the angular variation can be assumed to be low (~4 m), the crystal patterns could be different, to provide more energy bins from which to reconstruct the incident emission.

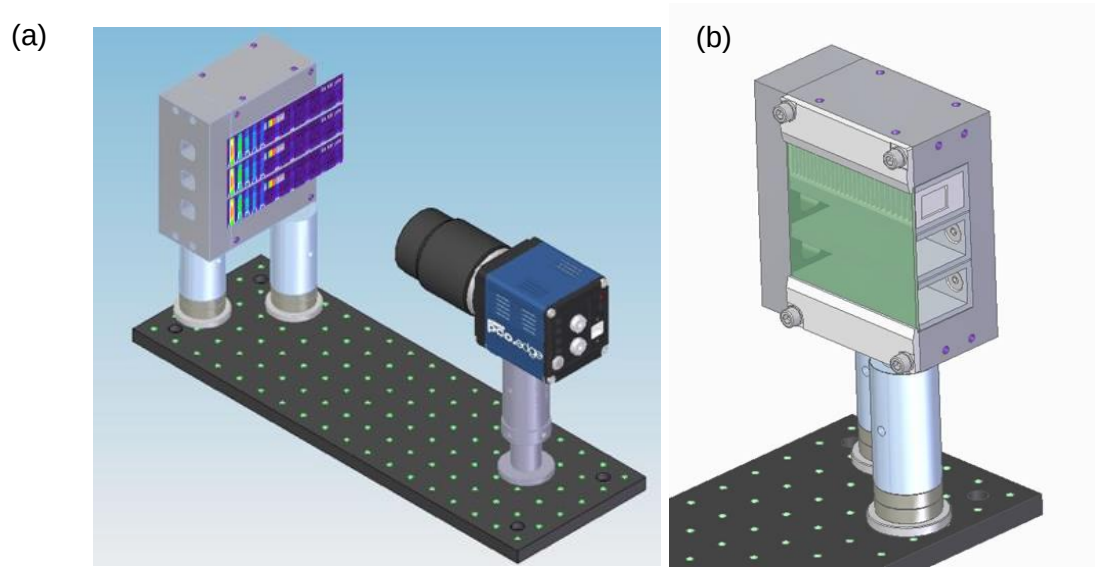

Figure 80: a) CAD model with representative LAS exposure images for the triple carriage design outlined in this report. b) Second view showing crystal holder and glass slide assembly.

4.2.3.2 Modelling of expected results

A synthetic diagnostic system was developed in Geant4 to model the expected results for the new crystal designs, following the outline in Swanson *et al.*[30] By factoring in hard hits, collection efficiency, and the x-ray deposition from Geant4, we are able to produce reasonable images for what we expect to measure when the device is built. **Figure 81** shows the expected working range of the device, spanning four orders of magnitude in photon flux (panel a) and an order of magnitude in critical energy (panel b) before the responses start to become difficult to analyse.

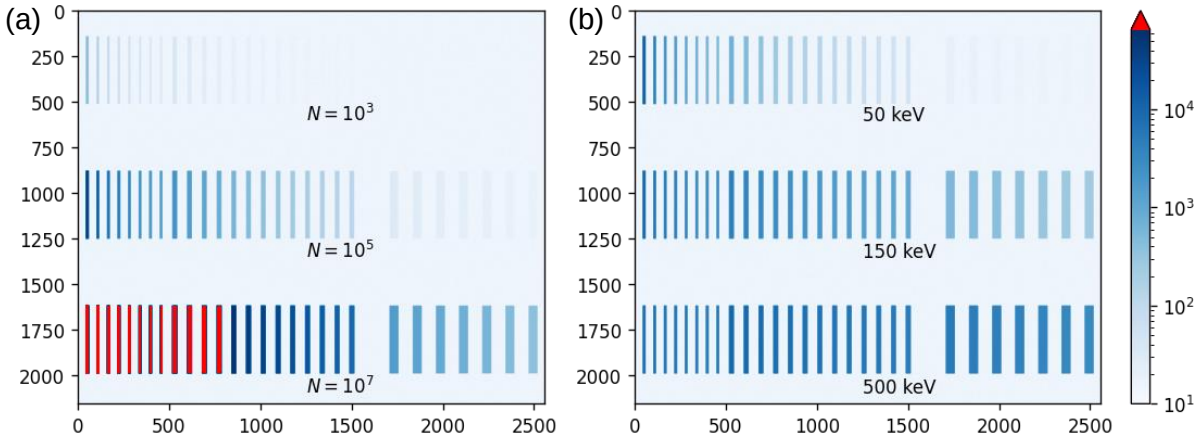

Figure 81: Synthetic image generated for a range of photon fluxes at a critical energy of 50 keV. b) Synthetic image generated for 10^5 photons at critical energies as indicated. Colourmap is shown in counts, where red indicates saturation.

These synthetic responses will be calibrated against measured results when the devices are built and tested later this year. However, synthetic images created based on existing LAS versions, shown in **Figure 82**, demonstrate the validity of this technique, with good agreement between the measured data and synthetically produced data. Here the noise term in the modelling was increased to match the camera performance, and the magnification of the lens was adjusted to match the FOV in the measured data.

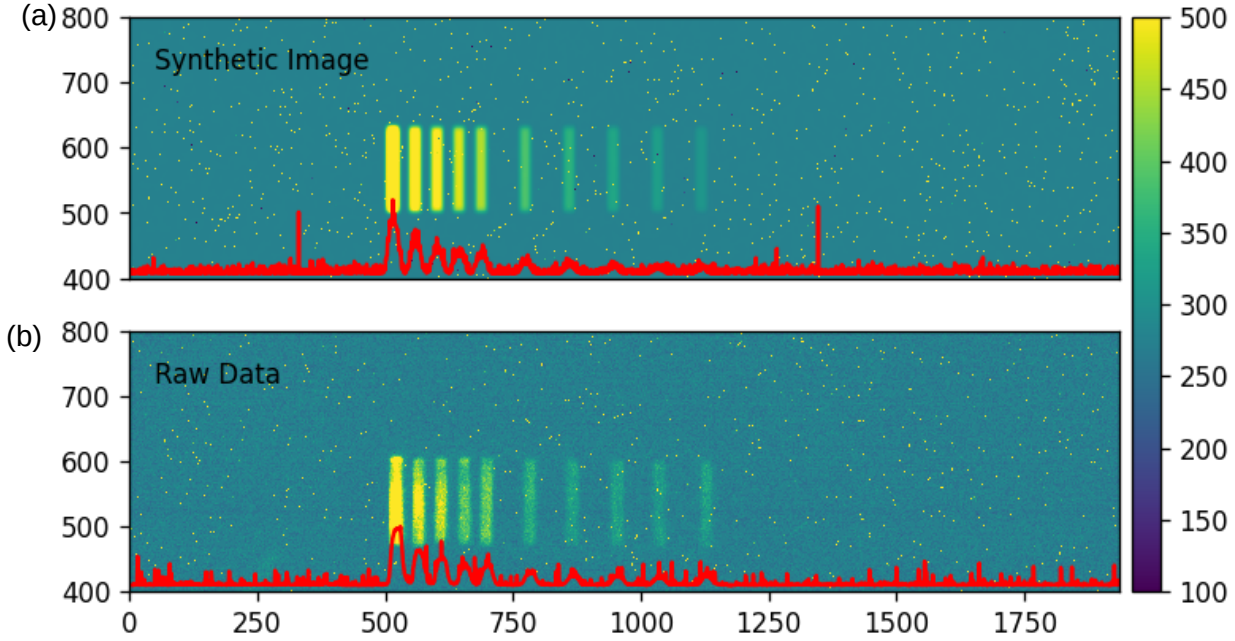

Figure 82: Comparison between synthetic images generated using the same process as described in [30] and real data measured from previous versions of the LAS [27]

4.2.4 THz interferometer design

4.2.4.1 Prototype results with broadband source

Last year, initial testing of several areal detectors for THz radiation took place; this year, we have implemented two of these sensors into a modified Mach-Zehnder interferometer design to permit broadband spectral characterisation of incident THz pulses, and have conducted testing on a further two. The setup is shown in **Figure 83 (left)**, showing the necessary delay line and position of each camera.

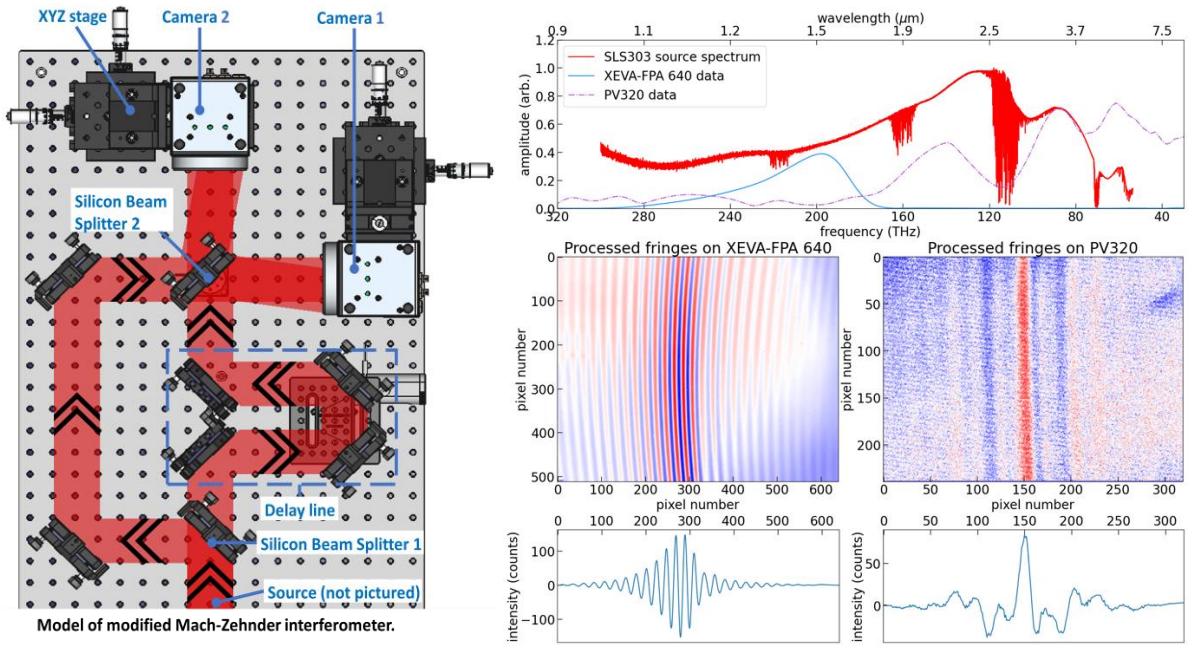

Figure 83: THz Spectrometer schematic and results from characterisation using a CW source

As with other emitted radiation, it is difficult to obtain similar pulse characteristics to those that we expect to measure on EPAC without an equivalent source. To characterise the performance of the system, we have used a broadband THz source to generate a controlled incident spectra; from this, the measured interferograms and Fourier transform (shown in **Figure 83 (right)**) provide a calibration to determine the response of the system. Work is underway to determine if the prominent gap in response at ~2 μm is due to the system efficiency or the source profile itself. For shorter wavelengths, we can introduce a near-IR spectrometer to provide further information at these frequencies.

4.2.4.2 Reconstruction of fs pulses

This spectrometer will be used in EPAC to provide longitudinal profile measurements of the accelerated electron beams. Using a combination of PIC simulations to generate the expected electron profiles, we were able to determine the expected coherent transition radiation (CTR) emission from such a profile, and then reconstruct the temporal profile from that expected emission. This required the implementation of Kramers-Kronig minimum phase retrieval algorithm[31] to convert the measured frequency space back to a temporal domain. The resolution of this process, factoring in the pixel resolution from the detectors, is expected to be ~1.7 fs, and a total temporal range of ~ps, providing sufficient resolution and range to characterise any trailing electron bunches.

In EPAC, the measurement sensitivity will be heavily dependent on the collection optic. As the electron beamline matures and the source is more understood, we will know the final resolution limits – or total sensitivity – that the instrument will have.

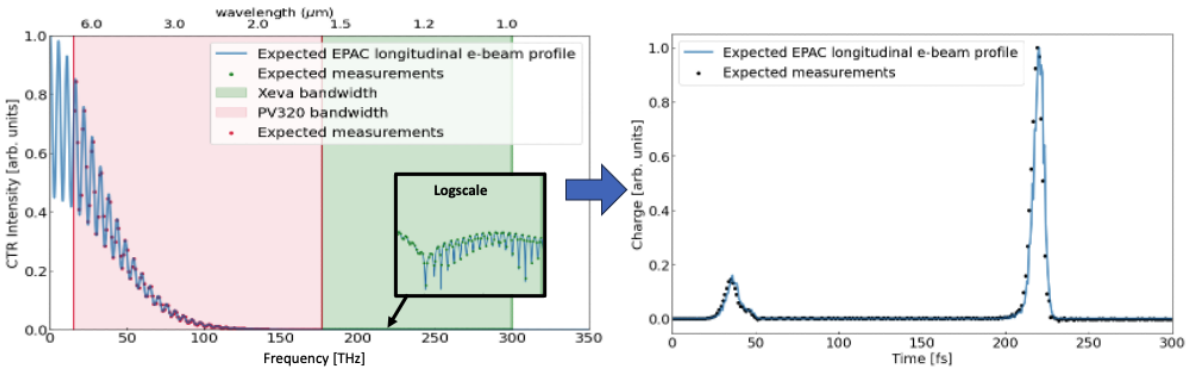

Figure 84: Reconstruction of simulated electron bunch structure from PIC simulations. The left panel shows the expected CTR measurement as a function of frequency, and the right panel shows the temporal profile extracted from EPOCH (blue) versus the reconstructed data the iterative Kramers Kronig algorithm.[31]

4.2.5 Ultra-fast nTOF instruments and calibration

An ellipsoidal capped conical scintillator is being developed for efficient and fast temporal resolution measurement of laser driven radiation sources: a schematic is shown in **Figure 85a**. In conventionally shaped scintillators (often cuboidal, cylindrical, spherical, or composites of these), the total internal reflection of isotropically emitted scintillation photons within the scintillator volume leads to a temporal dilation of the photon pulse that reaches the photo-detector, as photons take a myriad of paths and undergo multiple reflections to reach it.

An ellipsoidal capped cone design minimises the path length differences from scintillation event to detector location, therefore enhancing the temporal resolution capability. Residual total internal reflection can also be minimised by use of anti-reflective coating or by introducing roughness to the optical surface, as shown in **Figure 85b**. In this way we can take advantage of the detection efficiency of large volume scintillators, whilst preserving a fast temporal response. Simulations show that a temporal response of 250 ps is expected for the scintillator geometry we have chosen. Accordingly, to harness the temporal responsiveness of the detector, a scintillator has been manufactured to this shape using the fast scintillator BC-442Q, which has rise and decay times of 110 ps and 700 ps, respectively, coupled to a Photek DS006 MCP-PMT with a characteristic response time of 60 - 100 ps.

Initial testing of the shaped scintillator's response to protons has been conducted at the M40 cyclotron at the University of Birmingham. Single event analysis from the cyclotron demonstrates significant temporal response improvement for the shaped scintillator over the unshaped one for same scintillator compound BC-422Q: the decay time is observed to be 230±13 ps, a factor of three faster than the manufacturer's quote. Tests are ongoing using ^{60}Co and ^{241}AmBe sealed radiation sources to assess the response to MeV x-ray and neutrons.

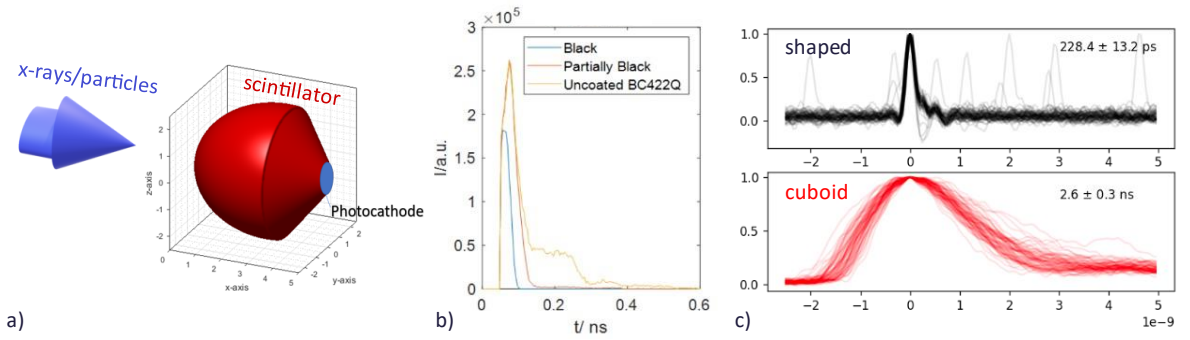

Figure 85: a) Schematic layout of ellipsoidal nTOF scintillator; b) the expected temporal response showing a volumetric limit of approximately 150 ps; c) the measured results from the initial testing, demonstrating a 228 +/- 13 ps response to incident protons

4.3 Community engagement

4.3.1 kHz x-ray characterisation (TIFR Hyderabad, EPIC)

Under the EPIC programme, we have been developing high repetition x-ray diagnostics with TIFR Hyderabad. The intent for EPAC is to use these fast systems to monitor the (γ, n) isomer activation of bismuth, which is expected to have a half-life of a few milliseconds and a critical energy at 1.5 MeV. The system at Hyderabad is not sufficient to generate the 10s of MeV required to activate bismuth, but it is sufficient to deposit the equivalent total energy in the scintillator at the desired repetition rate. As a test of the device, it was run concurrently with a large area sodium iodide detector: the difference in the response was used to determine the effective temperature of the incident x-rays and the flux.

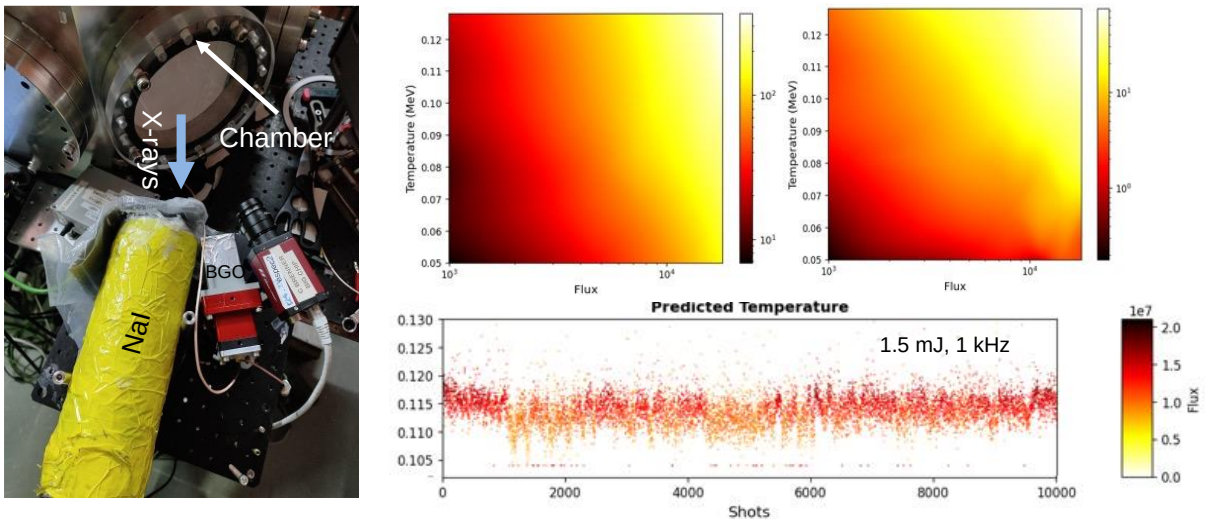

Figure 86: KHz x-rays measurements at TIFR.

4.3.2 Detector calibration facilities at the CLF (UCL)

Once EPAC operations begin, there is going to be a growing need for repeated calibrations with known sources as scintillator heads, and detector configurations will likely change or be exposed to different radiation types, energies, and fluences. To maximise the capabilities of EPAC, we have organised the loan of a dedicated shielding enclosure for a high brilliance x-ray tube source from UCL, and procured high activity sealed sources, including ^{60}Co, ^{22}Na and ^{152}Eu.

The x-ray tube is a 250 W, 160 kV liquid metal jet, with a Gd anode capable of producing 1.7 x 10^{10} photons per mRad per s, with the distribution as shown in **Figure 87**. Within the enclosure, this translates to 25 x 10^{6} x-ray photons per pixel per second (for the large area panel detector), which is approximately equivalent to the number of photons expected per shot from the betatron source in EPAC (150 x 10^{6}) at the same distance. Therefore, excluding the read noise from the sensor and the difference in spectral shape, the expected signal levels can be reached for all betatron detectors by exposing them to the new source for a period of six seconds. Varying the tube voltage from 30 kV to 160 kV also allows us to match the average deposition energy of betatron critical energies from 10 keV to 60 keV in the scintillator systems.

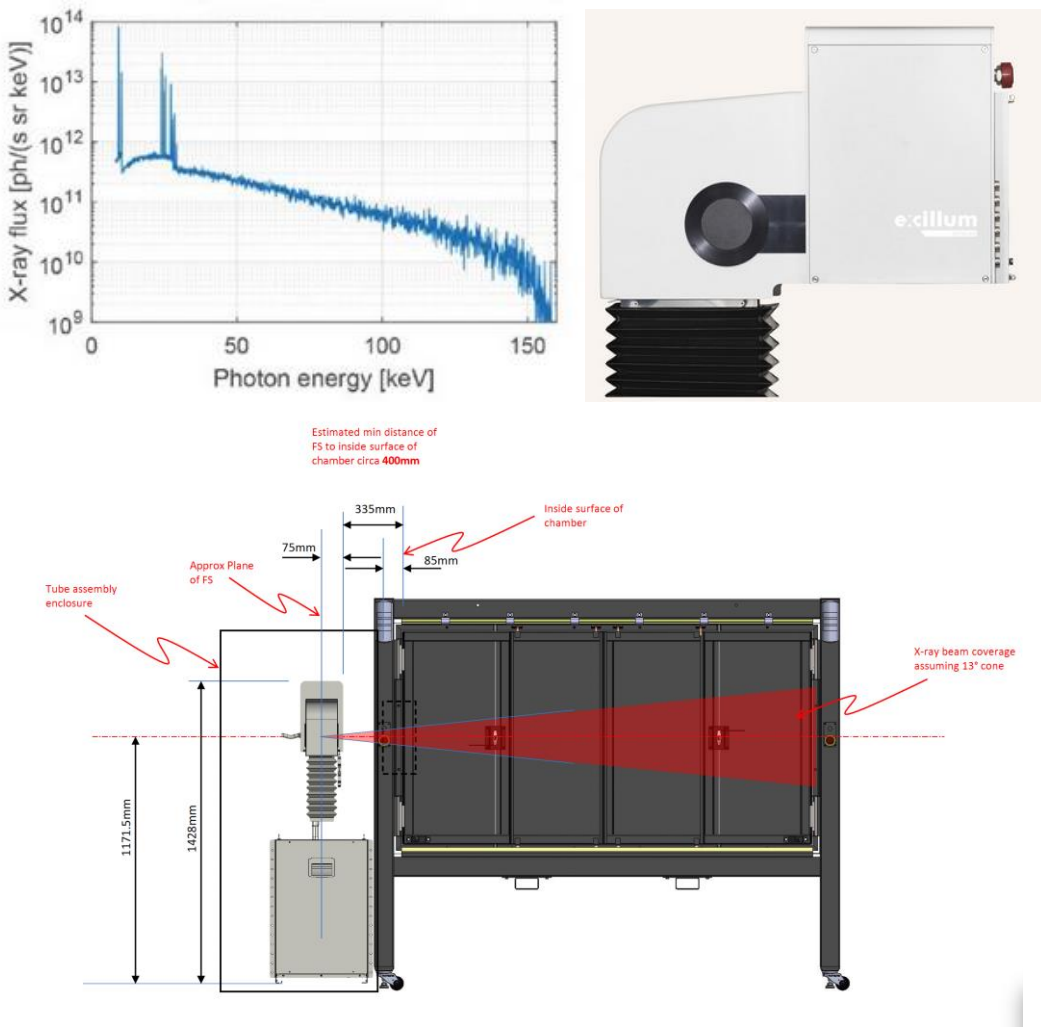

Figure 87: X-ray calibration tube for EPAC diagnostic development. Top panels show the expected spectra from the x-ray tube and an image from the suppliers of the tube-head. Bottom panel shows the layout for the shielding enclosure.

The sealed sources we have procured permit testing at x-ray energies far beyond these limits: the high activity ^{22}Na and ^{60}Co have 0.511 MeV and 1.1/1.2 MeV lines respectively. At these energies, the x-ray deposition profile is expected to be uniform through the thick detectors. This mitigates concerns related to non-uniform light emission in scintillators, and allows better (albeit slower and less efficient) calibration than expected with EPAC spectral profiles.

5. Data management and computed tomography

5.1 Overview

The data management system (DMS) in EPAC has the following functionalities:

- Acquires data from scientific instruments
- Provides an interface to orchestrate experiments and control the data flow from them
- Stores this data in a standard format
- Provides the tools to manage this data throughout its life
- Provides tools for facility users to analyse their data
- Archives the data for a long term.

The main components of the DMS include: (1) data acquisition and display; (2) data transfer pipelines and data broker (Apache Kafka); (3) data controllers and user interfaces; and (4) the scientific computing services (facility data pipelines) offered by STFC's Scientific Computing Department (SCD), which comprise data storage, archive and provisions for data access and analysis. (1) – (3) will be hosted in EPAC, while (4) will be operated from SCD in R89 on the STFC-RAL campus. An overview of the DMS architecture is shown in **Figure 88**.

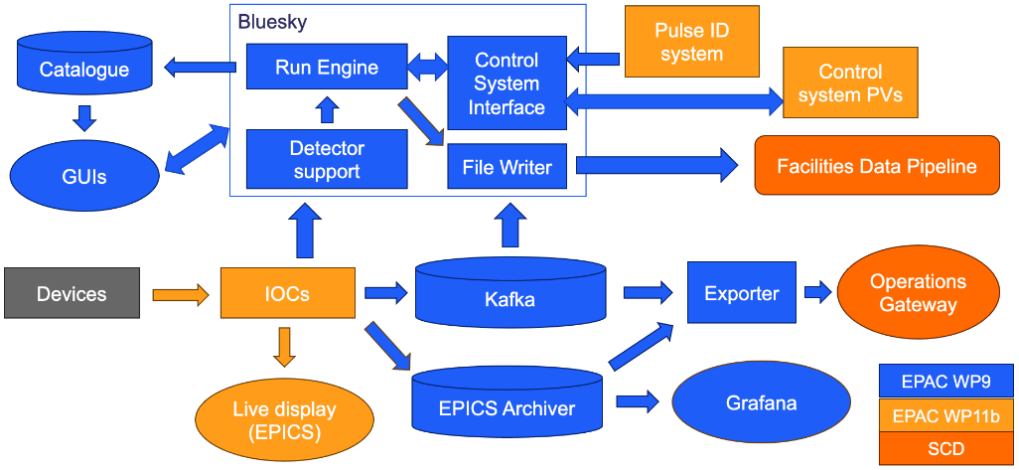

Figure 88: DMS architecture

Since the last report, the design of the data management system has become significantly more detailed. The main software components required for the early phase of EPAC are in an advanced stage of development. The hardware infrastructure required (network system, servers etc.) has been installed, so that initial tests can take place over the next few months. We are now concentrating on developing the connections between components, interfaces with the control system, and user interfaces, as well as advanced data acquisition features such as experiment orchestrators. In parallel, the Facilities Data Pipeline, comprising data storage, analysis and archiving suites, is being designed. We have also engaged with potential users and other stakeholders to ensure that our approach will be suitable for them.

In this report, we provide an update on the infrastructure behind the data management system, as well as progress on the development of key software solutions in EPAC. The main focus of the latter is on Bluesky, which is being adopted to fill the roles of *DAQ manager* and *experiment orchestrator* described in previous reports. We also cover proposed solutions for data display, updates on the Facilities Data Pipeline and the Computed Tomography package, and briefly outline plans for Digital Lab Books and EPAC's Data Policy.

5.2 Progress update on infrastructure installation

5.2.1 Network infrastructure in EPAC

The network infrastructure in EPAC is designed to cater for the high data rates (few GB/s) we anticipate in the facility. The initial network that came with the building has now been upgraded to employ a future-proof hub and spoke network topology, featuring two hubs on separate floors, as shown in **Figure 89** and **Figure 90**. This architecture provides enhanced redundancy and high availability. Each hub serves as a central point for connectivity, with spokes extending to various endpoints throughout the facility. With this architecture, even if one hub or floor experiences a disruption, the other hub can maintain network operations seamlessly. A single-mode fibre network fortifies reliability by ensuring consistent high-speed data transmission, critical for the facility's operations. This topology not only enhances the reliability and fault tolerance of the network by providing two distinct fibre routes, but also allows for scalability and adaptability to future technological advancements, providing reassurance about the network's longevity and relevance.

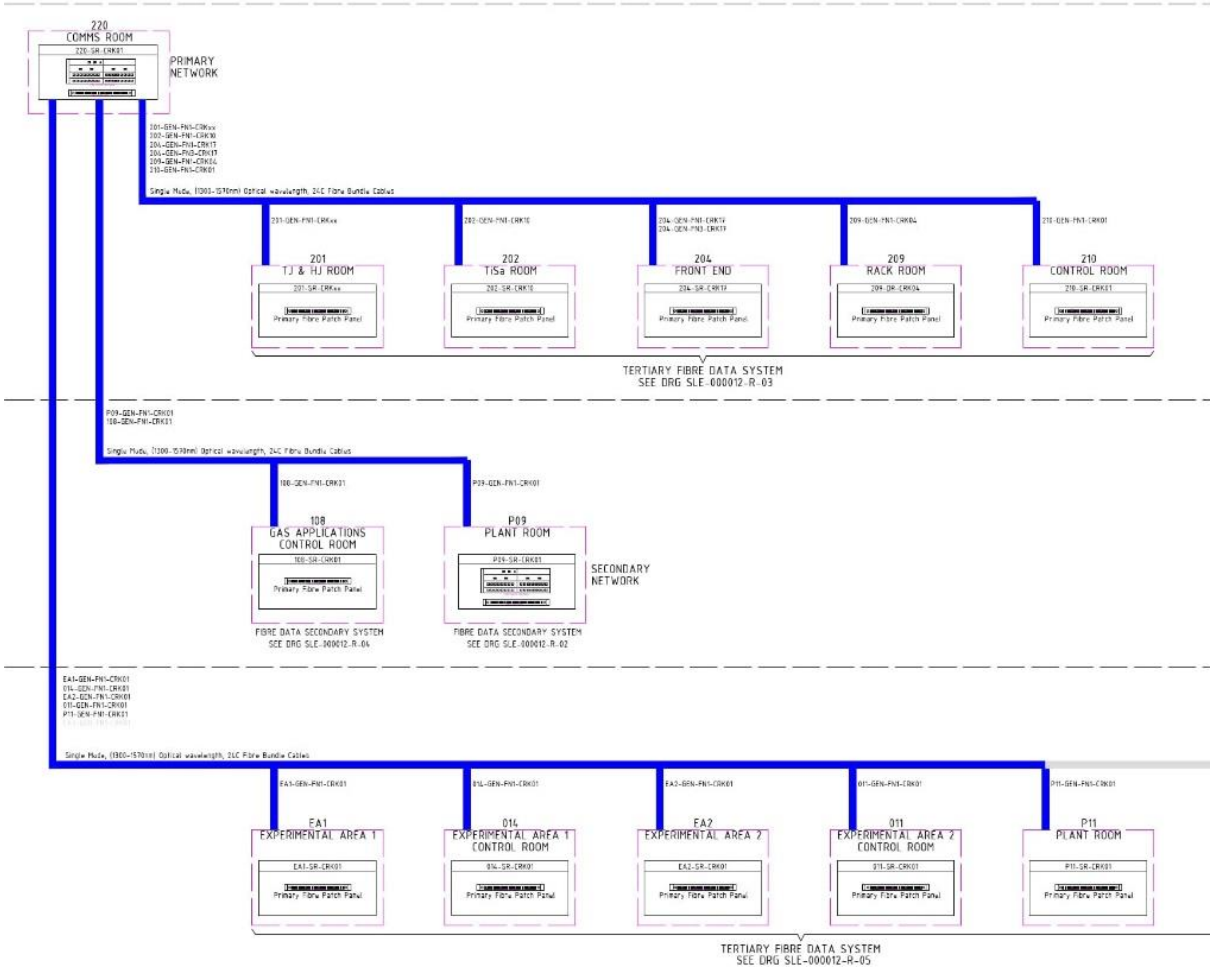

Figure 89: Primary network architecture in EPAC

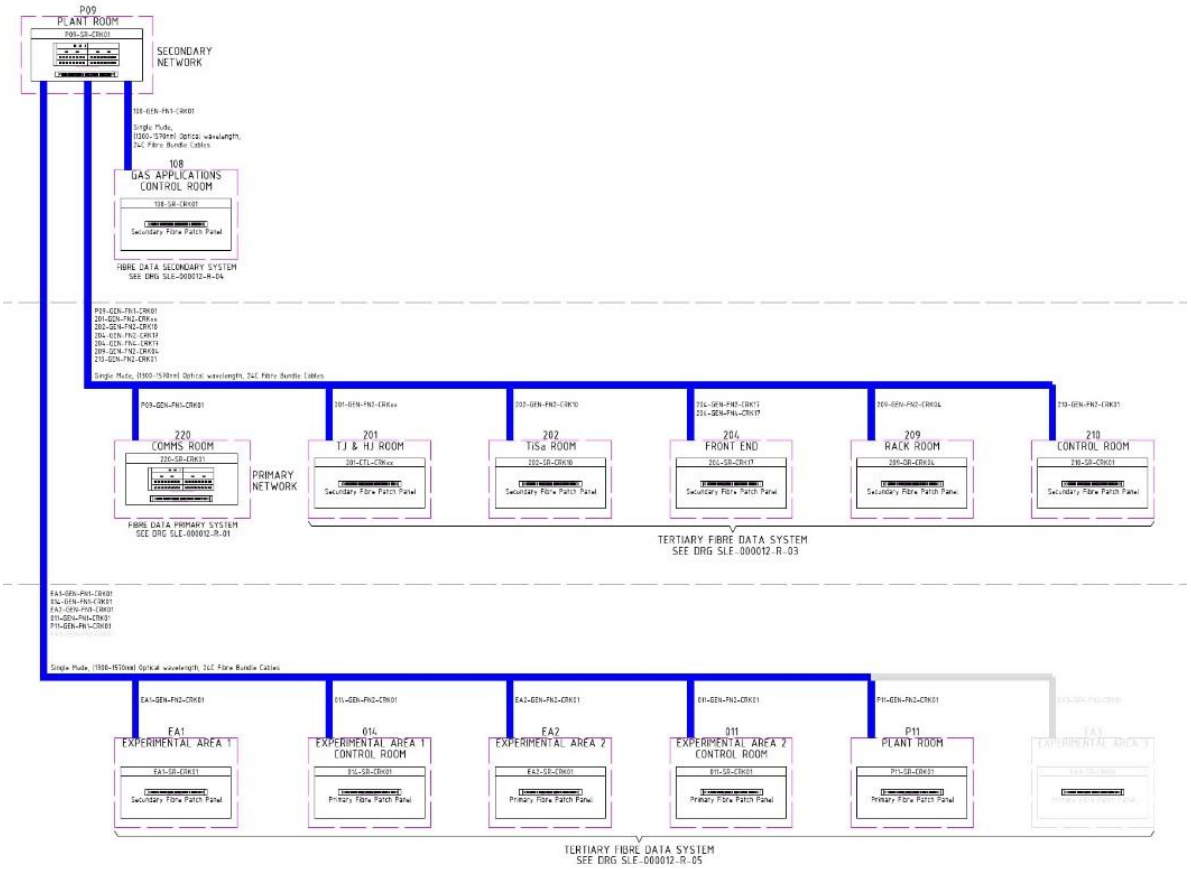

Figure 90: Secondary network architecture in EPAC

5.2.1.1 Network design approach in EPAC

A careful network design and segmentation approach is being implemented to ensure the physical separation of devices and infrastructure for different networks, such as the STFC-RAL network, PLC network, and other networks that use different IP subnet ranges in public and private address spaces, despite utilising the same redundant fibre backbone. This is achieved by separately setting up distinct network switches, routers, and security devices with varying topological requirements. Logical segmentation is achieved through Virtual LAN (VLAN) configurations, access control mechanisms, and firewall rules that control traffic between different networks. Only authorised communication is permitted to pass through.

The Interlocks network will use a separate hardware and cabling infrastructure, but a security bridge will connect it to the control network. Policies and rules will also be used to maintain stringent access to relevant data.

We have employed VLANs for organising and segregating devices within the EPAC LAB infrastructure. VLANs enable the creation of isolated broadcast domains, ensuring that devices with distinct purposes operate within dedicated segments. For instance, in Room 2.04 separate VLANs are assigned for diagnostics (192.168.214.0/24) and control devices (192.168.204.0/24), using VLANs 214 and 204. The numbers 2 and 4 act as identifiers for the room. Access control lists (ACLs) will reinforce network security by complementing VLANs and defining rules for controlled traffic flow between VLANs. **Figure 91** shows an example of the VLAN architecture. Aruba's Virtual Switching Extension (VSX) technology enables active-active high availability and seamless failover for critical network services. It enhances network resiliency by distributing traffic across multiple paths, minimising downtime due to hardware

failures or maintenance, and ensuring continuous operations. We also employ several ‘layer 2’ techniques for enhanced network security in EPAC.

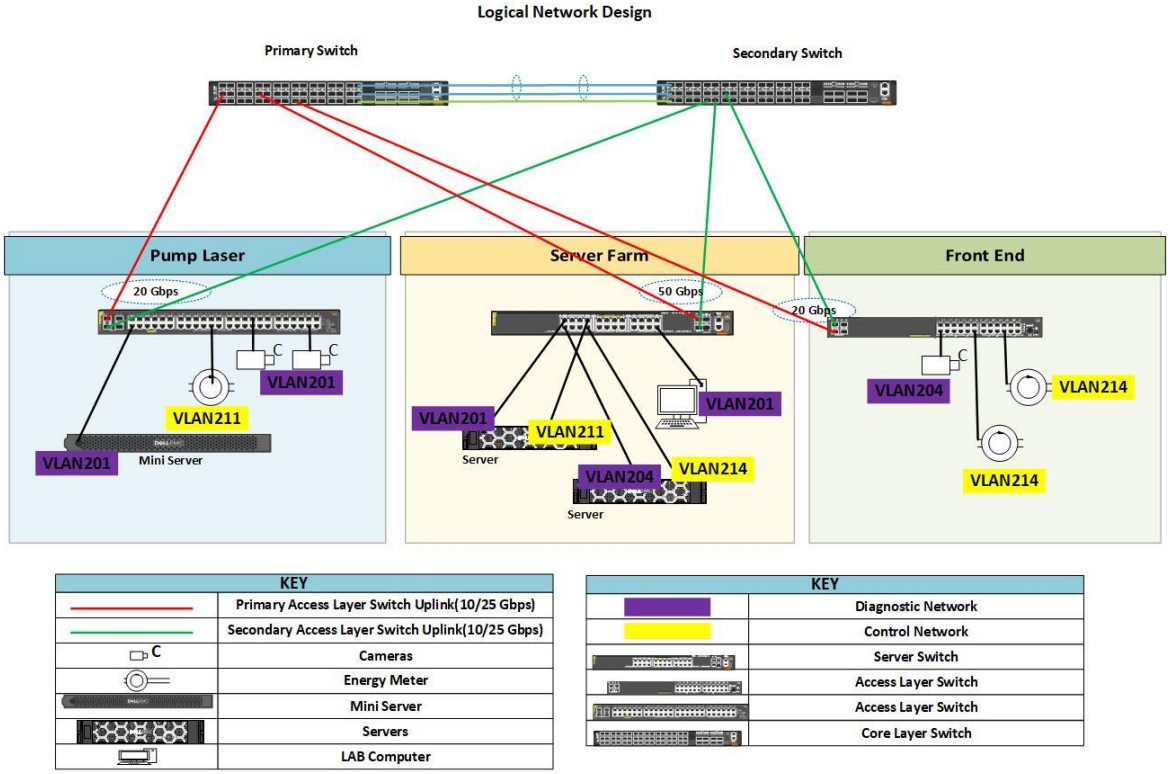

Figure 91: Example of VLAN architecture in EPAC

5.2.2 Data management infrastructure

The data management infrastructure consists of:

- the hardware on which the data management software will be running
- the libraries and services used to move data from one place to another.

The hardware for initial EPAC operations consists of six servers, which have been installed. Setting them up and installing software on them has been slightly delayed by the need to procure networking hardware.

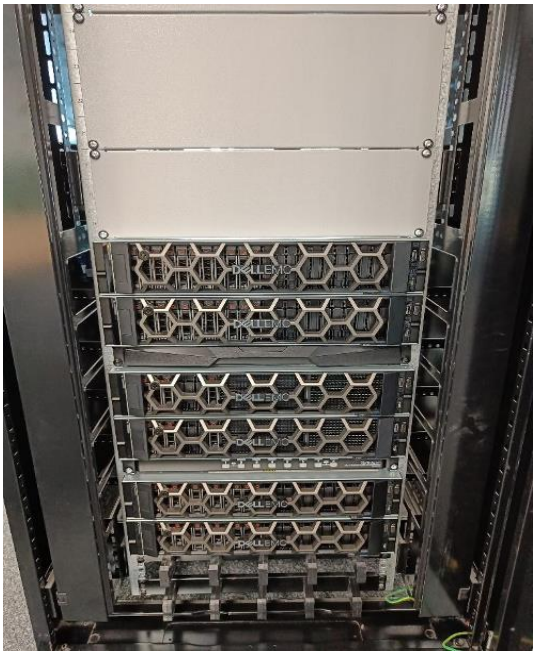

Figure 92: Initial data management servers installed in EPAC

Development of the main software components that go in them is largely complete. The integration of these components along with new features is yet to be done, but we now have a solid foundation on which to build them.

The file writer library is now functional. Full-featured Python and Rust applications using this library have been built, demonstrating that it is ready for widespread use. Additional features planned involve metadata support and additional customisation options. Former plans to develop a file writer service have been put on hold, with the functionality now implemented as a Bluesky “plugin” (see below).

In addition to ADKafka, which produces image data to Apache Kafka, we have implemented a “forwarder” to handle scalar and waveform data. This is a Python application built from scratch, rather than using the existing ESS forwarder, which was not considered flexible enough to handle all our needs.

Currently, the data formats used in Kafka are based on or identical to the formats developed by ESS. We have not found any technical problems with these formats and reusing them may allow us to reuse code in the future. We do, however, have some concerns about the uniform application of metadata to different data types, and we may migrate to our own data format in the future.

5.3 Progress update on software solutions

5.3.1 Experimental user interface: Bluesky

5.3.1.1 Overview

Although the GUI’s in the control system would provide sufficient levels of control for the operators of the facility, the experimental users in EPAC will require a separate interface for setting up and acquiring data, interfacing with the control system. This is especially true for the “scan” type data acquisition where a series of actions (such as movement of stages, triggering of diagnostics, acquisition, and movement of data into files) need to happen in a sequence. This requires a system with the capabilities of a *DAQ manager,* which will tie together other systems (principally the laser control system and the file writer) to provide basic data acquisition capabilities, as well as those of an *experiment orchestrator*, which can provide advanced data acquisition capabilities, interfacing with other systems directly.

5.3.1.2 Bluesky for EPAC

In EPAC, we are considering Bluesky as the system that can fulfill the roles of both *DAQ manager* and *experiment orchestrator.* Bluesky[20] is a framework for data acquisition and data management that was developed by a collaboration between several accelerator facilities in the USA and is now being adopted more widely, notably also at Diamond Light Source for the Diamond-II project. It is made of several Python libraries designed to work closely together, while still being extensible. The key components of Bluesky are:

- ophyd, an abstraction layer for accessing devices from Python
- bluesky, providing a RunEngine to execute “plans” and collect data
- databroker, an interface to access data previously collected by the RunEngine.

Bluesky is a powerful system and, since it has been adopted at many other user facilities, it would make an excellent foundation for data management at EPAC. Furthermore, the EPICS and Bluesky collaboration is open to new partners, and a local on-site collaboration of developers is growing with increased efforts from Diamond Light Source.

There are, however, certain assumptions built into Bluesky and its associated libraries that are not aligned with the operational philosophies of our existing facilities, and so some work will be needed to adopt it.

[20] https://blueskyproject.io/

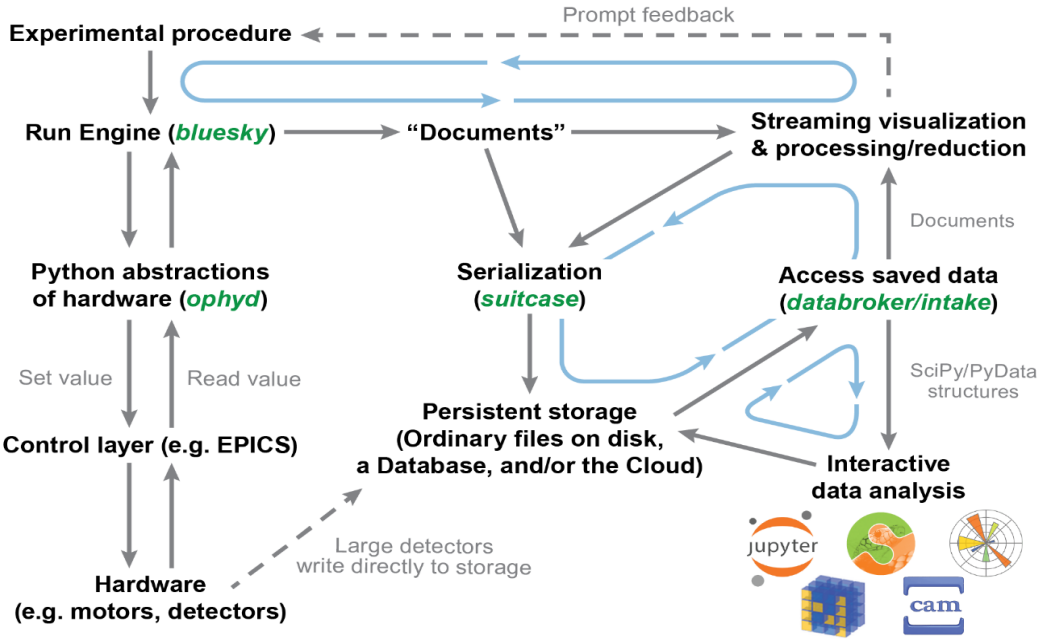

Figure 93: Concept of Bluesky

5.3.1.3 Limitations

The Bluesky data model assumes that no more data can be added to a run once it is complete. Many laser-plasma experiments, particularly low repetition rate ones, rely on image plate and RCF (radiochromic film). These cannot be developed and scanned until after the shots have taken place, and so the data is not available until after the fact. Although we are not expecting to use "single-shot" diagnostics of these types in EPAC, this makes it difficult to incorporate them into the Bluesky data model.

Bluesky assumes that each "event" will collect data from all detectors in use. There is no room for missing data in Bluesky. While this is an important simplification for the data analyst, it introduces challenges for data acquisition. With laser-plasma experiments typically having many diagnostics, transient failures are uncommon but not unheard-of. In such a case, depending on the importance of the diagnostic, the desired behaviour may be to carry on with missing data or to retry that measurement. The Bluesky data model makes the first option apparently impossible, and additional work may be needed to implement the second option. The default behaviour of Bluesky in such a case would be to abort the entire run.

These limitations for the use of Bluesky at a laser facility mean that resources must be invested in first understanding the detailed use-cases for Bluesky at EPAC, and then adopting and further developing Bluesky to meet the needs of EPAC. We are now engaging with Observatory Sciences for this development.

5.3.1.4 Role of Bluesky in EPAC

Bluesky will be the main data acquisition platform for users in EPAC. As well as taking on the role of the *experiment orchestrator*, it has also assumed the role of the *DAQ manager*. These are no longer considered separate components, and these two terms are no longer used in the design of the data management system. The Bluesky data broker will be the main cataloguing system for data and metadata.

Bluesky is not designed to handle large volumes of data directly, so we will still rely on Kafka for bulk data transport. The level of integration between Kafka and Bluesky will depend on requirements and availability of effort. One option is for Bluesky to handle metadata and experiment control only, while another option is for Bluesky to have direct access to data in Kafka using the same model it uses to access image files.

5.3.1.5 Experimental user interfaces

Bluesky is a Python library and is typically used as part of an interactive Python session. While this is suitable for those who originally developed Bluesky and for trained beamline scientists, it is not appropriate for most users. Several user interface concepts are being developed by the Bluesky community to address this shortcoming. Here, we describe the user interfaces we propose to provide to users, to control and monitor data acquisition through Bluesky.

The first will be an “advanced” or “programmer’s” interface. Like existing interfaces based on IPython, this will provide direct access to a Python interpreter running Bluesky. Important components will be pre-loaded and pre-configured, so that the user can start setting up scans and taking data immediately. It will be based on Jupyter Lab, running in a web browser, so that it can be accessed from any workstation in the control room and provide rich graphical output. The ability to save “notebooks” and re-run code will make it possible for users to establish a workflow that they can repeat multiple times, without needing advanced programming knowledge. The integration of data acquisition into a scientific Python environment allows a tight loop between data acquisition and data analysis. A proof-of-concept of such an interface has already been developed, as shown in **Figure 95**. This user interface should be available for use well before project completion.

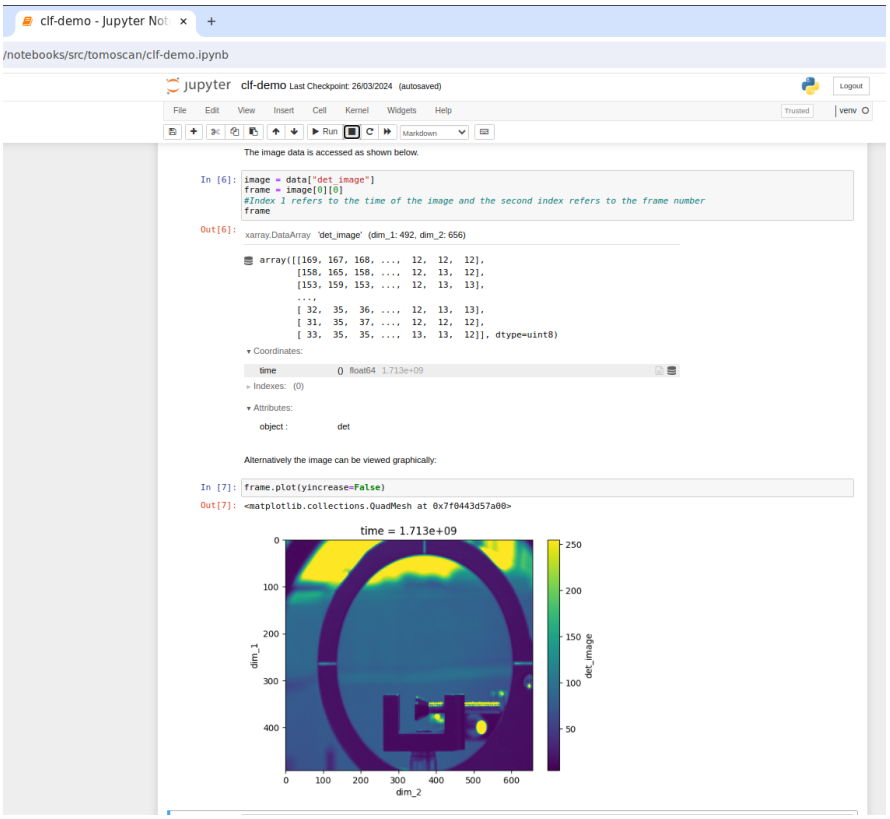

Figure 94: A screenshot of the work-in-progress “advanced mode” user interface, based on Jupyter Lab

In addition, there will be a set of “basic” and “intermediate” user interfaces. Each one will allow users to execute particular plans, offering them ways to customise those plans and display the results. These will be implemented as web applications, probably using the Dash framework[21] for data-driven Python web apps (due to the ability to create a full-featured web application using only Python). Each one will provide access to an underlying Bluesky run engine, probably through the Bluesky Queue Server.

This approach requires significant R&D effort. We need to decide what information needs to be displayed to end users and how to display it, and also what configuration options need to be user adjustable. We then need to create a complete web application offering all these features. Once this has been developed, it should be rather easier to develop additional applications to execute different types of plans. These user interfaces are likely to be a trial phase during commissioning experiments, but should be ready for more widespread use by the time EPAC opens up for wider user access.

5.3.1.6 Data acquisition flow

A plan is a sequence of instructions executed by the Bluesky run engine, usually but not always including data acquisition. A typical plan would be a CT scan, in which a rotation stage is stepped through 360 degrees of rotation, with projections being taken at each step. Some Bluesky plans are *adaptive*, meaning the instructions depend on what data was collected earlier, though most are not.

A user can start the execution of a plan either through the Jupyter Lab interface or through a more specialised user interface. The run engine begins executing the instructions in the plan, some of which will involve collecting data from detectors. There are two possible approaches to this. The first is that the run engine collects data from the detector directly. This is the preferred option, but it may lead to technical challenges when collecting data from multiple detectors simultaneously. We would like data collected by all detectors to relate to the same laser pulse, but Bluesky appears to offer no way of ensuring this. The second option is for Bluesky to record the pulse ID and delegate data collection to another subsystem. This has already been implemented, but has the significant drawback that the data is “invisible” to Bluesky.

In the current implementation, Bluesky will collect pulse IDs. The data corresponding to these pulse IDs will be sent to Kafka. By the end of the run, a component called the “file writer callback” will have collected a complete list of pulse IDs for that run. It will then collect the data for those pulse IDs from Kafka and write it into a file. The user will have to configure the file writer callback with the set of data sources and details of the desired file format. On completion, the file writer callback notifies the user, including any problems that were encountered.

5.3.1.7 Metadata flow

Bluesky is designed to handle metadata and can use multiple sources.

Firstly, the start of a run can be annotated with various kinds of metadata. This automatically includes information such as the time (and date) and the kind of plan being executed. We intend to add information to link the run to an experiment, and would like to add details such

[21] https://dash.plotly.com/

as the target in use automatically. Other details need to be provided by the users. As part of the Bluesky data model, this cannot be provided after the run has started.

Bluesky can also collect “baseline measurements” at the start of a run from any compatible detectors, as well as monitoring detectors during the run.

All metadata collected by Bluesky is inserted into the catalogue (see below). In addition, some metadata will be written into any data files produced.

5.3.1.8 Catalogue

All data and metadata collected by Bluesky can be inserted into a “Catalogue”. This is done using a Bluesky component called “databroker”, which then provides a programming interface to read data from the catalogue. Importantly, the interface does not depend on the details of how the data is stored.

Since many users will not be comfortable using this programming interface, applications will be provided to search and access the catalogue. If there is a preferred solution within the Bluesky community, we will use that; otherwise, we will develop an application of our own.

In addition, the contents of the Catalogue will be available to users after the experiment, as well as software to access it.

5.3.1.9 Implementation progress

Bluesky is already a complete product. The implementation work needed for EPAC consists of adapting it to EPAC’s systems, and adding the new features needed for our workflow.

We have begun work on an “EPAC toolkit” for Bluesky, to incorporate most of our custom code. So far, this includes integration with the pulse ID system and with the file writer. It is possible to run simple (non-adaptive) plans and create data files, which should be enough for routine data acquisition needs. We have now setup a data acquisition system in a tomographic scanning mode in Gemini TA1 (see **Figure 95**), in order to develop Bluesky for EPAC.

A demonstration of a simple tomography scan was created first in pure software simulation mode and then, when demonstrated to work, adapted to make use of hardware equipment in a laboratory.

The tomography scan was implemented as a step scan, where a motor rotates a sample through 360° stopping at a defined number of points at which images are captured by a camera. The triggering of the camera had to be timed to coincide with the illumination of a pulsed laser.

In simulation, a simulated camera, motor and laser were used. A custom Bluesky plan was created that waited for a laser pulse prior to trigger the camera, and then moved the motor to the next scan position once the image was captured.

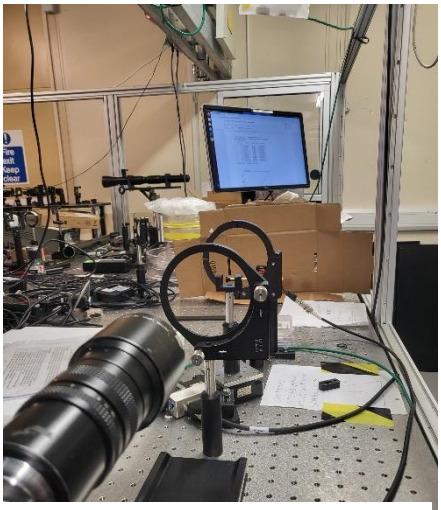

Figure 95: Experimental setup in “scan mode” to develop Bluesky for EPAC

The hardware demonstration used a camera, a rotating sample stage with a motor, an LED acting as the pulsed laser and a signal generator. The signal generator was used to trigger both the laser and the camera, such that images captured by the camera were always synchronised with the laser pulses. When the camera was commanded by the Bluesky software scan plan to acquire an image, it would then wait until it received a signal from the signal generator to capture the image. Using the Bluesky scan plan allowed the sample to be rotated, and images to be correctly captured, at each step of the scan.

The scan plan was then modified to capture multiple images at each point of the scan, to demonstrate the rate at which Bluesky could capture data in this mode. This allowed images to be captured at a rate of up to 5 Hz. This scan rate should be improved in future, by directly orchestrating the scan and hardware-triggering the camera using hardware such as a PandABox.

These demonstrations used the previously outlined “advanced” user interface in a Jupyter Lab notebook, and images captured were written directly to HDF5 files. These images, along with data such as the laser pulse ID, sample motor positions and metadata, were stored in the Bluesky Catalogue. The data were then demonstrated to be accessible as expected: directly available as multi-dimensional arrays in the Jupyter notebook, without the need for the user to first copy or open the data file manually.

5.3.1.10 Next steps

Now that basic functionality is in place, we need to work on more advanced features of Bluesky. These will involve adaptive scanning and improving user experience.

The immediate focus will be on integrating data more tightly with the Bluesky Catalogue, rather than keeping it only in separate files. This will involve connecting the Catalogue to the file storage, and possibly to Kafka. It will also involve acquiring data directly into Bluesky, where care will need to be taken to ensure that data corresponds to the correct laser pulse. This will also enable a wide range of adaptive scans.

We will also work to ensure that all necessary metadata is acquired and recorded. This includes metadata tied to a specific detector (such as the gain setting on a camera), and also metadata tied to the experiment generally. In the next few months, we will develop more use cases, including the use of continuous scan with PandABox etc.

5.3.2 Data display

EPAC will have multiple ways of displaying live and historical data, aimed at both users and facility staff. Here we describe some of those interfaces, their designs, their purposes, and the progress on them.

5.3.2.1 OperationsGateway

OperationsGateway is a solution being developed by SCD to provide a storage system for data related to facility operations, as well as user interfaces to access that data. It will allow operators to review historical data on laser performance, to check the health of the facility.

A detailed set of requirements and a rough design of the user interface were finished in 2022. Since then, development has begun and is proceeding on schedule, now jointly funded by the Ada Lovelace Centre (ALC) and the EPAC project.

As of April 2024, twenty-nine components of Operations Gateway have been completed, and three major components remain: Data Export, Data Display, and Functions. These three are all currently under development. Following completion of these, a final user feedback session will be held, following which any further modifications arising from the user feedback session will be addressed. OperationsGateway will then undergo end-to-end testing before being delivered to CLF as an operational system around January 2025. From this date, Operations-Gateway will operate further in test mode for several months, using real EPAC data as the EPAC laser is commissioned. Once EPAC has been fully commissioned, OperationsGateway will become fully operational.

The SCD/ALC team is currently working on the Data Display and Functions components. An early version of the browse screen display is shown in **Figure 96**. The CLF team is developing an "exporter" to generate periodic data dumps and send them to OperationsGateway. This will be configured with lists of data sources and time periods. Implementation of this has begun and is proceeding well. The integration of this would require the completion of other systems, mainly the EPAC control system and OperationsGateway itself.

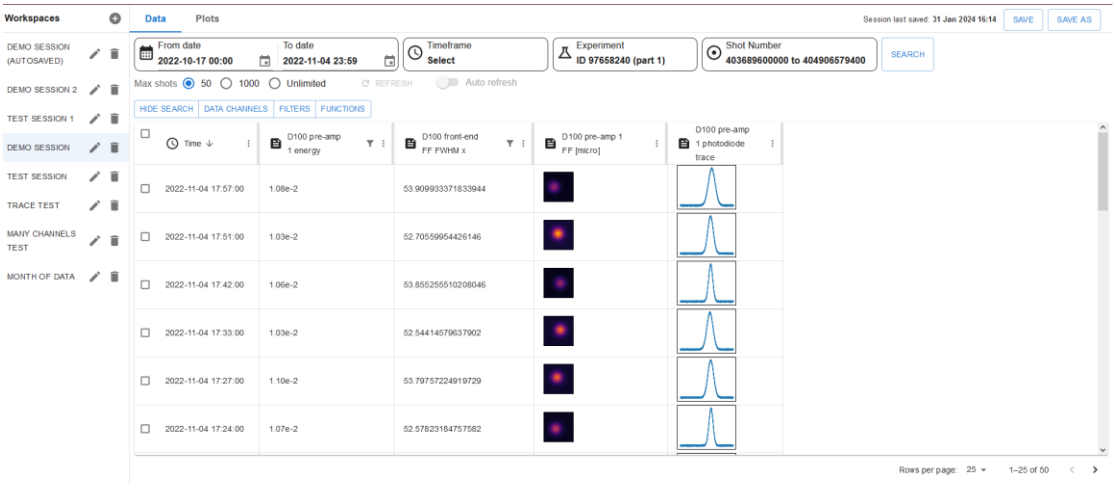

Figure 96: Screenshot of browse screen in OperationsGateway

5.3.2.2 Grafana

EPAC will produce a lot of data that we plan to display in a configurable dashboard for operators. This will help operators to understand the trend in various aspects of facility operations in a snapshot. We intend to use Grafana for this purpose.

Grafana[22] is a widely used web-based dashboarding system, mainly for monitoring and observability. For example, it is commonly used to display performance data from computer systems. It combines data into dashboards and allows its users to create, modify, and share those dashboards. It is useful mainly for scalar data rather than images and waveforms; while it would be useful for monitoring laser energy, it would be less useful for monitoring the laser spectrum or the shape of the focal spot.

There is an unofficial Grafana plugin[23] that allows it to access data from the EPICS Archiver Appliance[24]. The Archiver Appliance is used at many facilities to store data collected from their

[22] https://grafana.com/
[23] https://sasaki77.github.io/archiverappliance-datasource/
[24] https://slacmshankar.github.io/epicsarchiver_docs/

EPICS control systems. Data from laser diagnostics will be stored by the EPICS Archiver Appliance and visualised by Grafana. We expect that this will mainly be used to monitor the performance of the laser itself, with different groups of users developing dashboards for their own specific needs. This approach has been successful at ELI Beamlines.

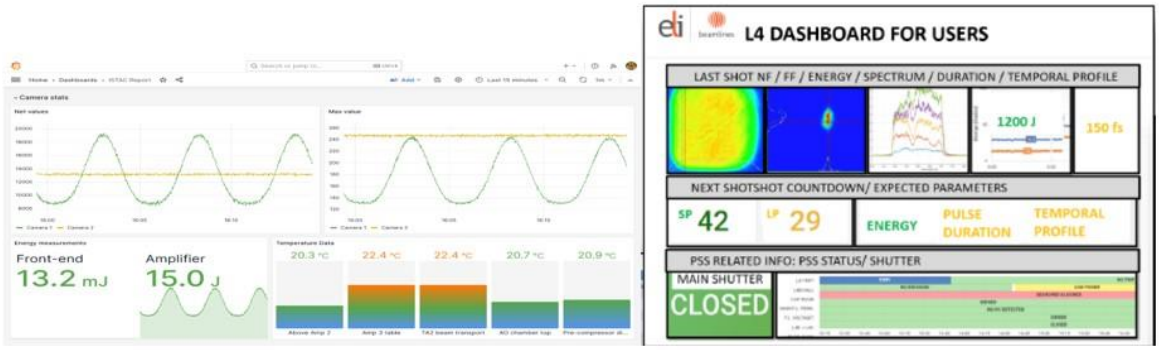

Figure 97: Grafana, showing data loaded from the EPICS Archiver Appliance. A screenshot of the Grafana dashboard in ELI Beamlines is also shown.

No significant development work is currently needed for Grafana, although some work would be needed if we wanted to display image data as well, as shown for ELI. We need to deploy and configure instances of the Archiver Appliance and Grafana. We will use the same Grafana instance (with some separation in place) to monitor the IT infrastructure in EPAC, so we expect this to be in place well before project completion.

5.3.2.3 Live data analysis and display

Users performing experiments need to be able to see the data they are collecting for many reasons. These include making sure the experiment is working as expected, checking useful data is being collected, and making scientific decisions on what to do next. While some of these needs can be met by the interfaces provided by the control system, and others by Bluesky, there is a need for dedicated software to plot data in real time. In addition, much of the raw data will require varying levels of processing before it is scientifically useful, for example electron and x-ray spectrometers. While traditionally this has been the responsibility of user groups, if these detectors are to be facility-owned, we must provide users with the analysed data (in addition to the raw data, and details of the analysis).

In the Gemini facility, a version of these “dashboards” is used, showing a combination of raw and lightly processed data, as shown in **Figure 98**. Experiences with these have informed the design of a live plotting and analysis package that we intend to implement in EPAC, with the following key features:

- Multiple sources of data displayed simultaneously as a dashboard
- “Playback” control, allowing older data to be recalled and displayed
- Custom plotting and analysis routines can be added.

The same application will be able to handle live data analysis by running in “headless” mode without a display. It will use the same analysis routines that would normally be used for plotting, but the results will be sent back into Kafka, where other systems can access the data.

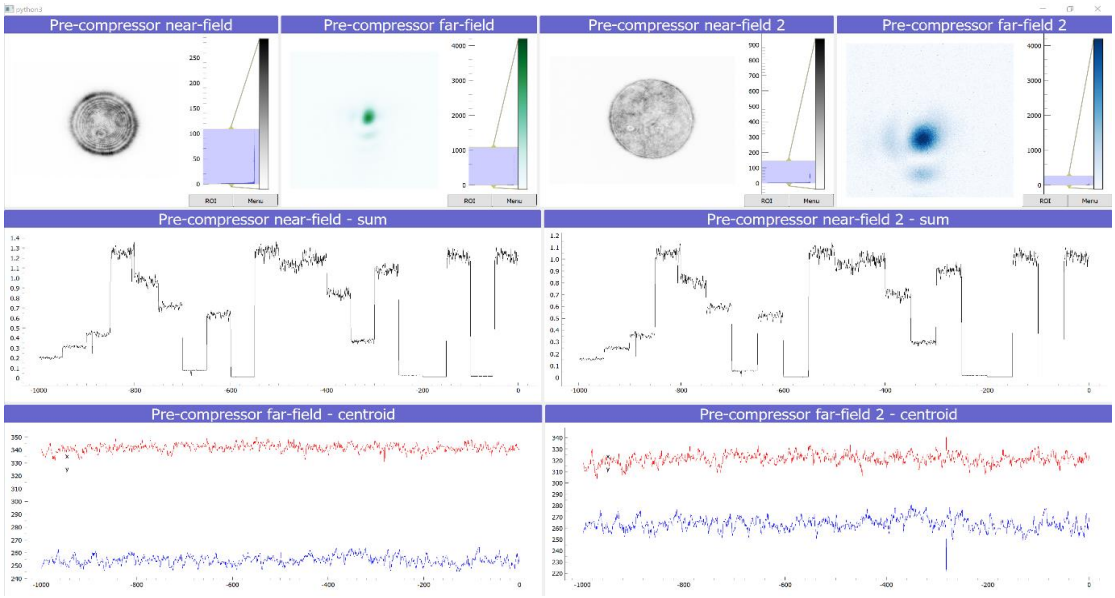

Figure 98: The Gemini live plotting system (mentioned above), displaying both raw and processed data in real-time

5.3.3 Facilities Data Pipeline – SCD

STFC's Scientific Computing Department (SCD) is designing a data pipeline for data storage, non-real-time data analysis, archival storage, and data management. The approach being taken is to design a modular pipeline where individual components can be upgraded and replaced, allowing flexibility to apply the same design to other, future STFC facilities. To improve commonality with other STFC facilities, existing platforms and services will be utilised and upgraded where possible.

Figure 99 shows a summary of the expected architecture, but this will continue to develop as requirements investigation progresses.

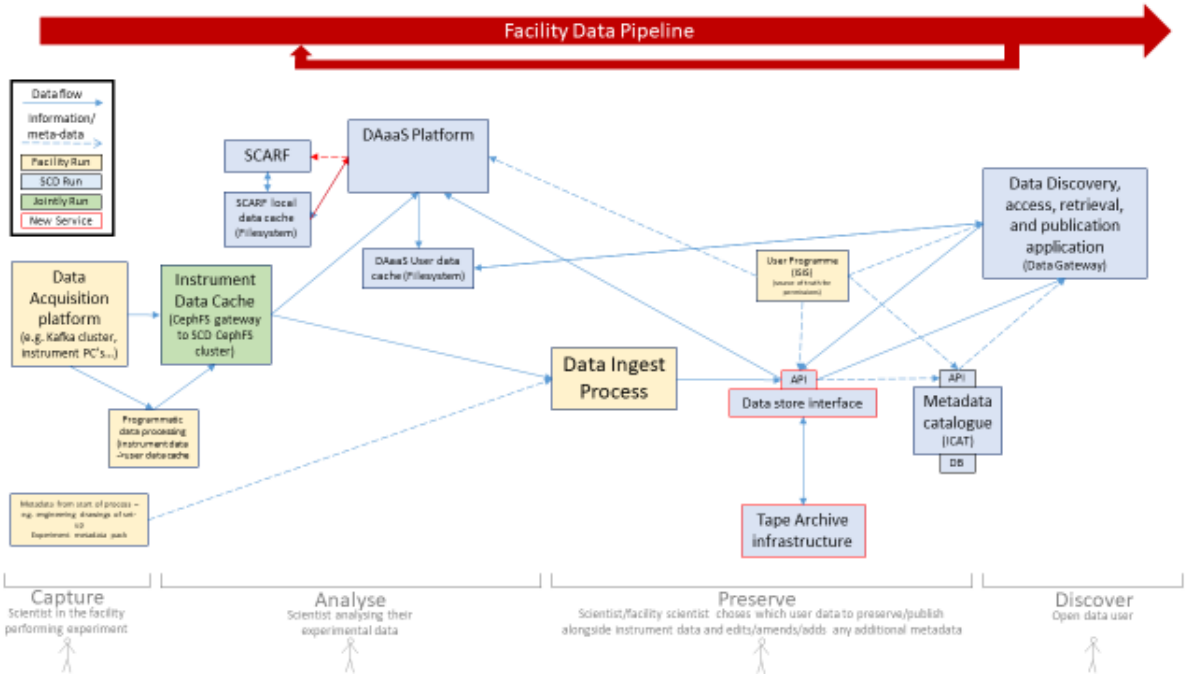

Figure 99: An overview of the design of the Facility Data Pipeline

5.3.3.1 Data caches

SCD will create two data caches on established Ceph clusters. The **instrument data cache** will have read only experimental data written from EPAC's data broker via a TBC ingest process, and will act as the handover point for data entering the pipeline. The **user data cache** will allow users of the Data Analysis as a Service (DAaaS) platform to store generated data as they work on analysis.

These caches are expanding existing systems that are well proven with other facilities. They are held on spinning disk storage, meaning that there is minimal delay in access; however, this will limit the data size that can cost effectively be stored in the caches, preventing them being used for archival purposes.

5.3.3.2 Data Analysis as a Service

To solve the problems associated with analysing large data sets, SCD has developed DAaaS, which provides users with on-demand access to a virtual machine (VM) in the STFC cloud. This VM has appropriate analysis software pre-installed, and access to the Instrument Data and User Data caches. This system has been run in production for several years for the ISIS Neutron and Muon Source; this year it has started to be rolled out to existing CLF facilities, including Gemini, and the user feedback so far is very positive. Roll out for EPAC is expected to be a relatively simple process and will not begin until analysis requirements for the facility are clearer. This year, work has been ongoing to coordinate with the team developing a CT graphical user interface (GUI) for EPAC, to ensure that the platform will be capable of supporting it.

5.3.3.3 Data store

SCD is creating an archival storage solution for EPAC. This will copy experimental data from the instrument data cache to SCD's existing tape storage systems for long term storage, integrate with metadata catalogues, and provide methods for users to find and retrieve data.

A new application programming interface (API) will require development to transport data between different platforms and services, and this represents significant development effort. A prototype is currently in development.

5.3.3.4 Data cataloguing and access

The data catalogue will be provided by ICAT: SCD is a part of the ICAT collaboration[25]. SCD currently runs production instances for both ISIS Neutron and Muon Source and Diamond Light Source. The codebase is also used by other facilities internationally. SCD has recently launched the Data Gateway, which is a web front-end for ICAT, and will ensure that the roadmap for the Data Gateway includes requirements for EPAC, including those around open data.

5.3.3.5 Progress and outlook

After a slow start, the Facility Data Pipeline for the EPAC project is now making good progress. Initial slow progress was driven by a high level of uncertainty on requirements, data volumes,

[25] The ICAT Collaboration | ICAT Project

and responsibilities. Work so far has focused on identifying requirements, system design, and prototyping connections between services.

The project team has been re-enforced with a project manager and additional support from ALC leadership. Additional development resources have also been secured from SCD, and prototyping is well underway on the API that will link components of this pipeline together.

Recently a workshop was held with EPAC to agree and prioritise the set of user requirements this project is delivering against, and this has helped to focus effort on the areas of highest value to EPAC. Following this meeting, a detailed review of architecture is underway to confirm that design choices will meet those requirements and align well with ALC and SCD's strategies. There is still a medium degree of uncertainty in the project, but following this prioritisation, it has been agreed that a Minimum Viable Product will be delivered in 2025, in line with EPAC commissioning timelines.

5.3.4 Computed Tomography package for EPAC

Development of the CT (Computed Tomography) pipeline for EPAC is ongoing, including a GUI for configuring and running pre-processing and reconstruction of tomographic data. The GUI brings together the Core Imaging Library (CIL) and CILViewer libraries for the computation and visualisation. CIL is an image processing and reconstruction package in Python and C++, developed by the Tomography team in the SCD in collaboration with CCPi (the Collaborative Computational Project in Tomographic imaging). The CILViewer is a 2D and 3D voxelised visualisation tool, allowing visualisation and interaction with the data in any orientation.

The CIL-GUI will allow users to easily configure pre-processing and reconstruction steps. They will then be able to run or save a chained list of processes forming a pipeline. This pipeline can be loaded and re-run or updated later. This output will be compatible with the CIL package, allowing it to be run on a server or on Diamond Light Source's HTTomo (High Throughput Tomography) pipeline.

5.3.4.1 Current status and future work

In June 2023, a major CIL-GUI version was released with enhanced process list functionality, increasing the speed of processor chaining. Users can now run, save, and reload their configured process list at any point, enabling them, for instance, to begin processing at STFC-RAL and resume later at their workplace. An example of this GUI is shown in **Figure 100**.

Enhancing GUI stability, workflow and usability are current priorities. An advanced dialogue tool (inset to **Figure 100**) has been developed, enabling work on simplifying the interface. The GUI now displays default configuration options with advanced settings in dialogs available to expert users.

CT functionality must be implemented and released in CIL before the GUI can expose it. Pre-processors identified as necessary or commonly needed are being added. Recent additions include improvements to the centre of rotation algorithm, supporting tilted centre of rotation axes, speed increase for downsampling, improved ring removal algorithm, and improvements to FBP (filtered back-projection) reconstruction, allowing split processing for parallel beam data and choice of filter. The next phase of the GUI will focus on integrating these new features. **Figure 100 (right)** shows current work integrating the choice of FBP filter into the GUI.

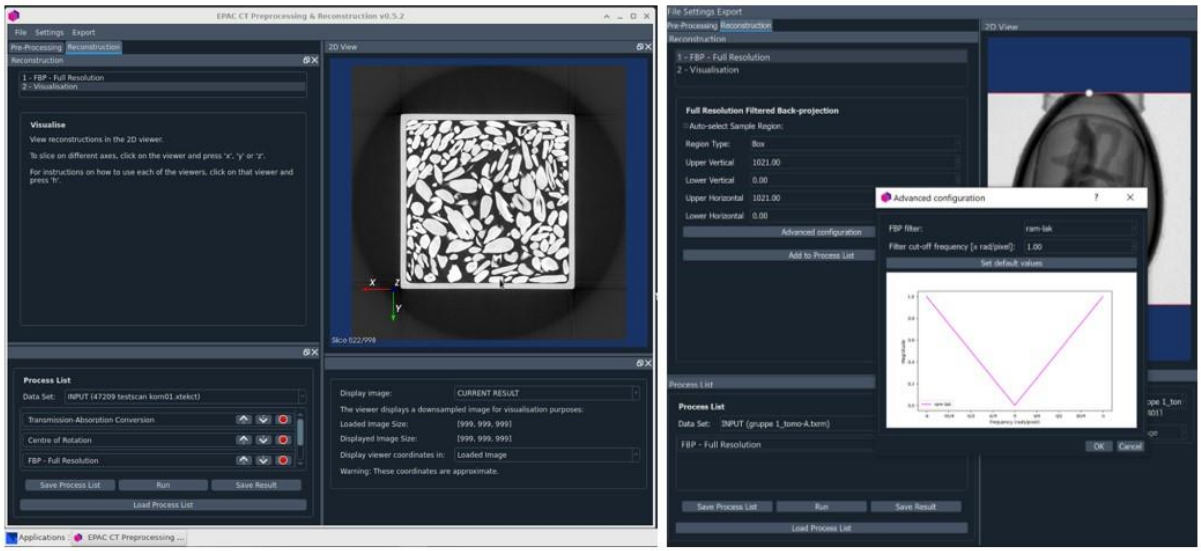

Figure 100: (Left) CIL-GUI running on the DAaaS platform; (Right) Selection of filter for Filtered Back Projection (FBP) reconstruction, currently under development in the GUI

Ongoing development work on pre-processors relevant to EPAC CT analysis includes addition of the Paganin phase retrieval algorithm for phase-contrast imaging, a single-material beam hardening corrector and commonly used pre-processing filters. **Figure 101** shows an example of CIL's recently improved Ring Removal processor in use[26]; however, different algorithms are suited to different datasets, making this an ongoing project to add further algorithms.

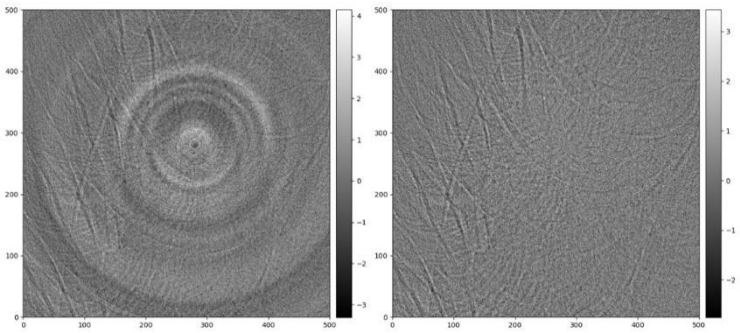

Figure 101: CIL's wavelet decomposition Ring Removal Algorithm applied to soft tissue data. Left: Reconstructed data, Right: Reconstructed data with ring removal algorithm applied.

Work on the CILViewer has improved stability and performance, and it is now released as a standalone tool for visualisation and interaction with reconstructed volumes. Integration of CIL with DLS's HTTomo has begun, starting with CIL's FBP reconstruction.

5.3.4.2 Deployment and workshops

The CIL-GUI and CILViewer are deployed on the DAaaS platform. New releases are now automatically available in the platform. The EPAC team have access to DAaaS and are able to test and raise issues as beta testers. In June 2023, a workshop was run with members of the EPAC team and Warwick Manufacturing Group (WMG) to demonstrate the GUI and DAaaS platform. At the demonstration we gathered feedback, including requested features, which are steering the project's roadmap. Further to this, the CT package is being tested by colleagues working closely with the WMG team, and their feedback will be critical in optimising the solutions we develop.

[26] Data: `tomo_00072` available at https://tomobank.readthedocs.io/en/latest/source/data/docs.data.rings.html

5.4 Next steps on developments and policy

5.4.1 Digital Lab books

As part of our commitment to the FAIR data principles[27], we need to ensure that all relevant metadata is collected and made available. Much of this metadata cannot be collected automatically and will only be recorded in a lab book. To meet our commitments, we will need to provide fully featured lab book software to our users and encourage them to make full use of it.

At a minimum, this must allow users to make notes, including images and tables. It must be searchable and must be accessible from the lab and the control room. Data must be stored centrally, so that it can be archived and released after an embargo period, as described in the Data Policy. Ideally, it will allow timestamping of entries, track or prevent modifications to older entries, and integrate with the data acquisition and cataloguing systems.

It is not practical to develop our own lab book software from scratch, so we are evaluating the existing options. Some commercial solutions such as Labfolder[28] exist. Other facilities (for example, Diamond) are also looking into similar solutions, so we are planning to collaborate with them to find a common solution that can be supported.

5.4.2 EPAC's Data Policy

We are currently in the process of developing a Data Policy for EPAC, which can be adopted by the CLF as a whole. So far, we have been operating under the principle that the experimental data we produce belongs to the user institutes and they curate the data. While this will continue to be applicable, with the amount of data EPAC will generate, the CLF will have an obligation to preserve and curate the data. Moreover, this also has a bearing on the design of the Facility Data Pipeline, which will provide storage and curation solutions for EPAC data. As such, this Data Policy will cover how the CLF handles curation, access, ownership, usage, and storage of data collected at the EPAC facility, along with the responsibilities that users of EPAC have pertaining to these topics.

The CLF, like the rest of STFC and UKRI, will be committed to the principles of FAIR data in order to support research, and the advancement of knowledge and technology. We intend to release data in common, accessible formats under a permissive Creative Commons licence, along with detailed metadata in a variety of human- and machine-readable formats. This will be applicable to all non-proprietary data (i.e. data obtained via open access). We are planning to conduct workshops over the next few months, involving CLF staff and facility users, as well as other facilities (such as ISIS and Diamond) to develop this further.

[27] https://www.go-fair.org/fair-principles/
[28] https://labfolder.com

6. Electrical control and safety systems

6.1 Introduction

The Electrical Control and Interlocks work is divided into three major deliverables: laser safety interlocks; motion control (alignment); and vacuum control systems. These systems spread across all three floors and multiple areas throughout the building. To deliver a user-friendly facility that operates efficiently and is able to increase its capability, the Electrical Control and Interlocks team has been working on providing solutions that are flexible, expandable, and maintainable. Feedback from users, and lessons learnt over the years in developing, commissioning, and supporting these systems, has also been taken into consideration.

This section details key progress on the motion control system since the last ISTAC report.

6.2 Motion control system updates

6.2.1 Development and testing

The motion control system plays an essential role in the operation of the facility across all laser and experimental areas. Under the current design for phase 1 of the project, it needs to allow the operation of more than 200 axes across EPAC, with expansion foreseen when the facility becomes fully operational.

In the **laser areas**, the motion control system is predominantly used for driving linear and rotation stages. For example, in the Front End, the drive system allows the movement of mirrors to ensure laser delays are correct. At the compressor end, the motion control system will be used to allow the operation, under vacuum conditions, of four grating mounts and one turning mirror with a total of 28 axes, using absolute encoders to measure their position accurately under closed loop control.

In the **experimental areas**, the system provides control of different mounts fitted with piezo and stepper motors, to allow closed loop control to achieve the requirements set in this area. For example, in EA1, the system will mainly be used on the turning, focusing and target chambers under vacuum conditions.

Procurement of major parts has been accomplished, with tailored control modules for the compressor delivered in 2023/24. Design has continued on two different control cabinet options, needed to accommodate different room layouts. We are focusing on providing a modular, flexible, scalable, and reliable system that can be quickly adapted to users' experimental configurations and requirements. We have continued to test the main control components in target and experimental areas in the Vulcan and Gemini facilities, and in the turning chamber in EPAC.

6.2.2 Collaborative input

6.2.2.1 CLF users

We are continuing to work closely with our Experimental Science Group (ESG) and user community in the development of the motion control system. We successfully tested the design and major hardware components on various experiments in Vulcan and Gemini, assessing both reliability and robustness. The motion control system to be used in EPAC has been running in Gemini LA3 and in the TA3 target, and has also been installed in Gemini's TA2 and TA1 target areas. This has provided the team with great real-life testing and learning

opportunities. We have received very positive feedback from users and ESG, which is directing the way forward. Additionally, the system has been used to test major components in EPAC EA1, and is currently in operation in the Pump and Front-End laser rooms.

6.2.2.2 Target fabrication

As part of our continued development, the Electrical Control Team collaborated with the CLF's Target Fabrication group on development of the Tape Drive System, using the current motion control system technology. As a result of this collaboration, a solution has been developed that has been successfully used in experiments at the CLF, and there is a commercial application to supply other institutions in the UK. This has increased our confidence that the motion control system will meet the requirements of the EPAC facility.

6.2.2.3 Engineering

Development of the motion control system has been an iterative procedure involving all the engineering fields – electrical, mechanical and software – with the aim of delivering a system that is not only capable of meeting the existing requirements, but that also provides the user community with the flexibility they need, and the possibility of speeding up the alignment of the laser. For example, the motion control system can provide the simultaneous, coordinated motion of multiple axes and set up the system to prevent any collisions of optical equipment, with the aim of reducing alignment time and therefore providing more experimental time. Such features have not been available in the past, but they present a considerable challenge as both engineers and scientists need to understand the impact and benefits of operating the facility this way.

Currently, we have a local graphical user interface (GUI) that allows users to operate the motion control system should the Main Control System be unavailable. A session was arranged to seek feedback from other Work Package Managers on the user-friendliness of the GUI, and positive feedback was received, as well as a few suggestions for improvements. We are also working with the Control Software Engineering Team to develop a user interface that allows integration with the Main Control System.

Additionally, we are working closely with the Mechanical Engineering Team to gain a better understanding of the motion requirements for each area, and to provide technical expertise and advice that will allow us collectively to deliver a better system for the project. The selection of absolute encoders to control gratings and monitor their positions on a closed loop feedback has been agreed by the two teams as a better solution for operating the gratings and turning mirror in the compressor.

6.2.3 Progress updates

6.2.3.1 Approach to delivery

Delivery of the motion control system hardware has involved a combination of sequential and iterative development. This approach has allowed us to agree and release requirements for the hardware, and to develop, test and refine the system with continuous feedback from ESG and CLF users.

Field trials have been carried out in Vulcan and Gemini, where users have used the hardware during their experiments. Improvements and additional features have been made as a result of their feedback. Our current approach and highlights of the delivery route are shown in **Figure 102**.

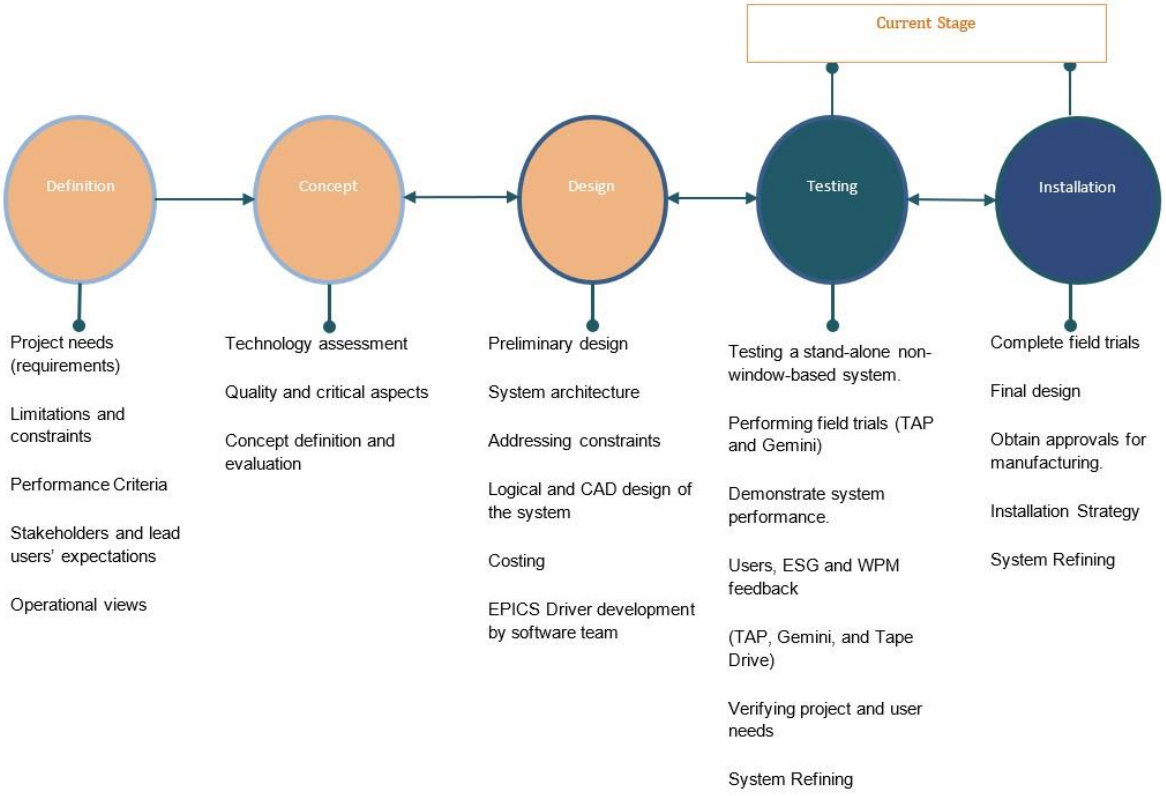

Figure 102: Iterative delivery approach to the motion control system hardware

6.2.3.2 System features

We have continued to learn from operational experience, and are taking a distributed approach for the delivery of the motion control system. We will provide the facility with a single system that offers a wider range of motor control technology (steppers, servo, piezo, encoders), and greater capacity than was previously available to our user community. To achieve this, the system uses a separate controller that communicates with a variety of drive modules, which can be tailored to the needs of laser and experimental areas. The controller and drive modules are linked using Ethernet cables, and thus they do not need to be in the same location. This allows drive modules to be located close to motors and encoders, reducing cabling.

One important feature of the system is that all the motion control happens at controller level, taking full advantage of the hardware features. This arrangement (**Figure 103**) minimises the amount of processing required by the Main Control System, and prevents unexpected motion should communications be lost.

Other additional features of the system include:

- Open and closed loop control
- The possibility of using up to six different types of incremental encoder and up to 12 different types of absolute encoder
- Point-to-point, relative, sequential, and simultaneous single and multi-axis motion.

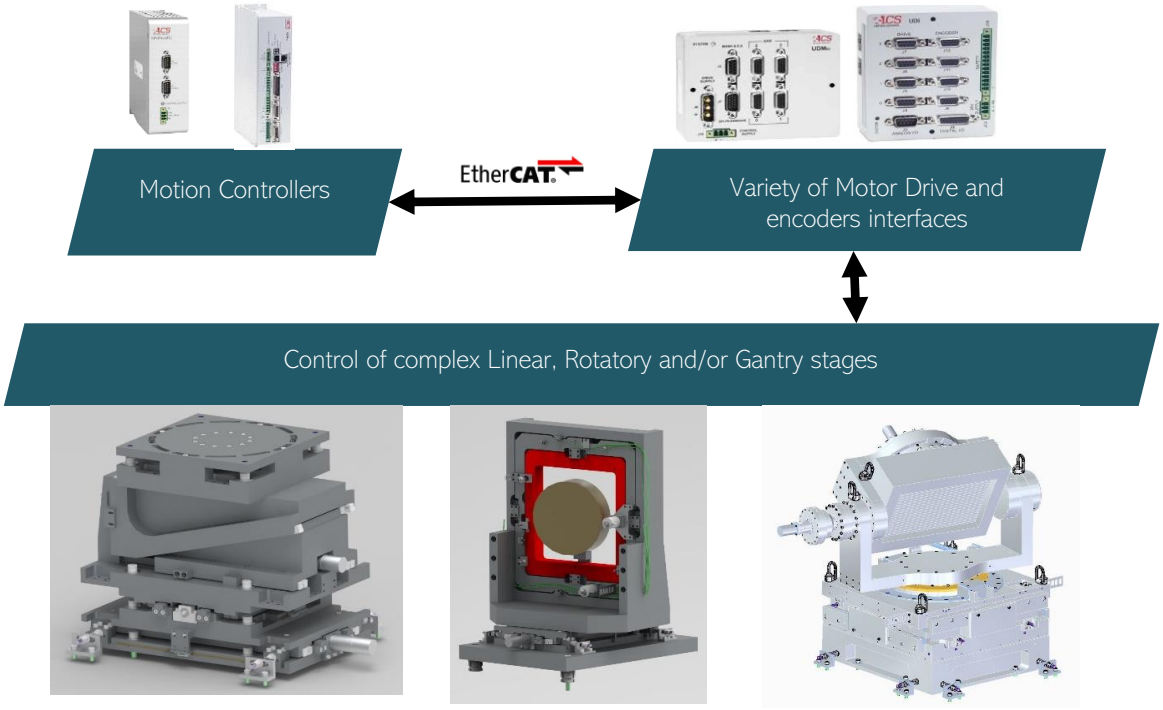

Figure 103: Motion control system hardware architecture, allowing flexibility and adaptability to user needs

Appendix A References

[1] First EPAC Technical Report for the ISTAC, EPAC-ISTAC-MN1-TR1, October 2020

[2] Second EPAC Technical Report for the ISTAC, EPAC-ISTAC-MN2-TR2, November 2021

[3] Third EPAC Technical Report for the ISTAC, EPAC-ISTAC-MN3-TR3, November 2022

[4] HiLASE Centre (www.hilase.cz/en/), Institute of Physics, Czech Academy of Sciences, Dolni Brezany, Czech Republic

[5] D. Clarke et al, "Improved stability second harmonic conversion of a diode-pumped Yb:YAG laser at the 0.5 kW level," Opt. Lett. 48, 6320-6323 (2023). doi: 10.1364/OL.497181

[6] M Divoky, J Phillips, J Pilar, *et al*. "Kilowatt-class high-energy frequency conversion to 95 J at 10 Hz at 515 nm," High Power Laser Science and Engineering, 11:e65 (2023) doi: 10.1017/hpl.2023.60.

[7] P. Poole, S. Trendafilov, G. Shvets, D. Smith, and E. Chowdhury, "Femtosecond Laser Damage Threshold of Pulse Compression Gratings for Petawatt Scale Laser Systems", Opt. Express 21, 26341 (2013) doi: 10.1364/OE.21.026341

[8] D. Doria *et al*. "Overview of ELI-NP status and laser commissioning experiments with 1 PW and 10 PW class-lasers," JINST, 15 C09053 (2020) doi: 10.1088/1748-0221/15/09/C09053

[9] https://multiscan3d-h2020.eu/

[10] P.L. Poole *et al*. "Liquid crystal films as on-demand, variable thickness (50–5000 nm) targets for intense lasers," Phys. Plasmas 21, 063109 (2014) doi: 10.1063/1.4885100

[11] P. Poole, A. Krygier, G. Cochran *et al*. "Experiment and simulation of novel liquid crystal plasma mirrors for high contrast, intense laser pulses," Sci Rep 6, 32041 (2016) doi: 10.1038/srep32041

[12] J. Hartmann *et al.* "Commissioning of the laser-driven ion acceleration beamline at the Centre for Advanced Laser Applications," Proc. SPIE 11779, Laser Acceleration of Electrons, Protons, and Ions VI, 117790N (2021) doi: 10.48550/arXiv.2111.08461

[13] E.J. Dolier *et al*. "Multi-parameter Bayesian optimisation of laser-driven ion acceleration in particle-in-cell simulations," New J. Phys. 24 073025 (2022) doi: 10.1088/1367-2630/ac7db4

[14] T.D. Arber *et al*. "Contemporary particle-in-cell approach to laser-plasma modelling," Plasma Phys. Control. Fusion 57 113001 (2015) doi: 10.1088/0741-3335/57/11/113001

[15] PWASC | Plasma Wakefield Accelerator Steering Committee

[16] J.S Green *et al*. "Scintillator-based ion beam profiler for diagnosing laser-accelerated ion beams," Proc. SPIE 8079, Laser Acceleration of Electrons, Protons, and Ions; and Medical Applications of Laser-Generated Secondary Sources of Radiation and Particles, 807919 (2011) doi: 10.1117/12.888967

[17] B. Loughran *et al*. (2023) "Automated control and optimization of laser-driven ion acceleration," High Power Laser Science and Engineering, 11, p. e35. doi: 10.1017/hpl.2023.23

[18] N. Booth *et al*. "Debris studies for high-repetition rate and high-power laser experiments at the Central Laser Facility," SPIE Optical Engineering + Applications, Proceedings Volume 10763, Radiation Detectors in Medicine, Industry, and National Security XIX; 107630S (2018) doi: 10.1117/12.2318946

[19] P.J. Phillips *et al.* "A kW-class nanosecond DPSSL operating at 100 J, 10 Hz for high energy density research at the European XFEL (Conference Presentation)," Proc. SPIE 10898, High Power Lasers for Fusion Research V, 108980K (2019) doi: 10.1117/12.2505605

[20] M.G. Gorman *et al.* "Shock compression experiments using the DiPOLE 100-X laser on the high energy density instrument at the European x-ray free electron laser: Quantitative structural analysis of liquid Sn," J. Appl. Phys. 135, 165902 (2024) doi: 10.1063/5.0201702

[21] P.J. Phillips *et al*. "Second and third harmonic conversion of a kilowatt average power, 100-J-level diode pumped Yb:YAG laser in large aperture LBO," Opt. Lett. 46, 1808-1811 (2021) doi: 10.1364/OL.419861

[22] Y. Wang *et al.* "0.85 PW laser operation at 3.3 Hz and high-contrast ultrahigh-intensity $\lambda = 400$ nm second-harmonic beamline," Opt. Lett. 42, 3828-3831 (2017) doi: 10.1364/OL.42.003828

[23] C. Armstrong *et al*. "X-ray detector requirements for laser-plasma accelerators," Front. Phys., Sec. Radiation Detectors and Imaging Volume 11 (2023) doi: 10.3389/fphy.2023.1286442

[24] M.C. Veale *et al*. "Characterization of the uniformity of high-flux CdZnTe material," Sensors, 20(10), 2747 (2020) doi: 10.3390/s20102747

[25] L. Jowitt *et al*. "HEXITEC 2 × 2 tiled hard X-ray spectroscopic imaging detector system," JINST 17 P01012 (2022) doi: 10.1088/1748-0221/17/01/P01012

[26] D.R. Rusby *et al.* "Novel scintillator-based x-ray spectrometer for use on high repetition laser plasma interaction experiments," Rev. Sci. Instrum. 89,073502 (2018) doi: 10.1063/1.5019213

[27] C.D. Armstrong *et al.* "Deconvolution of multi-Boltzmann x-ray distribution from linear absorption spectrometer via analytical parameter reduction," Rev. Sci. instrum. 92, 113102 (2021) doi: 10.1063/5.0057486

[28] K.T. Behm *et al*. "A spectrometer for ultrashort gamma-ray pulses with photon energies greater than 10 MeV," Rev. Sci. Instrum. 89, 113303 (2018) doi: 10.1063/1.5056248

[29] A. Laso Garcia *et al.* "Calorimeter with Baynesian unfolding of spectra of high-flux broadband x rays," Rev. Sci. Instrum. 93, 043102 (2022) doi: 10.1063/5.0078443

[30] K.K. Swanson *et al.* "Applications of machine learning to a compact magnetic spectrometer for high repetition rate, laser-driven particle acceleration," Rev. Sci. Instrum. 93, 103547 (2022) doi: 10.1063/5.0101857

[31] S.I. Bajlekov *et al*. "Longitudinal electron bunch profile reconstruction by performing phase retrieval on coherent transition radiation spectra," Phys. Rev. ST Accel. Beams 16, 040701 (2013) doi: 10.1103/PhysRevSTAB.16.040701

Appendix B EPAC Project team interactions

At the last ISTAC meeting, the committee recommended that EPAC participate in meetings where potential new users might be identified.

The EPAC team has continued to identify relevant meetings, conferences and workshops, attending where possible, and have organised many visits, particularly where potential suppliers or users are located close to such events.

In total, since the last ISTAC meeting, there have been some 203 interactions across the project team.

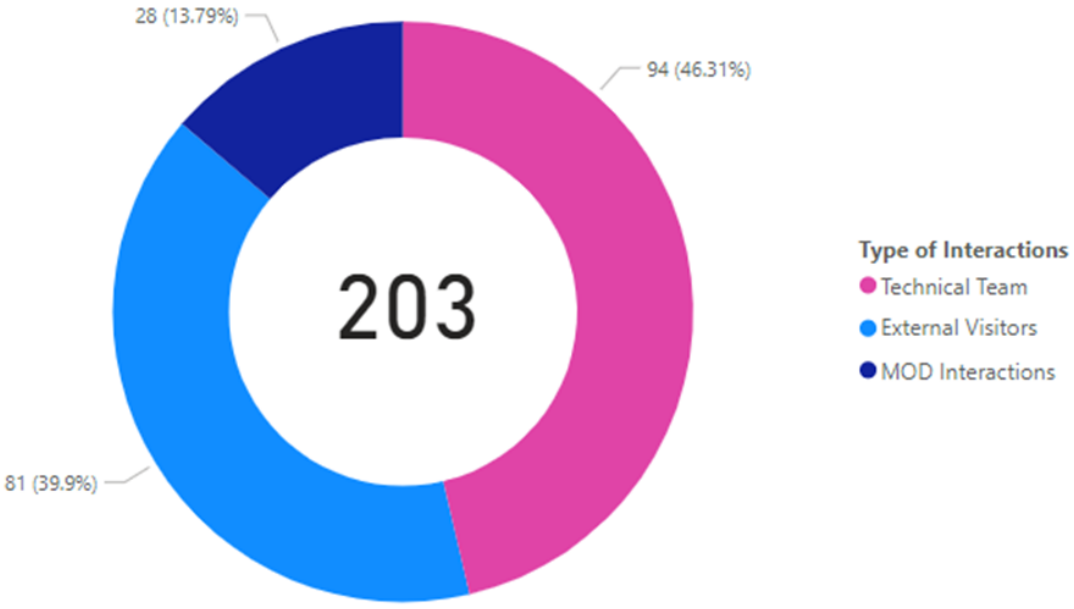

Figure 104: EPAC project team interactions during 2023/24

The EPAC technical team has actively engaged with users and suppliers across the world, delivering talks and presenting posters on EPAC innovations and opportunities to a wide audience of potential users and suppliers.

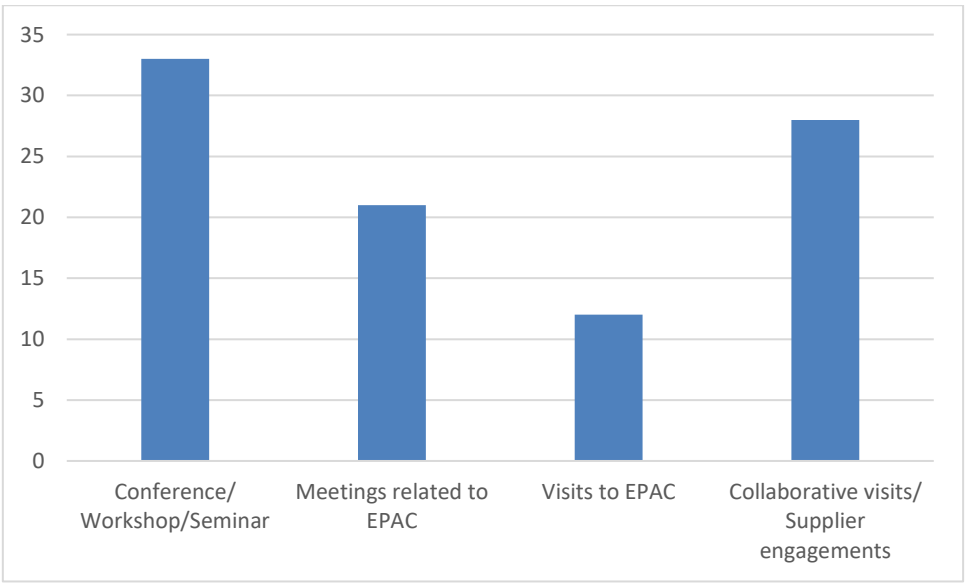

Figure 105: EPAC technical team interactions during 2023/24

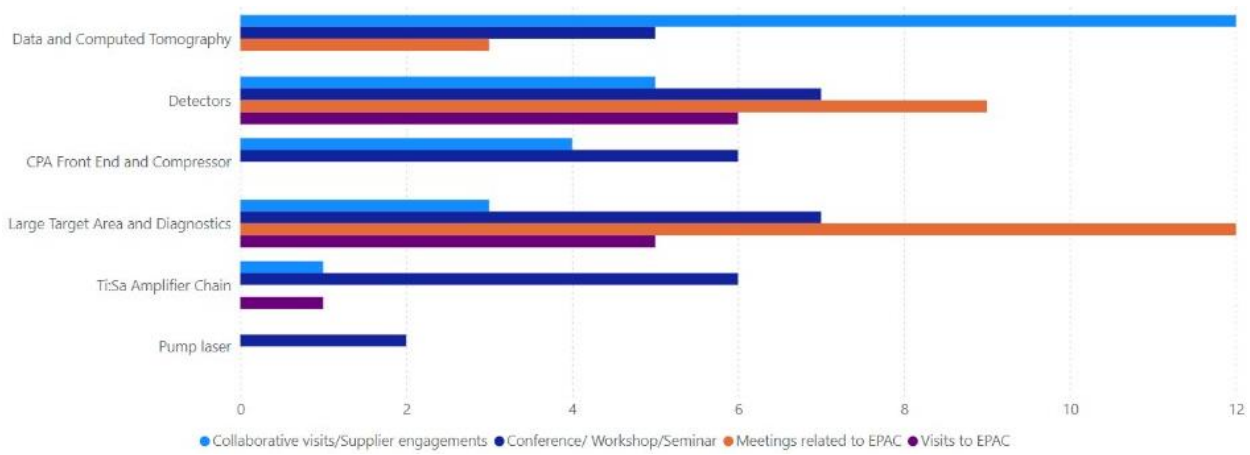

Figure 106: Interactions across the technical teams

Alongside visits captured here, there have been an additional 82 EPAC-related visits over the same period, with 610 visitors welcomed to EPAC building itself.

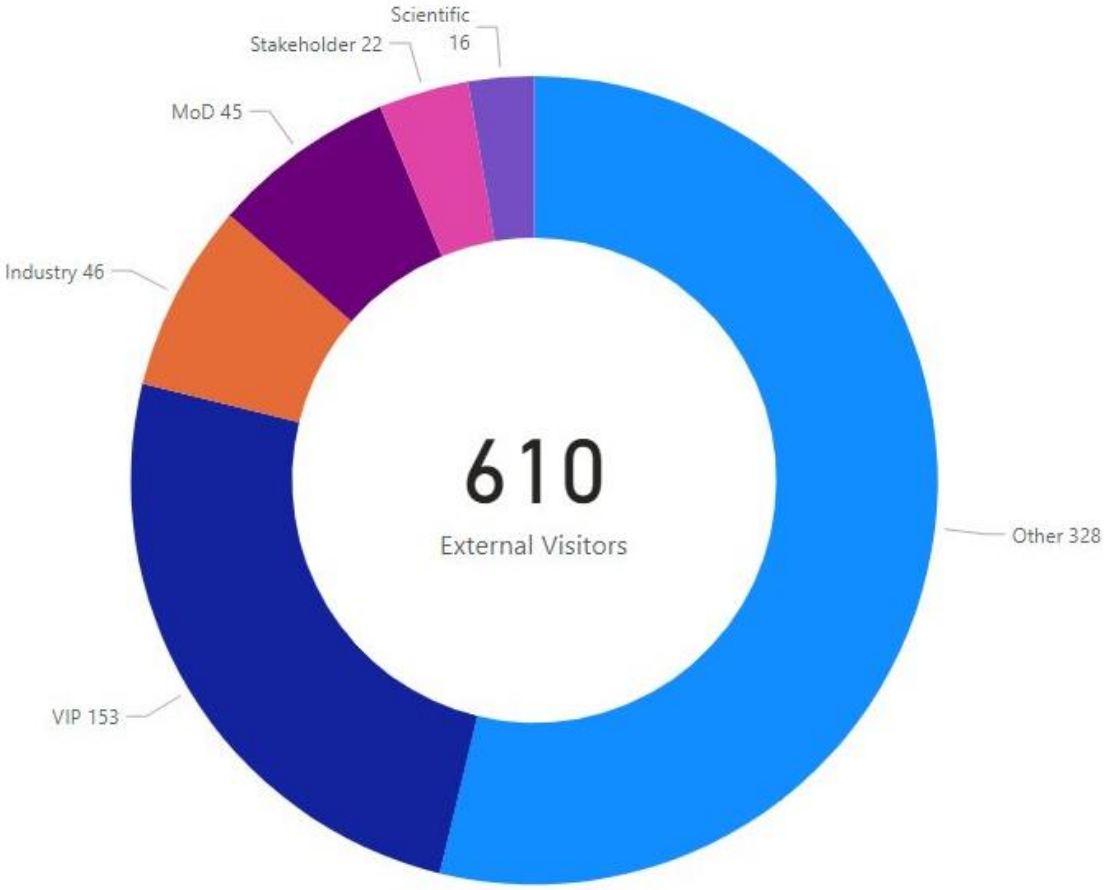

Figure 107: Visits to the EPAC facility during 2023/24